Université de Montréal

Directed evolution of human dihydrofolate reductase: towards a better understanding of binding at the active site

par
Elena Fossati

Département de biochimie
Faculté de médecine

Mémoire présenté à la Faculté des études supérieures
en vue de l'obtention du grade de
Maîtrise en biochimie

Novembre, 2008

Université de Montréal
Faculté des études supérieures

Ce mémoire intitulé:

Directed evolution of human dihydrofolate reductase: towards a better understanding of binding at the active site

présentée par :
Elena Fossati

a été évaluée par un jury composé des personnes suivantes :

Michel Bouvier, président-rapporteur
Joelle N. Pelletier, directeur de recherche
Serguei V. Chteinberg, membre du jury

Résumé

La dihydrofolate réductase humaine (DHFRh) est une enzyme essentielle à la prolifération cellulaire, ce qui en fait une cible de choix pour le traitement de différents cancers. À cet effet, plusieurs inhibiteurs spécifiques de la DHFRh, les antifolates, ont été mis au point : le méthotrexate (MTX) et le pemetrexed (PMTX) en sont de bons exemples. Malgré l'efficacité clinique certaine de ces antifolates, le développement de nouveaux traitements s'avère nécessaire afin de réduire les effets secondaires liés à leur utilisation. Enfin, dans l'optique d'orienter la synthèse de nouveaux composés inhibiteurs des DHFRh, une meilleure connaissance des interactions entre les antifolates et leur enzyme cible est primordiale.

À l'aide de l'évolution dirigée, il a été possible d'identifier des mutants de la DHFRh pour lesquels l'affinité envers des antifolates cliniquement actifs se voyait modifiée. La mutagenèse dite *de saturation* a été utilisée afin de générer des banques de mutants présentant une diversité génétique au niveau des résidus du site actif de l'enzyme d'intérêt. De plus, une nouvelle méthode de criblage a été mise au point, laquelle s'est avérée efficace pour départager les mutations ayant entrainé une résistance aux antifolates et/ou un maintient de l'activité enzymatique envers son substrat natif, soient les phénotypes d'activité. La méthode de criblage consiste dans un premier temps en une sélection bactérienne à haut débit, puis dans un second temps en un criblage sur plaques permettant d'identifier les meilleurs candidats. Plusieurs mutants actifs de la DHFRh, résistants aux antifolates, ont ainsi pu être identifiés et caractérisés lors d'études de cinétique enzymatique (k_{cat} *et* IC_{50}). Sur la base de ces résultats cinétiques, de la modélisation moléculaire et des données structurales de la littérature, une étude structure-activité a été effectuée. En regardant quelles mutations ont les effets les plus significatif sur la liaison, nous avons commencé à construire un carte moléculaire des contacts impliqués dans la liaison des ligands. Enfin, des connaissances supplémentaires sur les propriétés spécifiques de liaison ont put être acquises en variant l'inhibiteur testé, permettant ainsi une meilleure compréhension du phénomène de discrimination du ligand.

Mots clés : dihydrofolate réductases humaine, méthotrexate, pemetrexed, résistance aux médicaments, mutagenèse, évolution dirigée, criblage à haut débit, relation structure-fonction, cinétique enzymatique, modélisation moléculaire.

Abstract

Human dihydrofolate reductase (hDHFR) is an essential enzyme for cellular proliferation and it has long been the target of antifolate drugs for the treatment of various types of cancer. Despite the clinical effectiveness of current antifolate treatments, new drugs are required to reduce the side-effects associated with their use. An essential requirement for design of new antifolates is a better understanding of how these drugs interact with their targets.

We applied directed evolution to identify mutant hDHFR variants with modified binding to some clinically relevant antifolates. A saturation mutagenesis approach was used to create genetic diversity at active-site residues of hDHFR and a new, efficient screening strategy was developed to identify the amino acids that preserved native activity and/or conferred antifolate resistance. The screening method consists in a high-throughput first-tier bacterial selection coupled with a second-tier *in vitro* assay that allows for rapid detection of the best variants among the leads, according to user-defined parameters. Many active, antifolate-resistant mutants of hDHFR were identified. Moreover, the approach has proven efficient in rapidly assessing kinetic (k_{cat}) and inhibition parameters of the hDHFR variants (IC_{50}). Structure-function relationship analysis based on kinetic investigation, available structural and functional data as well as modeling were performed. By monitoring which mutations have the greatest effect on binding, we have begun to build a molecular picture of the contacts involved in drug binding. By varying the drugs we test against, we gain a better understanding of the specific binding properties that determine ligand discrimination.

Keywords : human dihydrofolate reductase, methotrexate, pemetrexed, drug-resistance, saturation and combinatorial mutagenesis, directed evolution, high-throughput screening, structure-function relationship, enzyme kinetics, molecular modeling.

Table of contents

List of tables

List of figures

Chapter 1

Chapter 2

Chapter 3

Chapter 4

Chapter 5

List of abbreviations

AICARFT	*Aminoimidazole carboxamide formyl transferase*
Amp	*Ampicillin*
DHF	*Dihydrofolate*
DHFR	*Dihydrofolate reductase*
E.C.	*Enzyme commission number*
E. coli	*Escherichia coli*
ecDHFR	*Escherichia coli dihydrofolate reductase*
FBP	*Folate binding protein*
FOL	*Folate*
FPGS	*Folypolygluatamate synthase*
GARFT	*Glycinamide ribonucleotide formyl transferase*
hDHFR	*Human dihydrofolate reductase*
IC_{50}	*Half maximal effective concentration for enzyme inhibition*
IPTG	*Isopropyl β-D-1-thiogalactopyranoside*
k_{cat}	*Catalytic constant (turnover number)*
k_{cat}/K_M	*Catalytic efficiency*
K_D	*Binding constant*
K_i	*Inhibitor constant*
K_M	*Affinity constant (Michaelis-Menten constant)*
k_{off}	*Dissociation rate*
k_{on}	*Association rate*
LB	*Luria-Bertani*
$NADP^+$	*Oxidized nicotinamide adenine dinucleotide phosphate*
NADPH	*Reduced nicotinamide adenine dinucleotide phosphate*
PDB	*Protein data bank*
RCF	*Reduced folate carrier*
RMSD	*Root mean square deviation*
SAR	*Structure-activity relationship*
SDS-PAGE	*Sodium dodecyl sulfate polyacrylamide gel electrophoresis*

THF	*Tetrahydrofolate*
TMP	*Trimethoprim*
TMTX	*Trimetrexate*
TS	*Thymidylate synthase*

Alla mia famiglia

Acknowledgements

After three years at the UdeM, here I am, finally finishing my Master degree, thinking about everything that has happened and about all the people I have met. Despite the sadness that comes with the choice of abandoning a project I know and I like for many new and still uncertain ones, I am excited and full of hope for my future. In fact, during my time at the UdeM I have grown as a scientist and as a person, and most of all I had the opportunity to meet a lot of interesting people and I feel I found another home in Québec.

First of all, I would like to thank my supervisor, Prof. Joelle Pelletier, for being such a dynamic and inspiring scientist. Joelle pushed me to my limits during my first and most difficult year, but she balanced this with compassion and patience, especially when my son arrived and when all the problems with the *train de banlieue* started! Her support, supervision and encouragement have been very precious, and her cakes and biscuits very appreciated!

Thanks to all the hDHFR gang. First of all to Jordan Volpato, for his scientific supervision and for making great Italian-like environment in the lab. Jordan is not only a brilliant scientist but an amazing communicator and…amazingly…he also knows the genetic code by heart, which may be useless, but it is certainly very impressive! Thanks to Lucie Poulin, who never missed either a sequencing gel or a chocolate cake! Lucie and I not only shared a bench but also a precious friendship. Thanks to Vanessa Guerrero for her good work and her flexibility around my 'not so flexible' working schedule…and for her desserts, obviously! Thanks also to Jonathan Blanchet and Mirja Krause.

Thanks to all the past and present members of the 'coffee club', first of all to Nicolas Chabot, the president! Thanks for *les vins et fromages*, *les Ricards*, *les grains de chocolat*, and the delicious *'saltinbocca alla romana'* receipe (imagine a French guy who gives to an Italian an Italian receipe! I know, I should have kept this a secret!). If it is true that real friends are rare and precious…bhe…Nico is certainly one of them. He was always there to listen and cheer me up me when I was afraid, sad, or disappointed and to celebrate all the good moments. Thanks Nico! Thanks to Krista Morley, Audrey Nisole,

Natalhie Campos Reales, Karine Caron and Rosine Pelletier for the dinners, laughs, long discussions, and for being good friends! Thanks to Christopher Clouthier for the discussion about science and life and for always making me laugh!

Thanks to all the other member of the Pelletier and the Keillor groups: Pierre-Yves De Wals (PY), Roberto Chica, Valerio Vinci, Claudio Gnaccarini, Natalia Kadnikova, Isabelle Roy, Julia Guy and Christophe Pardin. Thanks in particular to Nicolas Doucet, an extraordinary scientist with a deep love for knowledge, the ability of excel in everything he does and his natural gift of being a great pedagogue. Nicolas never hesistated to interrupt what he was doing to help or explain something to me. Thanks to Prof. Jeffrey Keillor, for being always very attentive, generous, and for being a great teacher.

Un ringraziamento speciale va ai miei genitori e a mio fratello Marco, per avermi continuamente incoraggiata nei miei progetti e per il loro amore incondizionato. Grazie di cuore anche ai miei nonni, Oreste e Ines, e ai miei zii, Rosa, Caludio e Mauro, per avere fatto razzia delle carte prepagate per chiamare il Nord America e per il loro affetto. Grazie anche a Sara, Maria, Cristina, Alessandra, Gonzalo, Andrea e Mattia, perche' hanno saputo dimostrarmi il loro affetto e la loro amicizia nonostante la distanza e le mie a volte troppo sintetiche e-mails.

Thanks to Maxime, my fantastic son, whose smiles, hugs and *'mama'* are worth more than any degree. Finally, a heartfelt thanks to Dominique, my husband, for his love, support and continuous encouragement, and without whom I probably would never had come to Quebec and all this would never had happened.

Chapter 1 - Introduction

Section 1.0 - Folate metabolism

Folic acid derivatives are essential coenzymes required by all living organisms in the *de novo* synthesis of thymidylate and purines, the building blocks for nucleic acid synthesis (**figure 1.1, 1.1a and 1.1b**) [1]. Thus, these cofactors have a crucial role during cell proliferation. Folate derivatives, in the form of a series of tetrahydrofolate (THF) compounds, act as cofactors in a number of one-carbon-transfer reactions within these biosyntheses, and they are also involved in homocysteine methylation and glycine and serine interconversion (**figure 1.1**) [1]. THF is obligatorily produced from 7,8-dihydrofolate (DHF) by the enzyme dihydrofolate reductase (DHFR) [2]. Enzymes depending on THF cofactors include thymidylate synthase (TS), glycinamide ribonucleotide formyl transferase (GARFT) and aminoimidazole carboxamide formyl transferase (AICARFT). TS uses the cofactor 5,10-methylene tetrahydrofolate to convert deoxyuridylate (dUMP) into thymidylate (dTMP)(**figure 1.1a**) [2]. GARFT and AICARFT add carbon 8 and 2, respectively to the ring structure of purine using N^{10}-formyl tetrahydrofolate as cofactor (**figure 1.1b**)[2].

Folates are mainly transported into cells by two energy-dependent carrier proteins: the reduced folate carrier (RFC) [3], which is bi-directional, and the folate binding protein (FBP) [4]. Intracellular concentration of folates is constantly maintained between 1 and 10 μM, compared to a plasma concentration of 10 to 30 nM [5]. This intracellular accumulation is mediated by polyglutamation. The enzyme folypolyglutamate synthase (FPGS) [1] adds 5 to 8 glutamate residues to the glutamate tail of folates *via* peptidic bonds. The enzyme γ-glutamyl hydrolase (GGH) [6], instead, removes terminal glutamate groups. Glutamation makes folates more polar and it can increase the affinity of folates for their target enzymes. The extent of polyglutamation of folates depends on their affinity for these two cytosolic enzymes.

Folate metabolism in cells is a dynamic process in which the levels of THF-cofactors and DHF vary with the intracellular activities. In resting cells (not in S-phase), DHFR activity is much higher than TS activity. This maintains cellular DHF at very low levels, in the range of the low nM [1, 7]. As the K_M^{DHF} for DHFR is < 75 nM [8], only a fraction of DHFR activity (< 5%) is sufficient to sustain normal rates of THF synthesis [1]. Inhibition of folate-dependent enzymes in actively proliferating cells leads to arrest of the synthesis of DNA precursors. Thus, these enzymes are major drug targets for the treatment of cancer diseases [5], as well as fungal [9, 10], microbial [11] and parasitic [12] infections that are dependent on cellular proliferation.

Section 1.1 - Dihyrofolate reductase

Dihydrofolate reductase (tetrahydrofolate: $NADP^+$ oxidoreductase; E.C.C. 1.5.1.3) is a cytosolic enzyme that catalyzes the NADPH-dependent reduction of 7,8-dihydrofolate (DHF) to 5,6,7,8-tetrahydrofolate (THF) in all living organisms (**figure 1.2A**) [1]. Vertebrate DHFRs also catalyse the reduction of folate (FOL) to DHF, at about one tenth the rate of DHF reduction (**figure 1.2A**) [1].

DHFR has attracted the attention of protein chemists and of molecular biologists as a model in many structural, kinetic and mutagenic studies due not only to its clinical relevance as a pharmacological target, but also to its small size (18-22 kDa), stability and relative ease of producing the recombinant enzyme. In fact, eukaryotic DHFRs are small monomeric proteins which does not require any post-translational modification and thus, can be easily expressed in heterologous bacterial hosts for ease of manipulation [13]. The human *dhfr* gene, for example, was cloned and expressed in *E. coli* in 1988 [14], and since then, extensive investigations of this enzyme have been performed.

Section 1.1.1 - Reaction mechanism

For the reduction of DHF to THF the hydride is transferred from the C4 of NADPH to the C6 of DHF, and this transfer is critically dependent on the distance between the two carbon atoms (optimal distance 2.6 Å) and the relative orientation of the NADPH nicotinamide ring and the DHF pteridine ring (**figure 1.2B**) [15]. Different studies [16-18] suggest that protonation of N5 in the transition state, which either

immediately precedes or is concerted with hydride transfer to the C6, promotes hydride transfer by delocalizing a positive charge to C6. Residue 30 is the catalytic active-site residue, which mediates, through intervening water molecules, the proton transfer component of the reduction [15, 19]. A similar mechanism has been proposed for the DHFR-dependent reduction of FOL to DHF, where protonation of N8 could be promoted by formation of a H-bond with the backbone carbonyl of Ile7, as observed in the crystal of the binary complex of human DHFR with 5-deazafolate, a tight-binding inhibitor of DHFR very similar to DHF [18].

Section 1.1.2 - Vertebrate and bacterial DHFRs: differences and similarities

Vertebrate DHFRs are highly homologous (72-89% sequence identities for DHFRs from chicken, mouse, bovine and human), but only ~25% identity is observed between animal and bacterial sequences or between different species of bacteria (**figure 1.3**) [20]. Despite the low sequence identity between bacterial and vertebrate DHFRs, structural analysis of DHFRs from different species has shown that the overall tertiary structures of these enzymes are very similar to one another (**figure 1.3**) [21, 22].

Notwithstanding the great structural similarity observed, this group of enzymes exhibits considerable species-to-species variability in sensitivity to different inhibitors [21]. *E. coli* DHFR (ecDHFR), for example, is 12000-fold more sensitive to the antifolate trimethoprim (TMP) than the human variant (hDHFR). Although active site residues are generally conserved, some differences exist and could partly explain this variability. Leu28 in *E. coli* DHFR, for example, which was reported to establish a major contact with the trimethoxybenzyl moiety of TMP [23], corresponds to Phe31 in hDHFR. However, mutation of Phe31 to Leu in hDHFR, did not increase TMP binding significantly, indicating that this residue was not the sole determinant of species selectivity of TMP [24]. Differences in active-site cavity were also reported to contribute to the observed differences in specificity [22, 25]. Despite extensive investigation, the structural basis for the various modes of binding in DHFR from different species still remains to be fully understood and it represents a crucial point for the design of species-

specific inhibitors [26]. Jordan Volpato, PhD student in the research group of Prof. Joelle Pelletier, has recently conducted a detailed review regarding this subject [27].

Section 1.1.3 - Human dihydrofolate reductase

Human DHFR (hDHFR) is a monomeric enzyme of 186 amino acids (21544 Da). The polypeptide backbone of hDHFR is folded into an eight-stranded twisted β-sheet, consisting of 7 parallel strands and one anti-parallel strand leading to the carboxyl terminus. Five α-helices and loops provide connectivity within the sheets (**figure 1.4**) [28]. Residues 21-26 (sequence DLPWPP) form two turns of a polyproline helix (left handed, typeII) (**figure 1.4**) [28].

Section 1.1.3.1 – Folate binding site

The structures of many complexes of hDHFR with cofactors, substrate or inhibitors have been determined both by X-ray diffraction methods [18, 22, 28, 29] and by NMR [30, 31]. Of the two substrates of hDHFR, only FOL has been crystallized in the binding cavity of the enzyme (in absence of the cofactor NADPH) (**figure 1.5A**) [18, 28]. FOL is a relatively stable molecule while DHF is readily oxidized to FOL, and therefore not suitable for protein co-cristallization [18]. The folate binding site is composed by residues in strands βA and βE, residues 61-70 and residues belonging to the left-handed polyproline helix and helices αB, αC [18].

The folate and folate-like molecules consist of polar pteridine and L-glutamate extremities, linked by a *p*-aminobenzoyl group (*p*-ABA) (**figure 1.7**). The active site of DHFR is a ~15 Å hydrophobic pocket in which the only polar side chain is the carbonyl of Glu30 [15]. The pteridine moiety of substrates and inhibitors binds nearly perpendicular to the benzoyl ring in the bottom of the hydrophobic pocket, with the benzoyl-glutamate side chain directed towards the surface of the protein. NADPH binds in an extended conformation with the reduced nicotinamide ring inserted into the active site pocket and the rest of the molecule along the surface of the protein. The nicotinamide ring is situated about 2.5 Å from the folate pteridine ring, with which it forms stacking interactions [18].

Table 1.1 lists the residues of hDHFR that directly interact with DHF. The 2-amino group, N3 and O4 of the pteridine moiety of folate interact specifically with residues Glu30, Thr136 and Trp24 by direct or water mediated H-bonds. Phe34 is within the van der Waals distance of the pteridine moiety. No specific interactions involve nitrogens N1, N5, N8 and N10 of folate. In DHF, which has a hydrogen atom attached to N8, a hydrogen bond between N8 and the carbonyl oxygen of Ile7 is likely to form, whereas an equivalent hydrogen bond to N8 of folate is likely to be formed only in the transition state [18].

The *p*-ABA moiety of folate is within van der Waals distance of the side chains of Phe31, Phe34, Ile60, Pro61 and Leu67. Moreover, the carbonyl oxygen of *p*-ABA forms a H-bond with the amide nitrogen of the Asn64 side chain [28].

The α-carboxylate portion of the glutamate fragment forms a salt bridge with the guanidinium of the conserved Arg70. Gln35 is in proximity to both the α-carboxylate and γ-carboxylate portions of DHF. The γ-carboxylate can form a H-bond mediated by a water molecule with the carbonyl oxygen of R28. However, this portion has a high B factor and the bond with R28 is not observed in all resolved structures, probably indicating that it is weak [18].

Section 1.2 – Antifolates

Antifolates constitute a large family of compounds which compete with folate derivatives for the binding to folate-dependent enzymes involved in nucleotide biosynthesis. Due to the role of their target enzymes in cellular proliferation, antifolates are used for the treatment of a broad range of proliferative diseases. Treatment of bacterial and parasitic infection is based on species-selectivities of some of these compounds. Trimethoprim (TMP), for example, is selective towards bacterial DHFRs [26] while pyrimethamine (PYR) towards malaria parasite DHFRs [26].

The importance of DHFR in bacterial, parasitic and cancer chemotherapy arises from its function in maintaining the pool of THF. Inhibition of DHFR leads to arrest of DHF recycling, and thus causes inhibition of cell growth and eventually cell death. It

should be noted that THF is regenerated in most one-carbon transfer reactions, with the exception of TS-catalyzed dTMP synthesis (**figure 1.1**). Therefore, in cells not actively synthesizing thymidylate and DNA, inhibition of DHFR does not result in any particular effect.

In 1947, pteroylaspartic acid, an antagonist of pteroyl glutamic acid (folic acid), was proved to interfere with folic acid metabolism and the normal growth of cells in *in vivo* test with both chicken and rats [32], and suggested that folic acid antagonists might be of value in patients with rapidly growing malignant disease. In 1948 the antifolate aminopterin (**figure 1.7**) was shown to be effective in children affected by acute leukemia at the terminal stage of the disease, marking the advent of cancer chemotherapy [33]. Soon after, aminopterin was replaced by the more effective and less toxic amethopterin (later named methotrexate (MTX), **figure 1.7**), which was approved by FDA in 1953. Since then, MTX has been the major antifolate used in cancer therapy [34].

Both aminopterin and MTX are strong competitive inhibitors of DHFR (for hDHFR, K_i aminopterin = 2 pM [35] and K_i MTX = 3.4 pM [13]).

Section 1.2.1 - Methotrexate

Methotrexate (MTX; 8-amino,10-methyl-pteryolglutamic acid) is a slow, tight binding, reversible inhibitor of the human enzyme dihydrofolate reductase (hDHFR) [13, 36]. The inhibition constant of hDHFR for MTX is of 3.4 pM [13, 36, 37]. MTX also inhibits human GARFT and human AICARFT, but the K_i values for the pentaglutamate forms of these enzymes (potency of DHFR inhibition depends on the polyglutamation status of the molecules) are of 2500 nM and 56 nM, respectively [5]. These kinetic data suggest that the main intracellular target is DHFR [5].

MTX shows high affinity for a wide range of DHFRs from different species (bacterial, parasitic, vertebrate). Due to its lack of specificity, it is mostly applied for the treatment of human proliferative diseases, both malignant (carcinoma, metastatic breast cancer, bladder cancer, lymphoma)[5] and not-malignant (rheumatoid arthritis [38], psoriasis [39] and graft versus host disease [40]). Despite the continuous discovery of

newer drugs, MTX often remains a component of the newer combination treatments [5, 34].

The kinetics of MTX binding to hDHFR was described extensively by Appleman *et al.* [13]. MTX binds rapidly and tightly (k_{on} = 1.0 x 10^{-8} M^{-1} s^{-1}; k_{off} < 1 s^{-1}; k_{off}/k_{on} = 210 pM), independently of the presence or absence of NADPH already bound to the enzyme [13]. The initial association of MTX to hDHFR is followed by some kind of conformational change of the complex, which increases the overall binding of 60-fold, leading to a K_i of 3.4 pM [13]. The authors also demonstrated that MTX polyglutamation, differently from what happens for TS, GARFT and AICARFT [5], does not affect binding to hDHFR. Like folate, MTX is transported into cells by both RFC and FBP [5, 41, 42].

Binding of MTX to hDHFR has been studied using X-ray crystallography [22, 43] (**table 1.1 and figure 1.5B)**. Despite its chemical and steric similarity with 4-oxo-folates (FOL, DHF, THF; **figure 1.7**), MTX binds in the active site with its pteridine moiety flipped 180° around the C_6-C_9 bond, relative to folate (**figure 1.6**). The main cause for this flip is probably the presence of the 4-amino group instead of a 4-oxo group. Consequently, active-site residues form different contacts with the two molecules, and binding of the inhibitor MTX is 2000-fold stronger than binding of the substrate DHF.

Table 1.1 lists the residues that directly interact with DHF and/or MTX in the hDHFR ternary complex. The hydrogen bonding network involving structural water, the conserved active site residues Thr136, Glu30, Trp24 and the pteridine moiety of the bound folate is maintained, but in the case of MTX it involves the N1 and N8 nitrogen and the 2-amino group [22]. The 4-amino group of MTX interacts with residues Ile7, Val115 and Tyr121 and with NADPH [22]. The backbone carbonyl groups of both residue 7 and 115 are within H-bonding distance with the 4-amino group of MTX [44]. Moreover, the side chains of these two residues are likely to form hydrophobic interactions with the inhibitor's pteridine moiety [44]. Residue Phe34 is also within the van der Waals distance with the pteridine moiety.[45]

As in the case of folate, the *p*-ABA moiety of MTX forms van der Waals and hydrophobic interactions with the side chains of Phe31, Phe34, Ile60, Pro61 and Leu67

[22]. The carbonyl oxygen of *p*-ABA also forms a H-bond with the amide nitrogen of the Asn64 side chain [22].

The α-carboxylate portion of the glutamate moiety makes close contacts with the side chains of Arg70 (charge interaction) and Gln35. When the inhibitor does not occupy the active site, a subdomain shift brings Arg70 into contact with Gln35 [46].

Section 1.2.1.1 - Mechanism of resistance to MTX

Some type of neoplastic diseases are intrinsically resistant to MTX whereas those that are responsive can develop resistance following repeated treatments (acquired resistance) [42]. MTX was brought into clinical use and became an established component of many clinical regimens right after the demonstration of its effectiveness in the late 1940s [33, 47], when its mechanism of action was not clearly understood. Between the end of the 1970s and the beginning of the 1990s, a better understanding of metabolism, transport and kinetics of binding of MTX to DHFR helped to elucidate the basis of MTX resistance. Different mechanisms of acquired resistance that impair efficiency of MTX-treatment have been described [5, 41, 42]. Amplification of the *dhfr* gene [48] or DHFR over-expression [49] were frequently observed. Moreover, mammalian DHFR expression is regulated by binding of its own mRNA at the active site [50]. In fact, hDHFR binds specifically to its own mRNA and this interaction represents a mechanism of inhibition of hDHFR mRNA translation [50]. Binding of MTX dislodges the DHFR mRNA, rendering it available for translation and therefore increasing protein expression. The higher the level of DHFR, the higher is the level of free-drug necessary to suppress THF regeneration. The free drug level is a critical parameter in the interactions between MTX and both hDHFR and folylpolyglutamate synthetase (FPGS; see section 1.0 for a detailed description of the carrier proteins and enzymes involved in folate metabolism). Transport mechanisms regulate the influx and efflux of drugs across the cell membrane, and the net effect of these processes determines the level of free MTX achieved intracellularly. Alteration in the expression or mutations of the reduced folate carrier protein (RFC) [51] and of FPGS [52] determine reduction of cellular uptake or allow more rapid efflux of MTX [41], respectively. MTX polyglutamates accumulate at different rates in a variety of tumor cells and ultimately become the predominant species

and the form of antifolate bound to hDHFR, and this is an important determinant of the pharmacologic activity of this drug. Impaired polyglutamation can therefore be a determinant cause of resistance together with the other possible resistance mechanisms.

The above-mentioned MTX resistance mechanisms have all been observed either in tumours isolated from patients that relapsed during or following MTX-treatment, and *ex vivo* (by exposing cells isolated from patients to MTX *in vitro*) [48, 53-55]. An additional resistance mechanism is the occurrence of mutations in the *dhfr* gene, resulting in expression of hDHFR variants with reduced affinity for MTX. This mechanism of resistance was first observed in *ex vivo* studies, but it has never been identified as a cause of resistance in tumours isolated from patients who relapsed following MTX treatment. Even if it has been long proposed that mutations that confer resistance to MTX could occur in tumural cell of patients receiving a MTX-based therapy, and therefore contributing to their clinical relapse, a study performed by Spencer *et al.* described why this is unlikely to happen [56]. Briefly, the authors demonstrated that different mutations that occurred spontaneously and conferred MTX-resistance in *ex vivo* experiments, conferred only modest protection to MTX when transduced into cells using a retroviral vector. Moreover, accumulation of mutations that increase total MTX resistance seems unlikely because other mechanisms of resistance, as discussed above, prevail. Because it does not occur clinically, hDHFR MTX-resistant mutants represent a promising tool for gene theraphy, as it will be discussed in paragraph 1.2.1.3. Moreover, a second possible application would involve the use of these hDHFR MTX-resistant variants as selection markers for gene transfer into eukaryotic cells [57, 58].

Section 1.2.1.2 - Mutations of hDHFR that confer resistance to MTX

MTX-resistant mutants of DHFR from mammalian sources have been identified either *in vivo*, *ex vivo* (by exposing mammalian cells to MTX *in vitro*) or *in vitro* (created by mutagenesis).

The MTX-resistant DHFR G15W was the only variant isolated *in vivo*, from a MTX-resistant subline of murine leukemic cells implanted in mice. Subsequent *in vitro* characterization of both the mouse and the human G15W variants, demonstrated that

although effectively resistant (200-fold increase in K_i^{MTX} for mouse DHFR), the mutant was too unstable to be the primary cause of the observed resistance [59].

The first *ex vivo* studies reported in literature aimed to better understand the causes of emergence of MTX resistance. Mutation L22R [60] and F31W [61] were identified from MTX-resistant mouse cells, F31S from both hamster [62] and human [63] cells and F31W from both hamster [62] and murine [61] cells. In parallel, *in vitro* mutagenesis studies on *E. coli*, mouse and human DHFRs allowed characterization of the above-mentioned variants and identification of further mutations that confer resistance to MTX. All mutations characterized showed decreased affinity for MTX but also loss of catalytic activity, generally due to reduced DHF affinity. This result is readily rationalized by the fact that MTX and DHF make similar contacts with the enzyme, as illustrated in **table 1.1** and **figure 1.5**.

Mutations of hDHFR that confer resistance to MTX and their kinetics and inhibition parameters are listed in **table 1.2**. Leu22 is a highly-conserved active site residue that establishes van der Waals contacts with the pterin ring of bound MTX and NADPH [35]. Variants substituted with Phe, Arg, Trp or Tyr at position 22 are all MTX-resistant and all exhibit a greater decrease in affinity for MTX than for DHF (**table 1.2**). Mutant L22F is the least resistant, presenting a moderate resistance and maintaining catalytic efficiency in the range of the native enzyme [43]. Decreased affinity for these mutants was associated with increased k_{off}, and this may be due both to a decreased affinity between MTX and the active site or/and to an increased diffusion of MTX from the active site. When the crystal structures of hHDFR mutants L22R [43] and L22Y [43] in the ternary complexes with NADPH and MTX were compared with the wild-type hDHFR·NADPH·MTX ternary complex structure [64], a rational common explanation was difficult to postulate. In fact, while Arg22 appeared to have lost all close contacts with MTX by adopting a low probability conformation, Tyr22 showed the same contacts with MTX as the native Leu residue. Therefore, while in the case of L22R a loss of binding energy could partly explain the loss of affinity for MTX, such explanation was not valid in the case of the L22Y variant [43].

Phe31 and Phe34 belong to α-helix B and they both interact by van der Waals interactions with the pteridine extremity and the *p*-ABA moiety of MTX and DHF [22]. Replacements of residue Phe31 with the small amino acids Ala, Gly and Ser gave rise to moderately MTX-resistant mutants (70 to100-fold increase in K_i^{MTX}), with little loss of catalytic activity and DHF binding comparable to the native enzyme (**table 1.2**) [65]. The authors proposed that decreased MTX binding was due to the loss of interaction between the side chain of residue 31 and bound the MTX. Moreover, the absence of isomerisation of the initial complex, which increases the MTX binding of about 60-fold in the native enzyme, was proposed as further potential cause for the increase in K_i^{MTX} and for a little variation of K_M^{DHF}. The authors proposed that isomerisation of the enzyme·MTX·NADPH complex could depend on the motion of residue 31 [65], which occupies two alternative conformations in one crystal structure of folate complexed with hDHFR [18]. When a small residue replaces the bulky Phe, this conformational change does not occur and further stabilization of the complex cannot take place. Mutations at position 31 with the more bulky and hydrophobic amino acids Leu, Val and Thr did not significantly affect either catalysis or inhibitor binding [65]. Finally, mutation F31R conferred the highest degree of MTX-resistance at this position, again with a small effect on DHF binding, but with a 10-fold decrease in reactivity [57].

Residue Phe34 is strictly conserved in DHFRs from all species. Nakano *et al.* [45] mutated residue 34 to Ala, Ile, Ser, Thr and Val and observed an important increase of both the ternary K_D^{MTX} and K_D^{DHF}. Mutation at residue 34 mainly increased the K_D^{MTX} by decreasing k_{on} and largely increasing k_{off}. In the case of F34T the effect on K_D^{DHF} was even more significant than the effect on K_D^{MTX}. The effect on reactivity was minimal in all cases. However, the effect of the described mutations on DHF binding indicates that position 34 in human DHFRs is likely essential for substrate binding, and therefore less tolerant to mutations.

The backbone carbonyl of Ile7 is within H-bonding distance of the 4-amino group of the bound MTX and its side chain is likely to form hydrophobic interactions with the pteridine ring of the inhibitor [22]. Since the H-bonding interaction is not observed in the binary complex structure with bound FOL, mutations that disrupt this bond could potentially reduce the affinity to MTX while maintaining a native-like binding to the

substrate. However, the resolution of the structure of the binary wild-type hDHFR·5-deazafolate complex indicates that it is possible that the N8 of DHF is protonated, contrary to folate, and that it can form an H-bond with the backbone carbonyl of Ile7. If this hypothesis is valid, mutation at residue 7 could also significantly affect the DHF binding. The only mutation described for hDHFR at this position is I7F. This mutation yielded a very unstable enzyme with a 7000-fold increase in K_i^{MTX} and a 370-fold drop in the DHF binding, suggesting that this highly conserved residue plays a role in both substrate and inhibitor recognition [57]. The Val115 backbone carbonyl also forms an H-bond with bound MTX [22], and this interaction was never reported with either FOL [28] or 5-deazafolate [18]. Thillet *et al.* created mutant V115P of murine DHFR to disrupt the H-bonding between V115 and MTX. The mutation gave rise to a very unstable enzyme with no significant decrease in the MTX binding.[44]

Arg70 is a highly conserved residue that forms a salt bridge with the α-carboxylate portion of the glutamate of both DHF and MTX. Mutation R70K generated a stable enzyme with an increase of 4 orders of magnitude of the binary K_D^{MTX} (with respect to WT K_i^{MTX}) [46], and a 100-fold decrease in catalytic efficiency, due to a combined effect on both k_{cat} and K_M^{DHF}. The authors proposed that the observed effect was due to the loss of protonation of Lys70. In fact, its pK_a was lowered due to the hydrophobic environment in which the amino acid was buried. This result suggests that the loss of the salt-bridge with the glutamate moiety of MTX has an effect on both the ligand and the inhibitor binding. However, it is interesting to observe that the glutamate moiety does not appear to be essential to have inhibition. In fact, the antifolate trimetrexate (TMTX, **figure 1.7**), which does not possess the glutamate tail, also binds to hDHFR with a strong affinity (K_i = 13 pM) [35].

Finally, highly MTX-resistant hDHFRs were obtained by combining the L22 and F31 point mutants, which individually conferred a moderate MTX-resistance [66]. All double mutants tested had a higher K_i^{MTX} (from 800 to 44000-fold) and only a slightly reduced (~5-fold) K_M^{DHF} than the native enzyme [66]. Both double mutants L22F-F31G and L22F-F31S showed a synergistic effect on the MTX binding [66].

1.2.1.3 - MTX cytotoxictiy and gene therapy

The therapeutic utility of MTX is impaired not only by the emergence of resistance but also by its indiscriminate cytotoxicity towards normal proliferative tissues, such as the gastrointestinal tract and the bone marrow (myelosuppression). Despite its toxicity, the safety and cost-effectiveness of MTX guarantees that it will continue to be administered in cancer therapy world-wide for the foreseeable future [5].

Toxicity can be partially managed clinically by modification of dosage and scheduling [5]. However, a more effective and durable approach could be to render normal tissues MTX-resistant by introducing a drug-resistant DHFR gene [57, 58]. The principle of protection of cells by means of a transgene is also known under the name of gene therapy. To overcome MTX-induced myelosuppression, this would involve transplantation of bone marrow with haematopoietic stem cell (HSCs; progenitor cells) previously transduced with retro-viruses introducing a resistant DHFR variant [67].

MTX-resistant mammalian DHFRs are potential candidates for gene therapy and in fact, they have already been tested for MTX-protection both in murine and human cells lines [68-72]. Despite the fact that different problems (e.g. low efficiency of gene transfer, low long term expression, engraftment failure of *ex-vivo* manipulated cells, silencing of the transgene) have to be addressed before this approach becomes effective in clinical trials, the potential of this application remain undoubted [67].

Section 1.2.2 - Other antifolates

MTX is the principal antifolate in use, but resistance and toxicity are current important limitations of a treatment with this drug [5, 41]. Attempts to improve the effectiveness and to overcome the side-effects related to the MTX treatment have promoted a search for alternative antifolates for the last 60 years, highlighting the importance of this area of investigation [73-76]. This research has led to the synthesis of inhibitors of different folate-requiring enzymes, inhibitors with multiple intracellular targets and inhibitors with different chemical and pharmacological features [74]. Pemetrexed (LY231514; **figure 1.7**), for example, inhibits four different folate-depending enzymes [77, 78] while trimetrexate (**figure 1.7**), being lipophilic and lacking the

glutamate tail portion, can circumvent the resistance associated with mutations of FPGS and with mutations of the folate transporters RFC and FBP [5].

This section will focus on antifolates, different from MTX, which will be discussed in this thesis. The structures of all the molecules discussed are illustrated in **figure 1.7**.

Trimethoprim (TMP; **figure 1.7),** a 2,4-diamino-pyrimidine ring connected with a trimethoxybenzyl moiety, is clinically used as an antibacterial drug [11]. TMP behaves as a classical competitive inhibitor of both bacterial and human DHFR [13]. However, it binds very tightly to DHFR from bacterial sources (K_i for ecDHFR = 80 pM) [13], but weakly to hDHFR (K_D ternary complex = 0.5 μM; Ki = 0.96 ± 0.3 μM) [13], which is the basis for its bacterial selectivity. Therefore, inhibition of hHDFR by TMP is 280000-fold weaker than the binding of MTX.

Trimetrexate (TMTX; **figure 1.7**) is a potent inhibitor of hDHFR (K_i = 13 pM) [35]. TMTX has structural and pharmacological properties different from MTX. First, it is lipophilic, and thus enters cells via passive or facilitated diffusion, without any need for folate transporter such as RFC and FBP. Then, it does not possess a glutamate tail and therefore it is not a substrate for FPGS. Unfortunately, this very promising antifolate failed phase II clinical trials for the treatment of different types of cancers, because it did not confer any real advantage with respect to the established treatments [79, 80]. From a structural point of view, TMTX remains interesting because, despite missing the glutamate tail, it binds very tightly to hDHFR.

Pemetrexed (PMTX or LY231514; **figure 1.7**) [77] is a multi-target antifolate which was approved by the FDA in 2004 and it is used for the treatment of lung cancer and of some other types of solid cancers (bladder, breast, gastric and pancreatic cancer) [78]. Its main target is TS (K_i = 1.3 nM), but it also inhibits DHFR (K_i = 7.2 nM), GARFT (K_i = 65 nM) and AICARFT (K_i = 265 nM) [81]. Targeting multiple enzymes involved in purine and thymidylate biosynthesis offers a lower risk of resistance development and a more limited toxicity profile than other approaches [5]. PMTX contains a 6-5 ring-fused pyrrolo[2,3-*d*]pyrimidine system. Using molecular modeling, Gangjee *et al*. [73] suggested that PMTX binds to DHFR in the same orientation of FOL.

This hypothesis is supported by the observation that 5-deazafolate (**figure 1.7**)[18], which is a 4-oxo pteridine system structurally similar to both FOL and PMTX, binds in the same orientation as FOL. The only difference with folate is the replacement of the pteridine ring's N5 with a carbon, which leads to a decrease of the polarity of this portion.

Section 1.3 – Drug discovery and structure-activity relationship analysis

To effectively prevent substrate binding and turnover efficient enzyme inhibitors must bind their target with both high affinity and high selectivity. Drug design consists in the tailored-synthesis of potential inhibitors based on detailed structural and functional information on the biological target of interest. Dorzolamide, an inhibitor of carbonic anhydrase, was approved in 1995 and it is one of the first examples of a structure-based drug design leading to an approved drug [82]. Drug discovery by high-throughput compound synthesis and screening is very expensive [76, 83, 84]. Therefore, to reduce costs and to increase efficiency, complementary approaches such structure-based computer assisted techniques (homology modeling [85], docking [86] and molecular dynamics simulations [87]) have been developed. Homology modeling, for example, allows building model structures for proteins by extrapolation of structural data from related proteins with homologous or similar sequences. Docking procedures allow fast screening of large compound libraries by evaluating the binding affinity to the target *in silico*. Molecular dynamics simulations, instead, can be used to model conformational changes upon binding. All these methods rely on structure-function information, and this is why structure-activity relationship (SAR) study is crucial for efficient drug discovery.

Despite the large amount of information about drug-target interactions and the continuously evolving informatics tools to support this approach, the design of new enzyme inhibitors with a high level of confidence is still a challenge. This is mainly due to the complexity of active sites, where small details can make a difference. However, the more we know about the ligand-binding cavity of a target enzyme, the further we can

improve structure-based approaches that currently drive the drug discovery process to identify new specific binders [88-91].

Section 1.4 – Presentation of the research project

Our principal goal is to better understand the molecular determinants of enzyme-ligand binding. In fact, notwithstanding the continuous increase in the number of ligand-bound enzyme structures being resolved, crystal structures provide limited information relative to the binding process. Even when high-resolution structures of a drug-bound target are available, it is challenging to predict effects of mutations on the binding, just as it is difficult to predict how the modification of the drug will alter binding. We generally possess limited information relative to the contribution of specific contacts to the overall binding efficiency and selectivity. Faced with an enormous number of potential drug and target modifications, we must continue to develop approaches to efficiently screen through potential interactions in order to focus on the most interesting ones.

Mutants with altered drug-binding properties represent a rich source of information about binding. We specifically focused on drug-resistance in the enzyme hDHFR, as a system to investigate the relation between structural variations of the target protein (using mutants) and/or of the drug (using different compounds), and their effect on binding. We propose to study the role of individual and combinatorial mutations of hDHFR on substrate binding and on antifolate sensitivity using directed evolution combined with structural and kinetic analysis.

Drug-resistant mutants of hDHFR from different species were previously characterized in order to elucidate the catalytic mechanism [19] and the role of some active site residues in structure maintenance [46] and in binding [65, 66, 92] (see also section 1.3.1.2). However, data available is limited and does not explore exhaustively the binding-site to systematically study the hDHFR structure-function relationship. We will consider different mutations at each targeted position (by saturation mutagenesis) and simultaneous mutations at different sites (by combinatorial mutagenesis). Binding properties are related to the specific environment and are not necessarily the sum of

single properties. In fact, upon simultaneous mutation, residues may behave either in an independent or in an interdependent fashion toward the protein function [93]. Moreover, the combination of mutations can yield additive or partially additive effects, multiplicative effects (synergy) or antagonist effects on the enzyme activity [66, 94, 95]. The elucidation of these combinatorial effects and the deconvolution of the single contributions to the total effect will give us information about the binding. The questions we want to answer are the following. How do mutations, individual and combinatorial, affect the energy of binding? Which residues are important for binding of all compounds and which ones are responsible for ligand discrimination? How important is a hydrophobic contact for the overall binding? How significant are distal effect on binding?

Human DHFR has been chosen due to its clinical relevance and to the fact that it is an ideal model system to verify the advantages of the proposed strategy. The findings of this study will increase our understanding of enzyme-inhibitor interactions and will provide a useful tool for the discovery of new and more efficient folate-analog inhibitors of hDHFR. Moreover, hDHFRs with an elevated resistance phenotype are interesting candidates for protection of healthy cells from the toxic side effects of MTX treatment using gene therapy (see section 1.2.1.3). To this aim, PhD student Jordan Volpato has devised a strategy for evaluating the protection efficiency of MTX-resistant hDHFR mutants in mammalian cells; this topic will not be covered in this M.Sc. thesis.

The first specific goal described in this M.Sc. thesis was to develop an efficient screening strategy to identify active and antifolate-resistant mutants of hDHFR from large libraries of mutants. Identification of the variants of interest from libraries of mutants represents the crucial step for success of the directed evolution approach and it is an obligatory step to identify relevant candidates for structure-activity relationship analysis.

The second specific goal was to participate in the development of a combined structural and kinetic strategy to analyse in detail the effect of mutations on binding.

Section 1.5 – Presentation of the experimental approach

1.5.1 - Directed evolution

Directed evolution is an efficient way to engineer the properties of proteins and to identify novel enzymes with tailor-made properties [96]. The approach mimics the principles of Darwinian evolution, but on a 'laboratory' scale-time, and it consists of two main steps: generation of genetic diversity (library creation) and selection/screening for the desired property (specificity, activity, catalytic efficiency, sensitivity to a drug etc.).

Creation of up to 10^{10} protein variants at the DNA level is presently an easy task, due to the advances in the recombinant protein engineering and the power of PCR techniques. Genetic diversity can be introduced by random mutagenesis (error prone-PCR) [97], or by recombination (DNA shuffling) [98]. These techniques do not require an in-depth understanding of structure/function relationships. However, in the cases where functional or structural information exists, it can be advantageous to apply a semi-random approach like saturation mutagenesis at specific residues [99, 100]. In this approach, directed evolution and rational design are combined in order to concentrate mutations where they offer a higher probability to be effective [100]. Variation and combination of these mutagenesis techniques have been extensively described in literature [100-103].

Once DNA libraries encoding the enzyme variants have been created, the hard task is to identify the variant(s) presenting the desired new property among all the possibilities available. This means that the likelihood of obtaining a variant of interest is limited by the effectiveness and the power of the selection/screening method available to detect it. When the enzymatic property of interest is essential for cell survival, it is possible to establish a selection strategy based on this feature [104]. Selection for survival is an ideal choice when it is applicable, its limit of detection being only the transformation efficiency for the type of cell utilized in the study (~10^8/μg DNA, maximum ~10^{10} for certain *E. coli* strains). Alternatively, screening methods could be applied. While different high-throughput screening (HTS) methods which can detect up to 10^{15} variants are available to detect binding interactions (two-hybrid systems [105],

phage-display [106], ribosome display [107], mRNA display [108], flow cytometry [109]), HTS for enzymatic activity is often harder to perform. The most commonly used screening methods are based on the assay of isolated bacterial cells on agar or in microtiter plates for the detection of coloured or fluorescent molecules, which are produced in a chemical reaction by means of the activity of interest, the major limit being the availability of robotic platforms to maximize screening capacity.

1.5.1.1 – Mutagenesis of hDHFR

First, active-site residues to be mutated were identified on the basis of crystallographic and/or functional data available for hDHFR. Since we are interested in binding at the folate–binding site, target amino acids were all chosen within or close to that area, were they were more likely to be effective [110]. Target residues were identified before my arrival in the laboratory by PhD student Jordan Volpato and they cover all the folate-binding site (**figure 1.8**). Among these, five residues have been the main target of the investigation presented in this thesis: Ile7, Gly15, Trp24, Arg70 and Val115 (**figure 1.8, in yellow)**. Each of the 5 targeted residues was randomized by saturation mutagenesis using NNS codon degeneracy (N: adenine/cytosine/guanine/thymine; S: cytosine/guanine). This means that at each position, all 20 amino acids were allowed.

1.5.1.2 - Screening for the properties of interest: activity and antifolate resistance

Previously, PhD student Jordan Volpato developed an efficient bacterial complementation approach to select MTX-resistant clones (described in chapter 2). Bacterial selection has the advantage of being very high-throughput, but unfortunately bacterial survival under selective conditions is not a direct read-out of catalytic activity and selected variants are not necessarily amenable to detailed characterization (where ‘amenable to’ refers to expression level, stability, solubility and/or activity) [111]. Since the subsequent steps of characterization are laborious and require the use of expensive compounds (NADPH and MTX), an improvement of the screening step was required. Therefore, a further step of screening using a plate reader-based activity assay in presence

of high concentrations of inhibitor was developed to identify only the best hits from bacterial selection, as it is described in chapter 3.

Moreover, in order to investigate discrimination in ligand binding, the scope of the project was extended by developing a screening strategy for further phenotypes of interest: activity (efficient binding of DHF upon mutation) and resistance/sensitivity to other antifolates (TMP and PMTX).

A protocol to quantify activity (k_{cat}) and MTX resistance (IC_{50}^{MTX}) directly from cell lysates in microtiter plates was also developed.

1.5.2 – Structure-function relationship analysis

1.5.2.1 – Kinetic characterization of the mutants: determination of kinetic inhibition constants

Positive hits from second-tier screening were over-expressed and purified in order to determine more precisely the kinetic and inhibition parameters *in vitro*. The kinetic parameters K_M and k_{cat} describe productive binding of the mutants for the substrate DHF and the reaction rate of reduction of DHF to THF, respectively. The inhibition constant K_i describes productive binding of a competitive inhibitor to the mutants' active-sites. The value obtained for these parameters were correlated to the different mutations for structure-activity relationship analysis.

We have also begun SAR with MTX by investigating the binding of its constituent fragments: DAP (2,4-diamino-6-(hydroxymethyl)pteridine), DAMPA (4-[N-(2,4-diamino-6-pteridinylmethyl)-N-methylamino]benzoic acid) and *p*-ABA-Glu (*para*-aminobenzoic acid-L-glutamate) to relevant MTX-resistant variants identified in our laboratory (**figure 1.7**; chapter 4).

1.5.2.2 – Structural characterization of the mutants by computer-based molecular modeling

As it is impossible to envisage resolving the structure of all the resistant variants identified, computer-based molecular modeling approaches were considered as tools for structural characterization.

First, energy minimization was used to compare the predicted structure of one novel identified MTX-resistant mutant to the crystal structure of the native enzyme complexed with MTX (chapter 2).

Then, docking was evaluated as a tool to mimic DHF and inhibitor binding in the active-site pocket of the native enzyme. Advantages and limits of this technique for SAR analysis will be discussed in chapter 5.

Table 1.1. Active-site interactions between hDHFR and folate or methotrexate

	Folate (1DHF.PDB)[28]		Methotrexate (1U72.PDB)[22]	
Dihydrofolate or methotrexate component	**hDHFR residue**	**Type of interaction**	**hDHFR residue**	**Type of interaction**
Pteridine ring	I7	Backbone carbonyl: hypothesized H-bond with N8 DHF (not observed with FOL in 1DHF.PDB structure). Side-chain: hydrophobic	I7	Backbone carbonyl: H-bond with 4-amino group. Side-chain: hydrophobic
			V115	
			T121	Side chain: H-bond with 4-amino group
			L22	
	F31	Van der Waals/hydrophobic	F31	Van der Waals/hydrophobic
	F34		F34	
	W24	H-bonding network involving structural waters, N3, O4 and 2-amino group	W24	H-bonding network involving structural water 216, N1, N8 and 2-amino group
	E30		E30	
	T136		T136	
N_{10}-methyl-*p*-ABA	F31	Van der Waals/hydrophobic	F31	Van der Waals/hydrophobic
	F34		F34	
	I60		I60	
	P61		P61	
	L67		L67	
	N64	H-bond to *p*-ABA carbonyl oxygen	N64	Side chain: H-bond to *p*-ABA carbonyl oxygen
L-glutamate	R28	Carbonyl backbone: H-bonding network between H_2O^{410} and γ-COOH FOL (rarely observed)	H_2O^{198}	H-bonding network between carbonyl backbone N64, backbone NH, K68, α-COOH MTX
	Q35	In proximity to both α– and γ–COOH FOL	Q35	In proximity to both α– and γ–COOH MTX
	R70	Salt-bridge with α–COOH FOL	R70	Salt-bridge with α–COOH MTX

Table 1.2. Mutations providing MTX-resistance in hDHFR

hDHFR variant		K_M^{DHF} (μM)	Ratio K_M mut/ K_M WT	k_{cat} (s^{-1})	k_{cat}/K_M ($\mu M^{-1}s^{-1}$)	K_i^{MTX} (nM)	Ratio K_i mut/ K_i WT
Native		≤0.075	1	10	92	0.034	1
Position 7	I7F [57]	20.5	270	5	0.25	24.6	7200
Position 15	G15W [59]	6.2	80	3.2	0.5	2.1	600
Position 22	L22F [43]	3.9	50	23.8	6.1	0.5	150
	L22R [43]	1.6	20	0.045	0.03	4.6	1300
	L22W [43]	0.4	5	4.2	10	4.3	1300
	L22Y [43]	0.5	5	6.1	12	11	3200
Position 31	F31A [65]	0.5	5	13.9	30	0.27	80
	F31G [65]	0.4	5	11.3	26	0.35	100
	F31S [65]	0.4	5	7.0	16	0.24	70
	F31R [57]	0.6	10	0.9	1.5	7.2	2100
Position 34	F34A [45]	36 [a]	480	8.4 [c]	0.2 [b]	34 [d]	10000
	F34I [45]	24 [a]	320	13.7 [c]	0.6 [b]	13 [d]	3800
	F34S [45]	350 [a]	4600	6.0 [c]	0.02 [b]	210 [d]	60000
	F34T [45]	300 [a]	4000	3.3 [c]	0.1 [b]	9.6 [d]	2800
	F34V [45]	63 [a]	800	30.7 [c]	0.5 [b]	10	3000
Position 70	R70K [46]	0.5	5	1.75	3.7	0.46 [e]	13
Double mutants	L22F/F31G [66]	0.4	5	1.3	3.3	29	850
	L22F/F31S [66]	0.4	5	1.6	3.6	26	7600
	L22Y/F31G [66]	0.3	5	0.5	1.4	150	44000
	L22Y/F31S [66]	0.3	5	1.3	3.8	42	12000

[a] Ternary K_D^{DHF} values. The K_M^{DHF} could not been determined cause of substrate inhibition. Since the rate of the chemical reaction is much slower than the rate of subsequent dissociation of THF, Nakano *et al.* used ternary K_D^{DHF} values as an approximation of K_M^{DHF} [45].

[b] Derived from plots of rate versus DHF concentration by least-square fit to the equation for substrate inhibition by Nakano *et al.*[45].

[c] Calculated from k_{cat}/K_M and K_M^{DHF}, using the approximation described in [a] and [b][45].

[d] Ternary K_D^{DHF} values [45].

[e] K_i^{MTX} calculated from data in figure 5a of Thompson and Freisheim (1991) [46].

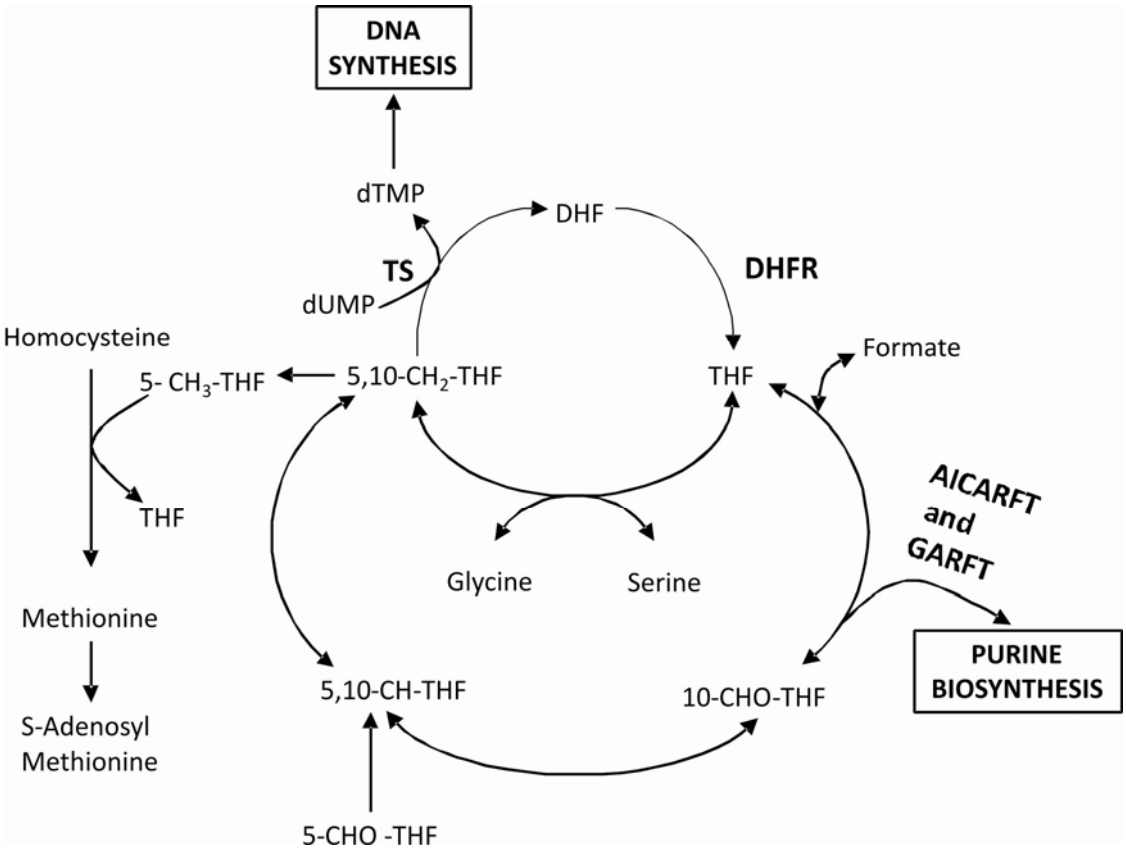

Figure 1.1. Folate–dependent metabolic reactions. The abbreviation are: DHFR, dihydrofolate reductase; TS, thymidylate synthase; GARFT, glycinamide ribonucleotide formyl transferase; AICARFT, aminoimidazole carboxamide formyl transferase; DHF, dihydrofolate; THF, tetrahydrofolate; 5-CH_3-THF, 5-methyl tetrahydrofolate; 5,10-CH_2-THF, 5,10-methylene tetrahydrofolate; 5,10-CH-THF, 5,10-methenyl tetrahydrofolate; 5-CHO-THF and 10-CHO-THF, 5-formyl- and 10 formyl tetrahydrofolate, respectively. Image was adapted from Figure 1 in Zhao *et al.* 2003 [41].

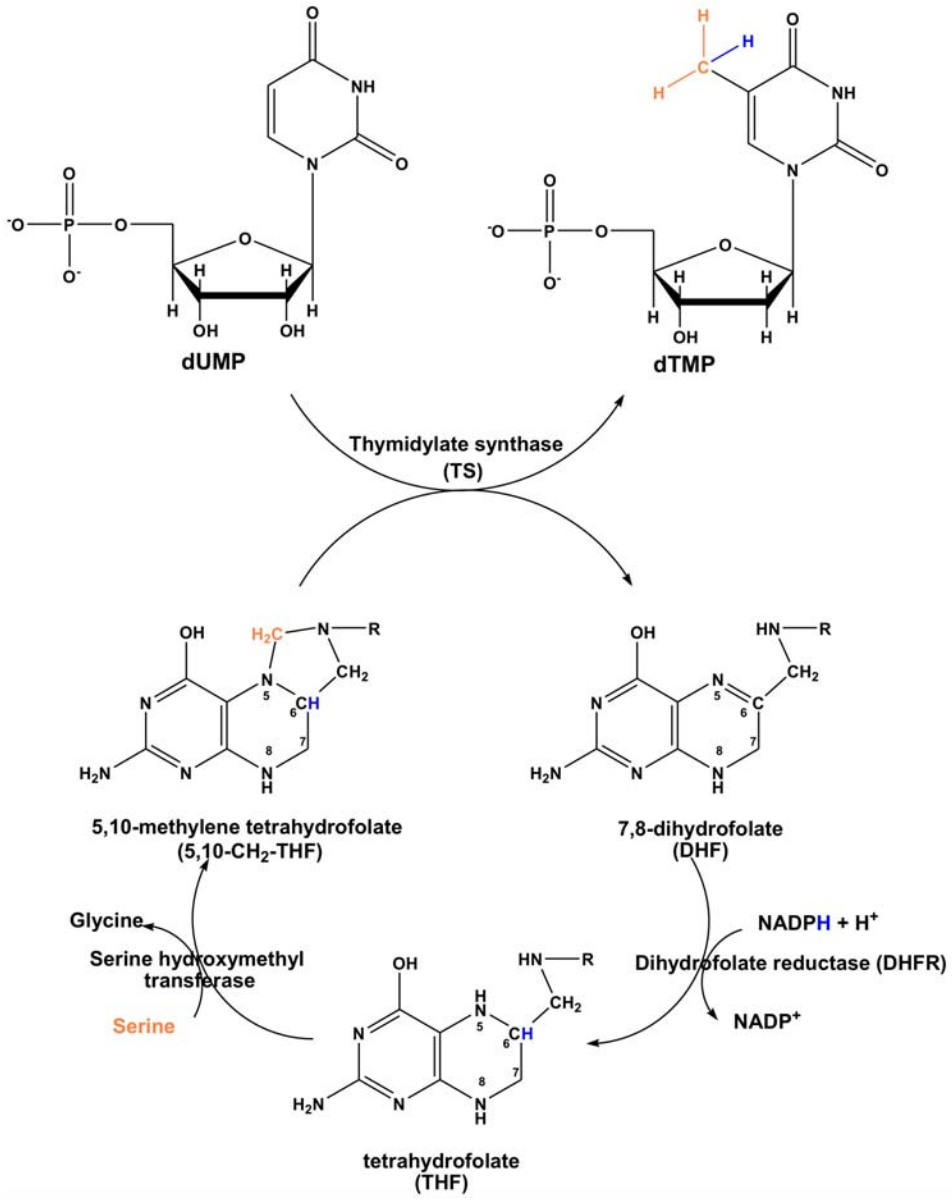

Figure 1.1a: Synthesis of thymidylate (dTMP) from deoxyuridine monophosphate (dUMP). The enzymes dihydrofolate reductase (DHFR) and Serine hydroxymethyl transferase are necessary for the recycling of the 5,5-CH_2-THF. In dTMP, all the methylic hydrogens (in red and blue) derive from 5,5-CH_2-THF. Figure adapted from reference [2].

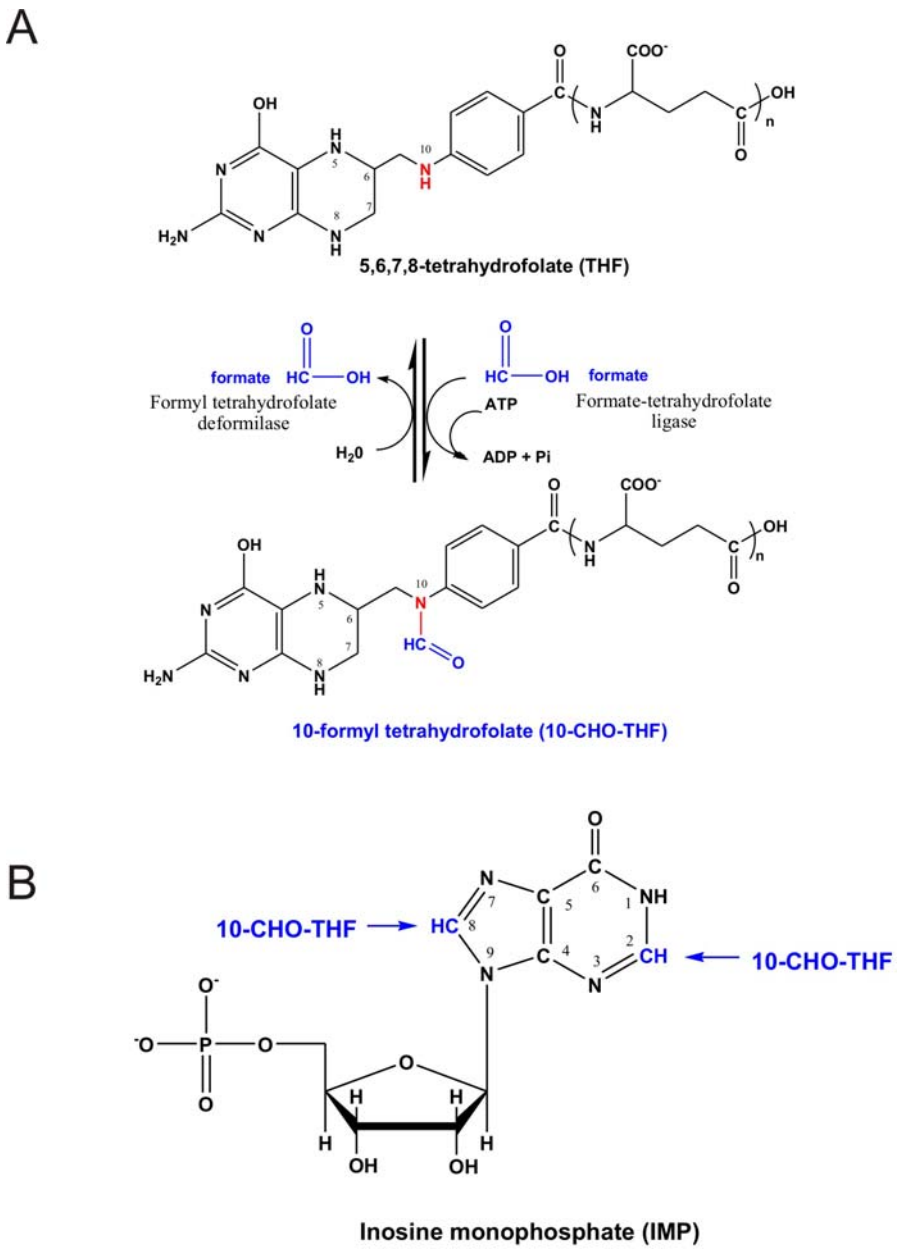

Figure 1.1b: Role of the folate cofactor 10-formyl tetrahydrofolate (10-CHO-THF) in the synthesis of the inosine nucleus. A) Conversion of tetrahydrofolate (THF) to 10-formyl tetrahydrofolate (10-CHO-THF). **B)** Structure of inosine monophosphate (IMP), first intermediate to posses a complete purine nucleus. The carbons added by GARFT (glycinamide ribonucleotide formyl transferase) and AICARFT (aminoimidazole carboxamide formyl transferase), derived from formate and provided by 10-CHO-THF, are indicated in blue. Figure adapted from reference [2].

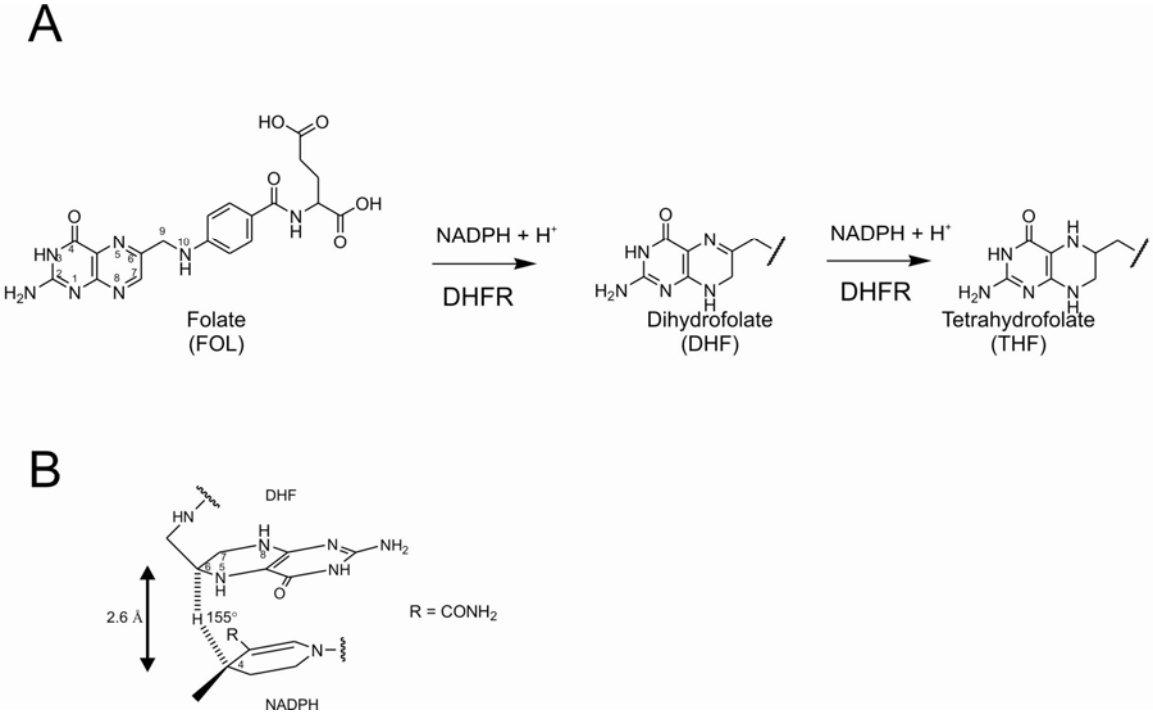

Figure 1.2. Reaction catalyzed by dihydrofolate reductase (DHFR). A) Reduction catalyzed by vertebrate DHFRs. **B)** Schematic representation of the hydride transfer in the transition state: optimal carbon-carbon bond distance and -C···H···C- bond angle are indicated. Image adapted from Benkovic *et al.* 1988 [15].

A

```
Human DHFR      MVGSLNCIVAVSQNMGIGKNGDLPWPPLRNEFRYFQRMTTTSSVEGKQNLVIMGKKTWFS 60
Mouse DHFR      MVRPLNCIVAVSQDMGIGKNGDLPWPPLRNEWKYFQRMTTTSSVEGKQNLVIMGRKTWFS 60
E.coli DHFR     ---MISLIAALAVDRVIGMENAMPWN-LPADLAWFKRNTLN-------KPVIMGRHTWES 49
                    :. *.*:: :  ** :. :**  *  :  :*:* * .       : ****::** *

Human DHFR      IPEKNRPLKGRINLVLSRELKEPPQGAHFLSRSLDDALKLTEQPELANKVDMVWIVGGSS 120
Mouse DHFR      IPEKNRPLKDRINIVLSRELKEPPRGAHFLAKSLDDALRLIEQPELASKVDMVWIVGGSS 120
E.coli DHFR     IG---RPLPGRKNIILSSQPG--TDDRVTWVKSVDEAIAACG------DVPEIMVIGGGR 98
                *    *** .* *::** :    . .     :*:*:*:          .*  : ::**.

Human DHFR      VYKEAMNHPGHLKLFVTRIMQDFESDTFFPEIDLEKYKLLPEYPGVLSDVQEEKGIKYKF 180
Mouse DHFR      VYQEAMNQPGHLRLFVTRIMQEFESDTFFPEIDLGKYKLLPEYPGVLSEVQEEKGIKYKF 180
E.coli DHFR     VYEQFL--PKAQKLYLTHIDAEVEGDTHFPDYEPDDWESVF---SEFHDADAQNSHSYCF 153
                **:: :  *   :*::*:*  :.*.**.**: :  .:: :    . : :.: ::. .* *

Human DHFR      EVYEKND 187
Mouse DHFR      EVYEKKD 187
E.coli DHFR     EILERR- 159
                *: *:.
```

B

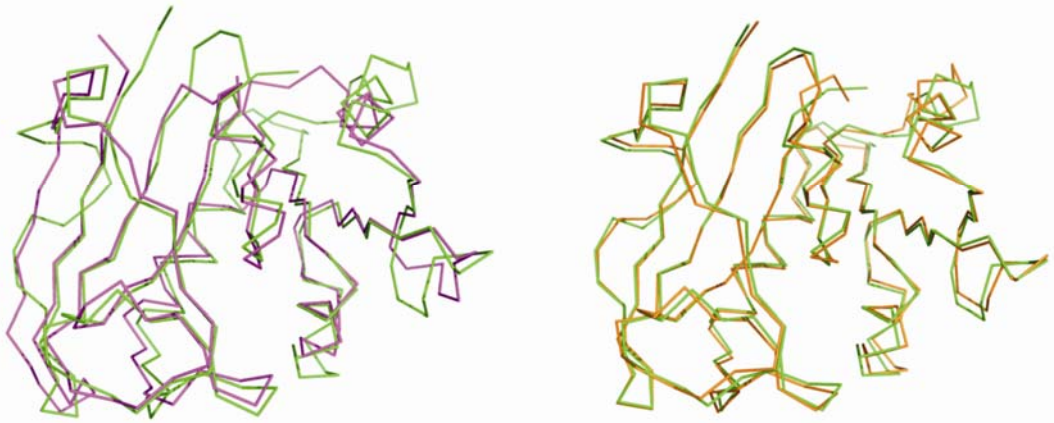

Figure 1.3. Sequence and structural comparison of human, murine and *E. coli* dihydrofolate reductases (DHFRs). **A)** Sequence comparison. Sequence differences from human DHFR are coloured in cyan for mouse DHFR and in red for *E. coli* DHFR. **B)** Comparison of the backbone of human (1U72.PDB; green) and *E. coli* (1RX3.PDB; magenta) and of human (1U72.PDB; green) and mouse (1U70.PDB; orange). Figure adapted from Cody *et al.* 2005 [22].

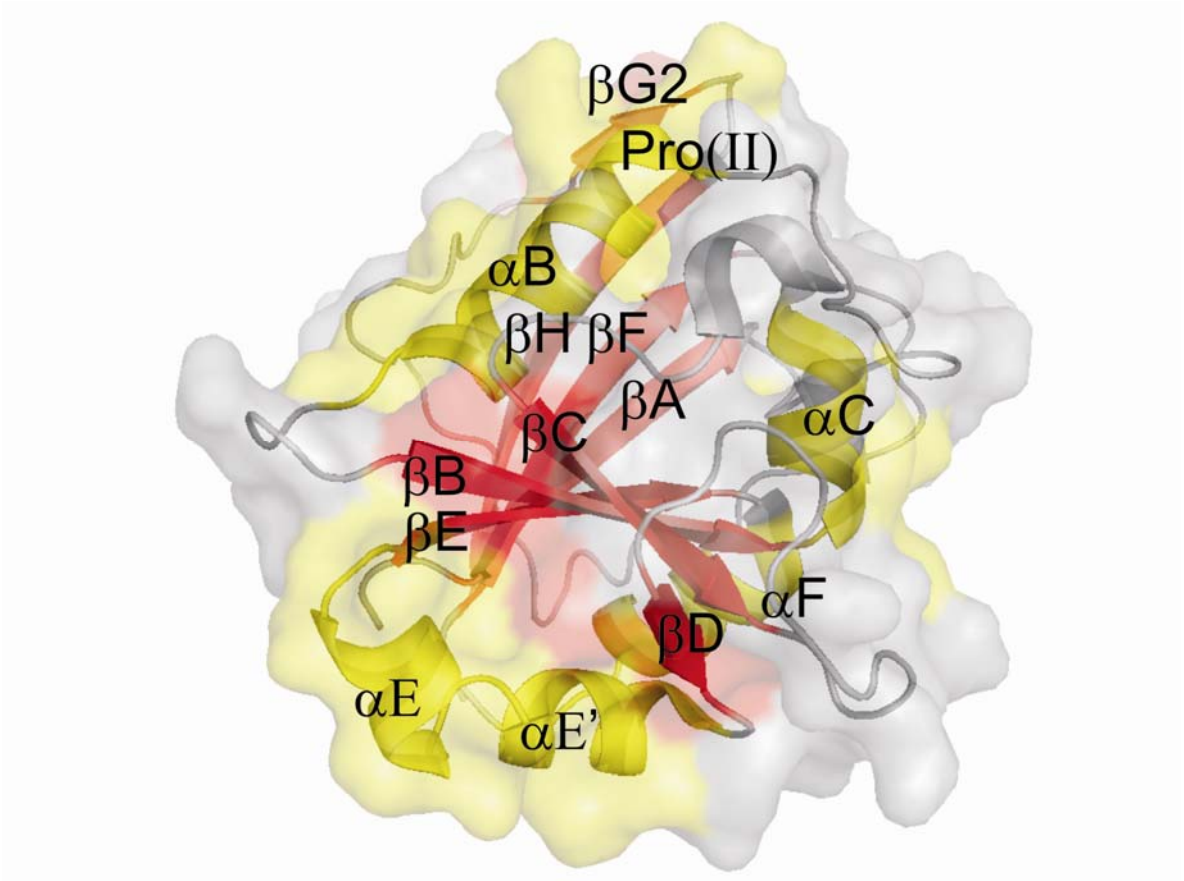

Figure 1.4. Secondary structure of hDHFR. Eight-stranded twisted β-sheet (βA, residues 4-10; βB, 47-53; βC, 71-76; βD, 88-90; βE, 108-116; βF, 130-139; βG, which is interrupted by a tight turn is composed by βG1, 157-159 and βG2, 168-172; βH, 175-185). Five α–helices (αB, 27-40; αC, 53-59; αE, 92–102 and αE', 102-109; αF, 117-127), a polyproline-like helix (Pro(II), residues 21-26) and eight tight turns (residues 11-14, 18-21, 43-46, 61-64, 67-70, 83-86, 162-165, 172-175) connect the β-sheets among them.

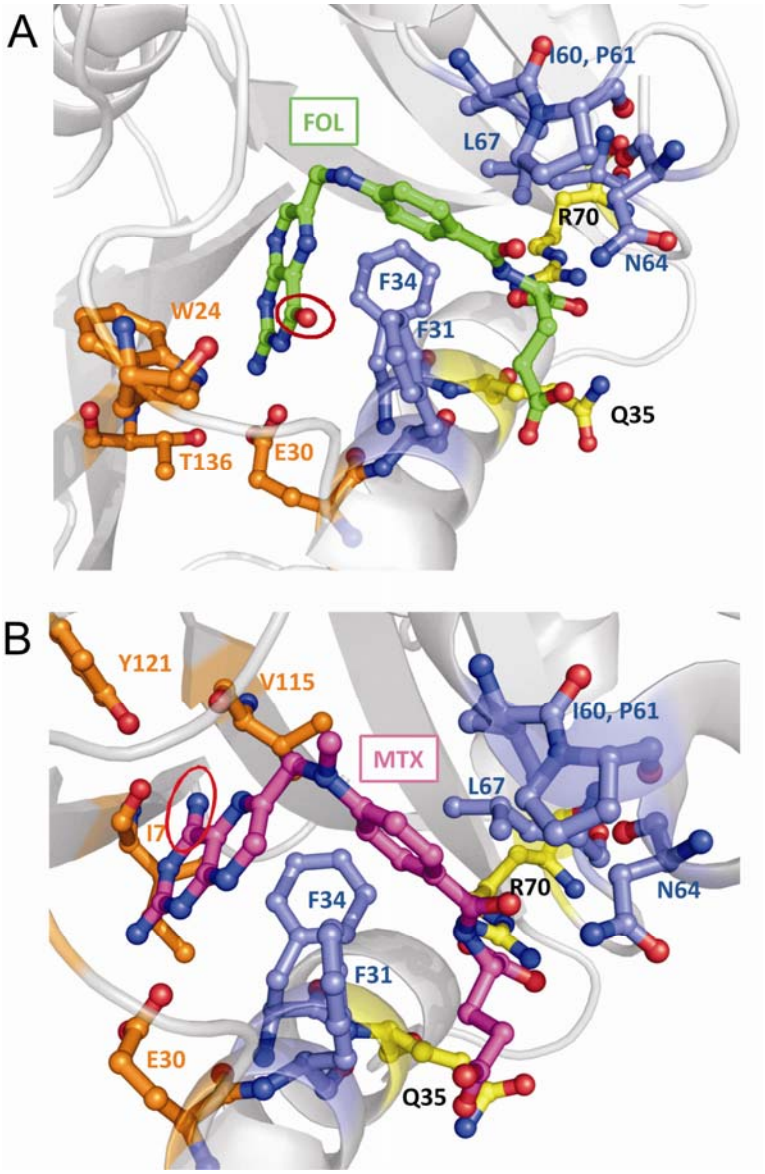

Figure 1.5. Ligand binding at the active site of WT hDHFR. A) Bound folate (FOL; in green) from 1DHF.PDB. **B)** Bound methotrexate (MTX; in magenta) from 1U72.PDB. The active site is shown. Active-site residues that interact with the ligands are shown in sticks representation and coloured in orange, yellow or blue to indicate interaction or proximity to the ligand's pteridine, *p*-ABA or glutamate moiety, respectively. The 4-carbonyl and the 4-amino group of FOL (in **A**) and of MTX (in **B**) are circled to highlight the pteridine ring flip.

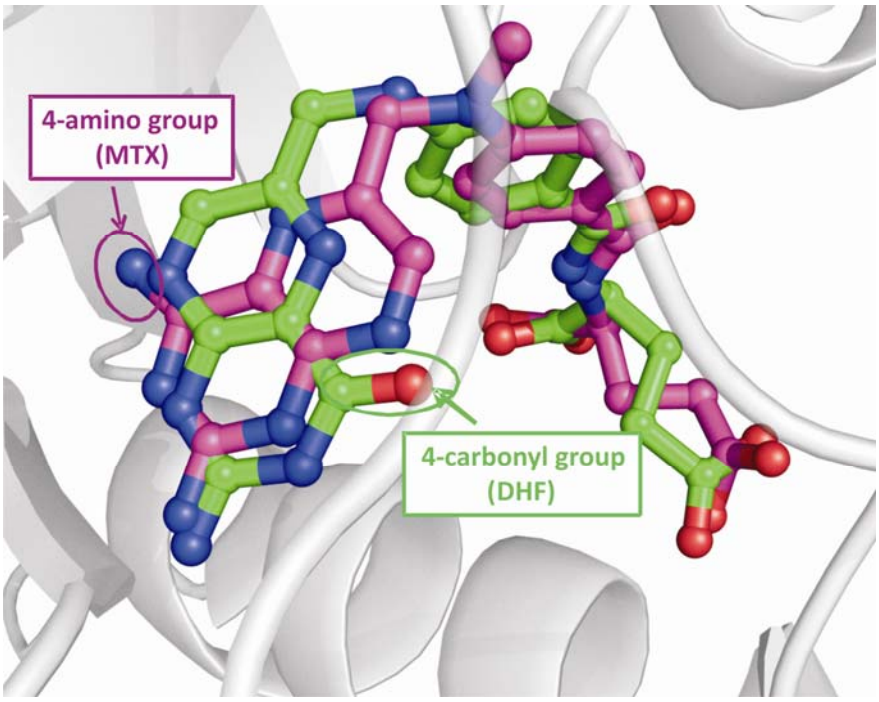

Figure 1.6. Binding of folate and methotrexate in the active site. Superimposition of 1DHF.PDB (binary complex WT hDHFR·folate) and 1U72.PDB (ternary complex WT hDHFR·NADPH·MTX). FOL (in green; from 1DHF.PDB) and MTX (in magenta; from 1U72.PDB) are visualized in the active site (from 1U72.PDB). The FOL 4-carbonyl group and the MTX amino group are indicated to show the pteridine ring flip between the two bound molecules.

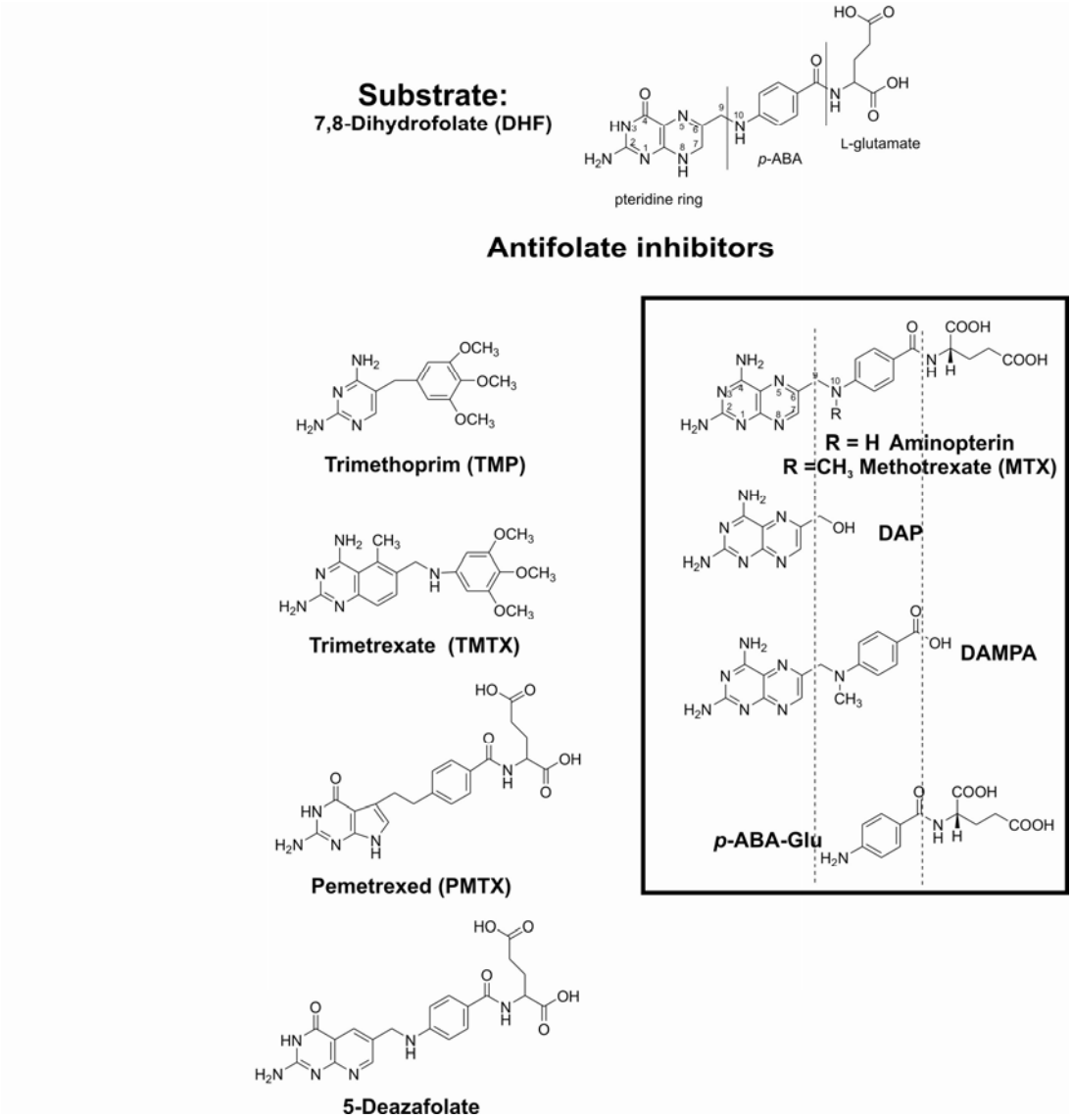

Figure 1.7. Structural representation of the DHFR substrate dihydrofolate (DHF) and different antifolates relevant to this study. Atom numbering is indicated for both DHF and MTX. The substrate and the inhibitors PMTX and 5-deazafolate carry a 4-oxo functionality, while all the other inhibitor illustrated carry an amino group at position 4. MTX and its fragments are represented in the box. DAP (2,4-diamino-6-(hydroxymethyl)pteridine), DAMPA (4-[N-(2,4-diamino-6-pteridinylmethyl)-N-methylamino] benzoic acid) and *p*-ABA-Glu (*para*-aminobenzoic acid-L-glutamate).

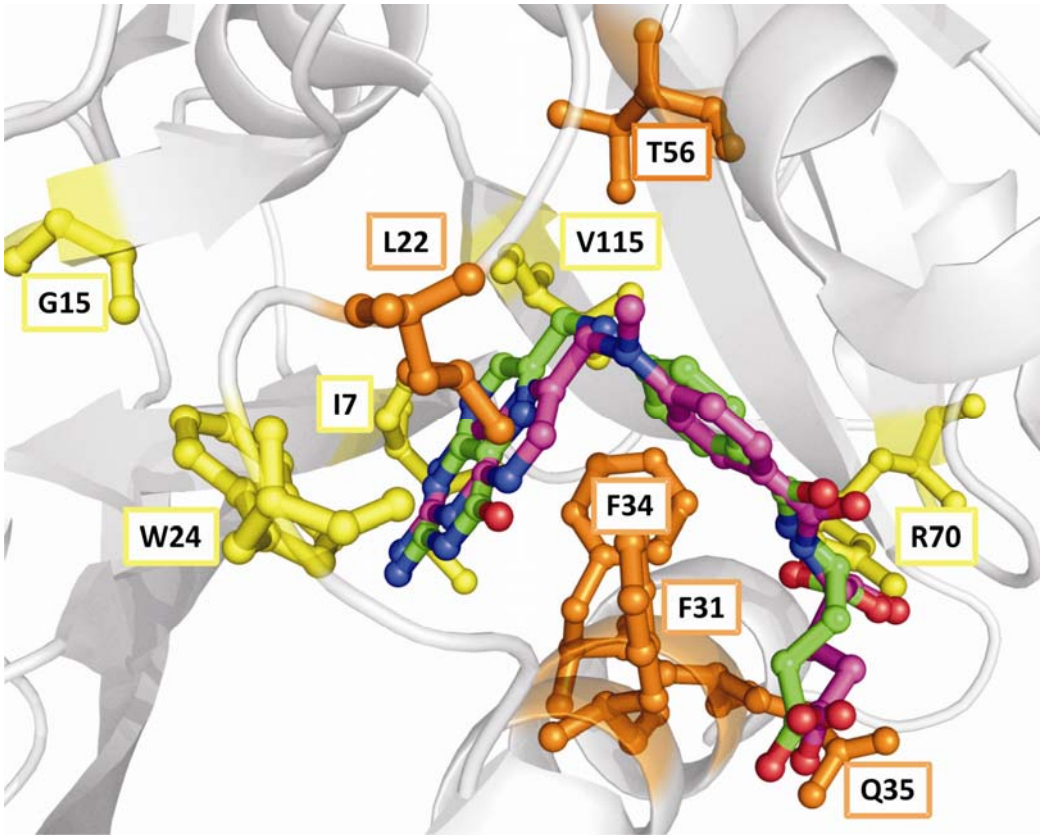

Figure 1.8. Active-site residues of hDHFR targeted by mutagenesis. Bound folate (FOL; in green) from 1DHF.PDB and bound methotrexate (MTX; in magenta) from 1U72.PDB are visualized in the active site (from 1U72.PDB). Active-site residues chosen as targets of this directed evolution study are shown in sticks and are coloured in yellow (principal targets discussed in this thesis) or orange. Residues Phe31, Phe34 and Gln35 (in orange) are also discussed in this thesis, but they were mainly studied by Ph.D. student Jordan Volpato.

Chapter 2 (Article 1) – Increasing methotrexate resistance by combination of active-site mutations in human dihydrofolate reductase

Section 2.0 – Preface

Highly MTX-resistant mutants of hDHFR are potential candidates for protection of healthy haematopoietic stem cells from the cytotoxicity of MTX by means of gene therapy [67]. Mutations of active site residues of hDHFR can reduce affinity of the inhibitor, thereby conferring MTX-resistance, while maintaining sufficient substrate binding to allow catalysis [112]. Synergistic effects on MTX-resistance have been previously described by combining two active-site mutations that individually conferred moderate resistance to the drug [66]. Article 1 describes the use of a directed evolution approach in order to obtain highly MTX-resistant mutants for protection of a model mammalian cell system from the toxicity of this drug.

Simultaneous mutagenesis to a variety of amino acids was performed at three specific active-site residues (Phe31, Phe34 and Gln35). Then, the development and application of an efficient selection strategy based on bacterial complementation allowed the identification of 10 highly MTX-resistant variants of hDHFR. While the residues targeted were all individually known to confer resistance to MTX upon mutation, characterization of the MTX inhibitory constant for the mutants identified showed that combinations of mutations can effectively lead to higher resistance, the most resistant mutant identified presenting three simultaneous mutations. This demonstrated the validity of the proposed approach for identification of mutants of interest. *In silico* energy minimization of the most MTX-resistant triple mutant and of the native enzyme was performed in order to postulate a structural explanation for the effects of mutation on inhibitor binding. Finally, mutants with the higher K_i^{MTX} were tested for their ability to

protect DHFR-knock-out Chinese hamster ovary cells from MTX-toxicity and showed 100 to 400-fold higher degree of protection than the native enzyme.

My contribution to the article was limited to molecular modeling. PhD student Jordan Volpato was responsible of the totality of the experimental work, and together with Prof. Joelle Pelletier provided the design of the project and the edition of the article. Although my contribution to this paper was minor, molecular modeling associated to kinetic analysis offers a powerful tool for structure-activity relationship (SAR) studies, which ultimately is one of the major goals of the project. While crystal structure resolution is certainly the best approach to investigate structural consequences of mutations, it has proven challenging in the context of this project, such that molecular modeling has been deemed an essential alternative. Therefore, my contribution added value to the article by allowing to propose a reasonable structural explanation for the decreased binding, in absence of experimental structural evidence. This subject will be further discussed in chapter 5.

INCREASING METHOTREXATE RESISTANCE BY COMBINATION OF ACTIVE-SITE MUTATIONS IN HUMAN DIHYDROFOLATE REDUCTASE

Jordan P. Volpato[1], Elena Fossati[1] and Joelle N. Pelletier[1,2]

[1]Département de biochimie and [2]Département de chimie
Université de Montréal
C.P. 6128, Succursale Centre-ville
Montréal (Québec)
H3C 3J7, CANADA

J. Mol. Biol., 2007, **373** (3), 599-611

ABSTRACT

Methotrexate-resistant forms of human dihydrofolate reductase have the potential to protect healthy cells from the toxicity of methotrexate (MTX), to improve prognosis during cancer therapy. It has been shown that synergistic MTX-resistance can be obtained by combining two active-site mutations that independently confer weak MTX-resistance. In order to obtain more highly MTX-resistant human dihydrofolate reductase (hDHFR) variants for this application, we used a semi-rational approach to obtain combinatorial active-site mutants of hDHFR that are highly resistant towards MTX. We created a combinatorial mutant library encoding various amino acids at residues Phe31, Phe34 and Gln35. *In vivo* library selection was achieved in a bacterial system on media containing high concentrations of MTX. We characterized ten novel MTX-resistant mutants with different amino acid combinations at residues 31, 34 and 35. Kinetic and inhibition parameters of the purified mutants revealed that higher MTX-resistance roughly correlated with a greater number of mutations, the most highly-resistant mutants containing three active site mutations (K_i^{MTX} = 59 to 180 nM; wild-type K_i^{MTX} < 0.03 nM). An inverse correlation was observed between resistance and catalytic efficiency, which decreased mostly as a result of increased K_M toward the substrate dihydrofolate. We verified that the MTX-resistant hDHFRs can protect eukaryotic cells from MTX toxicity by transfecting the most resistant mutants into DHFR-knock-out CHO cells. The transfected variants conferred survival at MTX concentrations between 100-fold and >4000-fold higher than the wild-type enzyme, the most resistant triple mutant offering protection beyond the maximal concentration of MTX that could be included in the medium. These highly resistant variants of hDHFR offer potential for myeloprotection during administration of MTX in cancer treatment.

Keywords

Dihydrofolate reductase; mutagenesis; drug resistance; enzyme kinetics; *in vivo* selection.

INTRODUCTION

Human DHFR (EC 1.5.1.3) is a ubiquitous cytosolic enzyme that catalyzes the reduction of 5,6-dihydrofolate (DHF) to 5,6,7,8-tetrahydrofolate (THF) in a nicotinamide adenine dinucleotide phosphate (reduced form) (NADPH)-dependent reaction. THF is an essential cofactor in several metabolic pathways, including purine and thymidylate biosynthesis. As a result of its importance in cellular proliferation, hDHFR has long been a key pharmacological target for the treatment of various types of cancer.[1] Methotrexate is a folate analogue that acts as a slow, tight binding competitive inhibitor of hDHFR, thereby inhibiting cellular THF synthesis and cellular proliferation. MTX is widely used for the treatment of acute lymphoblastic leukemia, [2] osteosarcoma, [3] breast cancer,[4] and head and neck cancer. [5]

Efficacy of MTX in cancer treatment is largely attributed to the high affinity of the drug for hDHFR (K_i = 3.4 pM).[6] Crystal structures of the wild-type (WT) hDHFR complexed with MTX have shown that, despite its high structural similarity to folate, MTX and folate bind at the active site in a different orientation.[7] Although the ρ-aminobenzoic acid and glutamate (ρ-ABA-Glu) portions of both ligands bind at the active site in a similar orientation, the pteroyl moiety of MTX is flipped 180° around the C6-C9 bond (**figure 2.1(a)**), such that its 4-amino group forms specific hydrogen bonds with the backbone carbonyls of residues Ile7 and Val115 (**figure 2.1(b)**), in contrast to bound folate, which does not form hydrogen bonds with these residues. The pteroyl moiety of MTX is also involved in hydrogen bonding with residue Trp24 *via* a conserved water molecule and with residue Glu30,[8] while the side chain of residues Leu22 and Phe34 are within van der Waals distance of this portion of the inhibitor (**figure 2.1(b)**).[9, 10] These interactions are also formed with the pteroyl moiety of folate, albeit with the opposite side of the pterin ring. The ρ-ABA moiety of MTX and DHF mainly interact *via* van der Waals interactions with residues Phe31 and Phe34 of α-helix 1 (residues 27-40), which also contains Gln35 that is proximal to the γ-glutamate moiety of the bound ligands. The glutamate moiety also forms a salt bridge with the guanidinium side chain of Arg70.

Previous studies of hDHFR and murine DHFR have shown that certain mutations at residues Leu22, Phe31, Phe34, Gln35 and Arg70 (**figure 2.1**) can yield catalytically-

active, MTX-resistant mutants.[11-17] Identification of MTX-resistant hDHFR mutants has been performed either *ex vivo* in cultured cells exposed to MTX[18-20] or by performing site-directed mutagenesis at the active site of hDHFR by rational design.[9, 11-15, 21] These studies have mostly yielded point mutants that maintain good catalytic efficiency while displaying moderate MTX resistance (e.g. F31S, K_i = 0.240 nM; L22R : K_i = 4.6 nM).[14, 15] However, some point mutations confer high MTX resistance (e.g. F34S : ternary K_D^{MTX} = 210 nM), albeit with considerably reduced catalytic efficiency.[10] These studies led to a better understanding of ligand binding at the enzyme active site and contributed to structure-based design of new antifolate inhibitors.[22]

Identifying more highly MTX-resistant hDHFR mutants offers important applications in the medical field. Because MTX-resistant hDHFRs have not been observed in clinical studies of acquired MTX-resistance in cancer patients,[23] MTX-resistant hDHFRs have the potential to protect healthy haematopoietic stem cells from MTX toxicity during chemotherapy,[24] thus protecting patients from immunosuppression. Gene therapy strategies have been used to transfer MTX-resistant hDHFRs into mouse and human bone marrow progenitor cells, efficiently ensuring stem cell survival upon exposure to MTX.[25, 26] Resistant cells transplanted in the bone marrow of mice ensured myeloprotection during treatment with MTX.[27, 28] For this application, ideal candidate hDHFR mutants should have a very high K_i for MTX (in the high nanomolar range), while maintaining the catalytic properties, including DHF binding , required to ensure cell survival.

Highly MTX-resistant hDHFR genes with good catalytic efficiencies have been obtained by the combination of the moderately MTX-resistant point mutants at active-site residues 22 and 31,[29] which generated synergistically resistant hDHFRs (e.g. L22Y-F31G, K_i = 150 nM *versus* L22Y, K_i = 11 nM and F31G, K_i = 0.35 nM) that conferred high MTX resistance in human and mouse stem cell lines. While those results are promising, variants that are yet more highly resistant and/or more active would hold greater potential for clinical application, by increasing the difference in cellular survival between cells harboring MTX-resistant hDHFR and those with native hDHFR (target of MTX).

On the basis of these considerations, we have devised a strategy based on directed evolution for the identification of novel hDHFR combinatorial mutants that are highly active and resistant to MTX. Directed evolution of ligand binding in an enzyme generally requires structure-based knowledge to pinpoint residues in the vicinity of the active site. These residues are mutated in combination and the resulting combinatorial mutant libraries are screened for a desired property. Application of such methods has provided new structural insight into ligand binding,[30,31] engineered new substrate specificity,[32] and resulted in the development of efficient biomarkers.[33,34] Using a semi-rational approach, we created a combinatorial library encoding mutations at residues Phe31, Phe34 and Gln35 of the hDHFR gene. These residues belong to α-helix 1 and are individually known to confer MTX resistance upon mutation.[10,14,17] We performed *in vivo* library selection in a bacterial system propagated on media containing a high concentration of MTX. Characterization of selected variants yielded novel MTX-resistant hDHFR mutants, including a variety of combinatorial mutants that displayed an important decrease in MTX binding, comparable to the weakest-binding hDHFR mutant reported to date, albeit with a greater residual specific activity. As a result, we obtained very efficient protection of a relevant mammalian cell model, *dhfr* $^-$ CHO DUKX B11 cells.

RESULTS

Creation of the hDHFR mutant library

A combinatorial library encoding 567 different mutants was created by mutating amino acids Phe31, Phe34 and Gln35 to a selection of amino acids, in order to identify novel MTX-resistant hDHFR mutants (**table 2.1**). The number of possibilities encoded was restricted in view of future recombination with other mutant hDHFR libraries. The three positions chosen for mutation belong to α-helix 1 (residues 27-40), which contains the catalytic residue Glu30, a highly-conserved residue that protonates N_5 of DHF prior to hydride transfer,[8] as well as residues Phe31, Phe34, Gln35, that have been shown to be important for substrate and/or inhibitor binding.[10,14,17] The selection of amino acids to be encoded at positions 31, 34 and 35 was based either on known mutations that individually

confer resistance to MTX or on the basis of *in silico* observations of hDHFR with bound MTX. We encoded the desired mutations at the three positions using a single degenerate oligonucleotide primer. As a result of codon degeneracy, other amino acids were encoded in addition to the amino acid variety of interest (**table 2.1**). Site-directed mutagenesis studies at residues 31 and 34 have shown that MTX-resistant mutants generally contain small polar or non-polar amino acids at these positions. Consequently, these types of residues were encoded in addition to the phenylalanine present at these positions in WT hDHFR. As noted in previous reports,[7,35-37] visualization of bound MTX or folate in the native enzyme (**figure 2.1**) suggests that these substitutions can reduce the contact surface with bound ligand, therefore reducing affinity for MTX and/or DHF. For residue 35, earlier studies of the murine DHFR gene have shown that the mutation Q35P can confer moderate resistance to MTX.[17] The location of the Q35P mutation in the middle of α-helix 1 suggests a change in α-helix geometry. Consequently, we mutated Gln 35 to amino acids with low α-helical propensity,[38] without encoding proline due to low stability of the Q35P point mutant.[17]

Selection and identification of MTX-resistant mutants

The hDHFR mutant library was transformed in *Escherichia coli* SK037, a MTX-sensitive strain. This strain is a knock-out for *tolC*, which encodes a protein essential to the function of a multi-drug-resistance (MDR) efflux pump.[39] The quality of the library was assessed by sequencing 70 clones that grew on non-selective media (LA-100). Nucleotide representation for each of the degenerate codons used at residues 31, 34 and 35 followed the expected statistical distribution, and no non-specific mutation was observed. The library was then selected on M9 minimal medium containing 1 mM MTX (ATM-1000). As negative controls for MTX-resistance, *E. coli* SK037 transformed with pQE32 or WT hDHFR-pQE32 were also plated on the selective medium. The survival rate of the library was 0.2%, whereas no bacterial growth was observed for the negative controls. *E. coli* SK037 transformed with hDHFR L22Y-pQE32, which encodes a MTX-resistant point mutant of hDHFR, were plated on the selective ATM-1000 medium as a positive control. This yielded a 100% survival rate relative to non-selective medium,

demonstrating that the selection stringency was appropriate for identification of MTX-resistant hDHFR mutants. Seventy colonies were picked following selection to identify the mutations at positions 31, 34 and 35. As shown in **figure 2.2**, ten different mutants were identified post-selection. The mutants are designated by the one-letter code of the amino acid occurring at positions 31, 34 and 35. The selection yielded 1 point mutant, five double mutants and four triple mutants. Mutant PFE was the most frequently selected combination (30%), followed by SFE (27%), RFE (20%) and PFH (11%). These variants, which are all double mutants, represent 88% of the selected clones and all contain the native Phe residue at codon 34. The last double mutant identified, GFN, also conserves the native Phe at position 34, but was identified only once (1%). The most frequently observed triple mutant is AVH, identified 5 times (7%), followed by RTR (1%), RTS (1%) and RAN (1%). Finally, a point mutant, PFQ (F31P) was identified once (1%). This point mutant had not yet been characterized in MTX-resistance studies. Retransformation and plating in the presence (ATM-1000) or absence (LA-100) of MTX gave rise to a similar number of colonies for all selected variants, confirming that the observed resistance is solely due to the MTX-resistant hDHFRs.

Binding and kinetic characterization of MTX-resistant hDHFR mutants

For determination of kinetic and binding parameters, the retransformed MTX-resistant hDHFR variants were purified in one step to 90-95% purity, with yields ranging between 1-30 mg/L of culture (data not shown). Solubility and relative expression level of all variants upon over-expression was verified by loading volume-equivalent amounts of total cell extracts, cell pellet and supernatant for resolution by SDS-PAGE. All His_6-hDHFR variants were approximately 50% soluble, as reported for the native recombinant hDHFR,[40] ruling out solubility differences in explaining the observed variations in yield of purified variants. In addition, all mutants (soluble + insoluble) were expressed at similar levels. The mock-purified supernatant of *E. coli* SK037 transformed with the vector pQE32 served as a negative control in all kinetic and binding experiments.

Michaelis constants for the substrate DHF (K_M^{DHF}) and reactivity (k_{cat}) were determined for the ten selected mutants and for WT His_6-hDHFR. K_M^{DHF} of WT His_6-hDHFR was determined to be <75 nM. At this concentration of DHF, the enzyme was

already saturated. It was not possible to obtain a more precise value due to the weak signal observed at such a low concentration of substrate. Previously reported K_M^{DHF} values for recombinant, native (non-His-tagged) WT hDHFR are in the range of 33 to 120 nM,[6,15,20] suggesting that the His_6-tag has little effect on DHF affinity. K_M^{DHF} was increased at least ninefold to 57-fold for the selected mutants relative to WT His_6-hDHFR as a result of the mutations introduced at positions 31, 34 and/or 35. This was not unexpected, as the residues chosen for mutagenesis are known to be involved in DHF binding. As shown in **table 2.2**, k_{cat} values were reduced by at most a factor of 10, except for mutant RAN (20-fold decrease); mutants PFQ, GFN and SFE displayed k_{cat} values similar to that of native enzyme. The lowest reactivities were generally displayed by mutants containing a F31R substitution, which is consistent with previous reports of this point mutant (k_{cat} = 0.93 s^{-1}).[41] As a result of the k_{cat} and K_M^{DHF}variations, the catalytic efficiencies (k_{cat}/K_M^{DHF}) for all selected mutants were reduced, ranging from a 30-fold decrease for point mutant PFQ to a 700-fold decrease for triple mutant RAN (**table 2.2**).

The inhibition constants for MTX (K_i^{MTX}; **table 2.2**) reveal that all selected mutants were resistant to MTX, the most highly resistant being the AVH triple mutant (K_i^{MTX} = 180 nM), with K_i^{MTX} almost 4 orders of magnitude greater than WT. The mutant with the lowest K_i is the point mutant PFQ (K_i^{MTX} = 1.7 nM), which was inhibited 50-fold less efficiently by MTX than the WT enzyme, while the other combinatorial double and triple mutants showed K_i increases of at least 2 orders of magnitude (**table 2.2, figure 2.3**). Ternary binding constants for MTX were also determined, to verify that the observed loss of inhibition correlated with reduced binding. The ternary K_D^{MTX} values obtained were similar to the K_i^{MTX} values for all mutants (**table 2.2**), indicating a direct relation between binding and inhibition in all cases. The greatest difference between K_i and K_D was for mutant RTR (eightfold). It was not possible to determine the K_D values precisely for WT His_6-hDHFR, PFQ and RAN mutants by this method, the fluorescence quenching detection limit being ~2 nM MTX in our system. Binary K_D^{MTX} values were also obtained in absence of NADPH for the MTX-resistant mutants (results not shown). In all cases, the value for the binary K_D^{MTX} was greater than the ternary K_D^{MTX} (fourfold to 19-fold difference for tested mutants RTR, RTS, RFE and AVH). This is consistent with

bound NADPH promoting tighter binding of MTX to the selected hDHFR variants, as demonstrated for the native enzyme.[6]

Protection of mammalian cells with mutant hDHFRs

We verified the efficacy of eukaryotic cell protection with four of the selected mutants (**table 2.3**). CHO DUKX B11 cells (*dhfr*$^-$) were transfected with mutant RFE, SFE, RTS or AVH. These variants were chosen because they displayed the highest K_i^{MTX} values while maintaining catalytic efficiency comparable to MTX-resistant hDHFRs used in similar studies.[42-44] WT hDHFR and the MTX-resistant point-mutant L22Y served as negative and positive controls, respectively. A mock experiment consisted in transfecting pcDNA 3.1 vector (null). Transfection efficiency was evaluated at approximately 50% for all constructs. Transfected cells were exposed to various concentrations of MTX for 48 hrs in α-MEM medium containing no nucleotides, ensuring that cell survival was based solely on activity of the transfected hDHFRs. **Figure 2.4** presents cell survival data; EC_{50}^{MTX} values are given in **table 2.3**. All mutants tested conferred MTX-resistance to CHO DUKX B11 cells. The point mutant L22Y (EC_{50}^{MTX} = 12 μM) provided a 220-fold increase in EC_{50}^{MTX} relative to the WT hDHFR (EC_{50}^{MTX} = 0.054 μM). The double mutants RFE (EC_{50}^{MTX} = 31 μM) and SFE (EC_{50}^{MTX} = 32 μM) provided a 570-fold increase, while the triple mutant RTS (EC_{50}^{MTX} = 56 μM) provided a 1030-fold increase relative to WT. The EC_{50}^{MTX} for the triple mutant AVH (>4000-fold increase) could not be determined because dissolution of higher concentrations of MTX in the medium perturbed the pH. Mutant AVH allowed survival of 73% of the cell population at 200 μM MTX. Enzyme expression under these conditions was confirmed by Western blot analysis (data not shown). The null control showed no cell survival, confirming that survival was due solely to the presence of MTX-resistant hDHFRs, and that no secondary resistance mechanism had been acquired upon exposure to MTX. Cells expressing WT hDHFR were sensitive to low concentrations of MTX, ruling out gene amplification.

DISCUSSION

Of 567 possibilities encoded in the hDHFR mutant library, ten MTX-resistant mutants were identified following selection on solid media containing 1 mM MTX. The chosen selection strategy yielded one novel single mutant and nine novel combinatorial MTX-resistant mutants, providing new insight into the role of residues at positions 31, 34 and 35 in ligand binding and selectivity, while generating novel hDHFR mutants that efficiently protect CHO (*dhfr-)* eukaryotic cell line from MTX-cytotoxicity. All of the resistant mutants displayed reduced catalytic efficiencies compared to WT His_6-hDHFR (30 to 700-fold decrease), mainly as a result of decreased productive binding of DHF (tenfold to 60-fold K_M^{DHF} increase). The reduction in MTX affinity was much greater, with K_i^{MTX} increased 54 to 5800-fold. Thus, we identified a variety of patterns of mutations at active-site residues 31, 34 and/or 35 that greatly reduce the binding of MTX while maintaining sufficient affinity for DHF to provide the level of catalytic activity required for bacterial propagation. The various sequence patterns obtained are indicative of significant plasticity and robustness in these active-site residues: a low number of mutations were sufficient to induce a new phenotype (high MTX resistance resulting from plasticity) while the native function, THF synthesis, endured the effect of the mutations to an important degree as a result of robustness.[45]

Consistent with previous reports of hDHFR point mutants of Phe31,[14] we observed the bulky, positively-charged Arg and small residues, whether polar or non-polar (Gly, Ala and Ser) at position 31 (**table 2.4**). The variety of amino acids identified at position 31 (five of the nine encoded) confirms that this position can tolerate a variety of side-chain volumes and functional groups. Arg31 was encoded in four of the resistant mutants, consistent with F31R being the most resistant Phe31 point mutant reported (K_i^{MTX} = 7.2 nM).[41] In addition, we observed the structurally-constraining proline at position 31 (point mutant F31P, or PFQ). Never previously reported, this MTX-resistant point mutant exhibits resistance and catalytic efficiency intermediate between the previously-reported F31R and F31S point mutants.[14,41]

Phe34 was the most strongly conserved native residue, consistent with previous studies qualifying the importance of Phe34 in binding either MTX or DHF at the active

site.[10] Three of the four amino acids encoded were observed in the four triple mutants we identified (Ala, Thr or Val). Previously-characterized point mutants were not identified by our screening strategy, likely because the *in vivo* MTX-resistance trait that we selected for is complex, requiring low MTX binding combined with sufficiently high specific activity as well as good expression and stability. The F34S mutant is an important example: despite having the highest ternary K_D^{MTX} reported for any hDHFR mutant (210 nM), its very poor catalytic efficiency (0.017 $\mu M^{-1}s^{-1}$)[10] apparently decreases enzyme function to a level too low for cellular propagation.

A diversity of mutations was also observed at position 35 (five out of nine amino acids encoded); no resistant point mutants were identified. The Gln35Glu substitution occurred in the three most frequently observed selected mutants (**figure 2.2**), that all conserved Phe34. The introduction of a negative charge at this location may introduce electrostatic repulsion of the γ-glutamate tail (**figure 2.1(b)**).While this effect is also expected to reduce DHF binding, we note that MTX binding is more importantly reduced than productive DHF binding (K_M^{DHF}), by a factor of at least 10 (mutant PFE) to more than 70 (mutant RFE). The differing binding and kinetic properties of mutants PFE, RFE and SFE highlight the impact of combining mutations at position 31 (Pro, Arg or Ser) with the Gln35Glu substitution. A positively charged residue at position 35 also supports MTX-resistance, as evidenced by the Gln35Arg (mutant RTR) and the Gln35His substitutions (mutants AVH and PFH). The side chain of Gln35 has been proposed to hydrogen bond with the guanidinium group of Arg70 in the apoenzyme or when the ligand does not contain a *p*-aminobenzoyl function,[7,46,47] while in the presence of ligands Arg70 forms a conserved salt bridge with the α-carboxylate of the glutamate moiety.[12] The mutations selected at position 35 may render the active site less propitious to ligand binding, by forming a Glu35-Arg70 salt-bridge in the apoenzyme or as a result of electrostatic repulsion with Arg70 in the case of an Arg35 or His35 mutation. Structural data are required to confirm these hypotheses.

In addition to the correlation of the conserved Phe34 with Q35E, other correlations were observed. Mutants PFQ, PFE and PFH equally conserve Phe34 while displaying a Phe31 to Pro substitution. Mutants RTR and RTS, two triple mutants, also

displayed correlation at positions 31 and 34. In no case was a strict co-variation observed. Considering the restricted subset of amino acids encoded at each of the three positions, it is likely that greater sequence diversity at positions 31, 34 and 35 can promote resistance.

How effective is the accumulation of mutations in providing increased MTX resistance? Combining the F31P substitution with mutations at position 35 (mutants PFE and PFH) resulted in a six-to seven-fold increase in K_i^{MTX} accompanied by a five-to seven-fold decrease in catalytic efficiency (**table 2.4**). Double mutant GFN displayed a nearly 40-fold increase in K_i^{MTX} and a tenfold decrease in catalytic efficiency relative to the point mutant F31G, contributed mainly by a sixfold increase in K_M^{DHF}.[14] The point mutant F31S[14] provides only modest MTX-resistance; the addition of mutation Q35E (mutant SFE) resulted in a 125-fold increase in K_i^{MTX}. In counterpart, the catalytic efficiency was reduced sixfold relative to F31S, due solely to decreased DHF affinity. The same Q35E mutation had a smaller effect when combined with mutation F31R (mutant RFE; **table 2.4**). Comparison of these double mutants highlights the complexity of cumulating active-site mutations: the effect of mutation Q35E differs according to its environment (i.e. the amino acid at position 31).

The selected triple mutants provided further evidence of the impact of multiple mutations on resistance: the most highly MTX-resistant hDHFR variants were all triple mutants (**table 2.2; figure 2.3**). While the F31R point mutant alone provides good MTX resistance (K_i^{MTX} = 7.2 nM)[41], additional mutations increased resistance, as evidenced by triple mutants RTS (K_i^{MTX} = 59 nM) and RTR (K_i^{MTX} = 86 nM). The frequently observed F31R appears to provide a good basis for further mutations to increase resistance.

The current data set is consistent with synergistic effects of many of the mutations toward MTX binding, as opposed to additive effects.[48] A striking example is triple mutant AVH, which displayed the weakest MTX binding out of the selected mutants (K_i^{MTX} = 180 nM), an almost 6000-fold increase in K_i^{MTX} relative to the WT. This combinatorial mutant nearly matches the best-reported K_D^{MTX} (F34S = 210 nM).[10] However, it boasts a catalytic efficiency that is almost 20-fold superior to the F34S point mutant. The point mutant Q35H was not selected, suggesting that it does not confer a high level of resistance. Nonetheless, Q35H increased the K_i^{MTX} of the point mutant F31P

in mutant PFH; combined with F31A (K_i^{MTX} = 0.27 nM)[14] and F34V (K_i^{MTX} = 10 nM)[10], it contributed to the highest resistance in mutant AVH. In a similar fashion, the Q35R mutation (the murine Q35R mutant displays only a tenfold increase in K_i^{MTX}),[17] combined with F31R (K_i^{MTX} = 7.2 nM)[41] and F34T (K_i^{MTX} = 9.6 nM),[10] contributed to resistance in mutant RTR (K_i^{MTX} = 86 nM). No resistant triple mutant was identified that was only one mutation away from a characterized double mutant, precluding a direct assessment of the effect of one additional mutation in these cases. It is not currently possible to predict synergistic effects of mutations on specific protein functions; our success in identifying multiple active-site environments providing the desired properties resulted from searching an area of sequence space that was likely, according to prior knowledge, to harbour positive solutions. Despite the fact that F34 was highly conserved during selection, likely as a result of its role in DHF binding, mutations at this position in the context of neighbouring mutations provided the highest level of resistance. We are currently combining this triply-mutated library with further libraries mutated at active-site residues previously shown to specifically interact with MTX, to attempt to further increase MTX resistance while maintaining catalytic efficiency. Rather than restricting the identity of mutations to specific point mutants known to confer resistance, each position encodes a variety of amino acids, allowing for the possibility of unpredicted combinatorial effects.

As made evident above, the trade-off to decreased MTX binding with the greater number of mutations was a general correlation with decreased catalytic efficiency. The most important contributor to decreased catalytic efficiency was decreased productive binding of DHF: the variation in K_M^{DHF} was 1.5 to 44-fold greater than the change in k_{cat}. Surprisingly, while the impact of point mutations at positions 31 and 34 on K_M^{DHF} was great, there was no significant further increase of K_M^{DHF} upon accumulating mutations. The additional mutations did, however, greatly increase K_i^{MTX}. These differences in the effect of the mutations toward either ligand may result from the different binding modes for the pteroyl moiety of DHF and MTX at the active site of hDHFR (**figure 2.1**), despite the fact that residues 31 and 35 do not directly interact with the pteroyl moiety. We are currently testing further ligands of DHFR to verify whether there is a relation between the decreased MTX and DHF affinity, and affinity for other ligands. Trimethoprim (TMP),

an antibiotic that targets bacterial DHFR with a high degree of specificity (K_i^{TMP} *E. coli* DHFR: 80 pM) binds hDHFR 12,000-fold more weakly,[49] justifying its use in our selection strategy to knock out background *E. coli* DHFR activity. While most of the mutants selected for MTX resistance showed no change of *in vitro* resistance to TMP relative to the WT hDHFR, double mutant RFE and triple mutants RTR and RTS showed significant resistance (data not shown). Our results are consistent with the observation that the Leu28Arg substitution in *E. coli*, homologous to hDHFR mutation Phe31Arg, contributes to TMP-resistance in addition to MTX resistance.

The AVH mutant bound to MTX was created *in silico* to gain insight into the effects of the mutations on MTX binding (**figure 2.5**). While this simple molecular visualization does not provide structural evidence, it is clear that the combinatorial F31A/F34V mutations enlarge the volume of the active-site cavity proximal to MTX, simply as a consequence of the smaller volumes of the substituted amino acids.[50] The F31A mutation is likely to reduce van der Waals interactions with the *p*-ABA moiety of MTX relative to the WT. The F34V mutation likely has a similar effect in addition to reducing van der Waals interactions with the pterin moiety. The effect of the Q35H mutation is not as apparent in this visualization. We are presently obtaining structural information for mutant AVH by X-ray crystallography.

We have shown that CHO *dhfr*$^-$ cells containing double mutants RFE or SFE and triple mutants RTS or AVH were all protected, to some extent, from the toxic effects of MTX (**table 2.3; figure 2.4**). The positive control, point mutant L22Y, confers good MTX-resistance in mammalian cells as a result of its good catalytic efficiency (12 $s^{-1}\mu M^{-1}$) and high K_i^{MTX} (10.9 nM).[15] Previously reported transfections of hDHFR point mutants (F31S, F34S, G15W and L22R) in CHO *dhfr*$^-$ cells[43,44] yielded between 2 to 7% cell survival in presence of 1 μM MTX. In our similar system, the resistance conferred by our double mutants was greater than that for any of the point mutants. In turn, the triple mutants offered a better protection than the double mutants. The triple mutant AVH, exhibiting the highest K_i^{MTX}, conferred the best protection with 70% cell survival at 200 μM MTX, despite the fact that it displayed the lowest catalytic efficiency among our sample. This suggests that weak MTX binding is a more important feature than catalytic

efficiency in protecting the CHO cells. This result provides an interesting tool for further increasing MTX resistance, given that most MTX-resistant mutants previously used to protect mammalian cells had catalytic efficiencies at least tenfold higher than the AVH mutant.[51]

Combining active-site mutations in hDHFR yielded novel insights concerning increased MTX resistance. Ideally, one would like to predict the capacity of a mutant to confer MTX resistance to mammalian cells from assessment of a specific *in vitro* parameter, be it K_i^{MTX}, IC_{50}^{MTX} or K_D^{MTX}, or yet a combination such as K_i^{MTX} × catalytic efficiency.[10,14,16] While each of these provided a rough estimate of resistance, we did not succeed in ranking the *in vivo* effect of the MTX resistant mutants according to *in vitro* parameters. We believe factors such as expression level, folding, stability and cell type all contribute to the *in vivo* effect. Given the correlation between the efficiency of MTX-protection in CHO *dhfr*$^-$ and in haematopoietic stem cells for a given MTX-resistant mutant,[43,52] we are currently investigating the potential for the most highly MTX-resistant combinatorial mutants to protect haematopoietic stem cells, *via* retroviral infections. Preliminary results in haematopoietic stem cells (J.P.V. *et al.,* unpublished results) suggest that, despite the fact that mutant AVH confers a high level of MTX-resistance, it is not our most effective mutant at conferring resistance in that specific *in vivo* context. This underscores the difficulty of identifying an *in vitro* indicator for ranking *in vivo* effects, and supports further identification of a variety of MTX-resistant hDHFR variants for application in different contexts.

MATERIALS AND METHODS

Reagents

Restriction and DNA modifying enzymes were purchased from MBI Fermentas (Burlington, ON). Folic acid, methotrexate, β-NADPH, adenine, deoxyadenine and thymidine were purchased from Sigma-Aldrich (Oakville, ON). Dihydrofolic acid (DHF) was synthesized from folic acid as described.[53] Ni-NTA was purchased from Qiagen (Mississauga, ON). Cell culture media and reagents were purchased from Invitrogen

(Burlington, ON), with the exception of dialyzed fetal bovine serum (FBS), which was obtained from HyClone (Logan, UT), and 5-bromo-4-chloro-3-indoyl-β-D-galactopyranoside (X-Gal), which was purchased from US biological (Swampscott, MA). CHO DUKX B11 (*dhfr*-) cells were a generous gift from Ingrid Remy and Stephen W. Michnick (Université de Montréal, Montréal, QC).

Bacterial strains and plasmids

E. coli strain SS320 was used for propagation of the DNA library.[54] *E. coli* strain SK037,[39] which was used for selection and over-expression of MTX-resistant mutants, was a generous gift from Gwen S. Snapp and James C. Hu (Texas A&M University, College Station, TX). The pQE32 expression vector was purchased from Qiagen. The WT hDHFR (MRA-91) and hDHFR L22Y (MRA-90) genes contained in pBluescript vector[55] were obtained from the Malaria Research and Reference Reagent Resource center (Manassas, VA).

Oligonucleotides and DNA constructions

Standard oligonucleotide primers used for mutagenesis were purchased from Alpha DNA (Montréal, QC). Primers containing degenerate codons were purchased from Integrated DNA Technologies (Coralville, IA). Dye-labelled oligonucleotide primers for DNA sequencing were purchased from Li-Cor Biotechnology (Lincoln, NB). The external primer set 1 (primer 1A: *fwd* $^{5'}$ ACACAC*GGATCC*AAATGGTTGGTTCGCTAAACTGCATC (BamHI restriction site in italics) and primer 1B: *rev* $^{5'}$ CAATTTCACACAGGAAACAGCT) was designed for PCR amplification of the entire coding region of the WT hDHFR and hDHFR L22Y genes and subcloning into pQE32 vector between the BamHI and HindIII restriction sites. An AflII restriction site (in italics) was introduced for ulterior recombination work *via* silent mutations between codons 26 and 28 of WT hDHFR by mega-primer PCR,[56] using primer 2: *rev* $^{5'}$ TGGAAATATCTAAATTCGTTC*CTTAAG*GGTGGCCACGGCAGGT and the external primer set 1. The resulting construct, WT hDHFR-pQE32, expressed WT His_6-hDHFR

(N-terminally His_6-tagged) and served as a template for the creation of the hDHFR mutant library as well as for the creation of eukaryotic transfection DNA constructs.

Creation of the hDHFR mutant library at positions Phe31, Phe34 and Gln35

The hDHFR mutant library was created by megaprimer PCR,[56] using degenerate primers encoding a variety of amino acids at positions Phe31, Phe34 and Gln35 (see **table 2.1**) using primer 3: *rev* 5' AGAGGTTGTGGTCATTCT*SYBKRH*ATATCT*GVV*TTCGTTCCTTAAGGGTGG (degenerate codons in italics) as well as primer 1A and primer 4B: *rev* 5' GTTCTGAGGTCATTACTGG as external primers (external primer set 2). The resulting library was cloned into pQE32 using the BamHI and HindIII restriction sites and transformed in *E. coli* SS320, yielding approximately 1×10^4 colonies. The quality of the library was evaluated by sequencing the entire hDHFR gene from 70 colonies picked on Luria-Bertani (LB) medium containing 100 μg/mL ampicillin (LA-100; non-selective conditions). Sequencing was performed by the dideoxy-chain termination method using a Thermo Sequenase Cycle Sequencing kit (GE Healthcare, Piscataway, NJ) and a dye-labelled primer with a Li-Cor 4200 automated sequencer (Lincoln, NB).

Selection and identification of highly MTX-resistant mutants

Plasmid DNA from the pooled hDHFR mutant library was isolated and transformed into electrocompetent *E. coli* SK037 cells for selection. The cells were plated in equal dilutions on LA-100 (non-selective) or on M9 minimal medium containing 0.08% (w/v) casamino acids, 100 μg/mL ampicillin, 1 μg/mL trimethoprim (TMP) and 1 mM MTX (dissolved in 0.05M KOH) (ATM-1000 medium; selective conditions). Colony formation took place at 37°C for 16 hrs on the non-selective medium and for 36 hrs on the selective medium. The survival rate of the library was calculated from the ratio of colonies formed on selective ATM-1000 relative to non-selective LA-100 medium. Seventy colonies were picked on ATM-1000 media, and the plasmid DNA was sequenced to identify mutations at positions 31, 34 and 35. In all cases, the entire coding sequence was verified.

Expression and purification of selected hDHFR variants

For expression of both WT His_6-hDHFR and MTX-resistant mutants identified by selection, the plasmids of interest were isolated and retransformed into *E. coli* SK037 cells. Overnight cultures were used to inoculate 50 mL of LB media and were propagated at 37°C until $A_{600\ nm} \approx 0.7$. Protein expression was induced with the addition of 1 mM isopropyl 1-thio-β-D-galactopyranoside (IPTG), after which cells were further propagated for 3 hrs at 37°C. Induced cells were harvested by centrifugation (4000*g* for 30 min at 4°C). The cell pellet was resuspended in 0.1M potassium phosphate buffer (pH 8.0), 5 mM imidazole. The cells were lysed on ice using a Branson sonicator (three pulses at 200 W for 30 s with a tapered micro-tip). Cellular debris were pelleted by centrifugation (4000*g* for 30 min at 4 °C) and 1 mL of pre-equilibrated Ni-NTA resin (Qiagen) was added to the supernatant. The slurry was mixed by inversion at 4°C for 1 h, after which it was transferred to a column (Bio-Rad Polyprep Chromatography columns, 0.8 x 4 cm) for gravity-flow purification. The column was washed with 5 mL each of 0.1M phosphate buffers (pH 8.0) containing increasing concentrations of imidazole (5, 10, 15 and 20 mM). Elution of bound protein was achieved using 2 mL of 0.1M phosphate buffer (pH 7.5), 50 mM imidazole. Eluted protein was dialyzed overnight against 0.1M phosphate buffer (pH 7.5) at 4°C for 16 hrs. Expression pattern and purity of enzymes were evaluated using the public domain image analysis software Scion Image (NIH, rsb.info.nih.gov/nih-image) following separation by SDS-PAGE (15% (w/v) polyacylamide gel) stained by the zinc-imidazole method.[57] Protein concentration was determined using the Bradford assay (Bio-Rad, Hercules, CA).

Determination of kinetic and inhibition parameters

All kinetic and inhibition assays were conducted in MATS buffer (25 mM Mes, 25 mM acetate, 50 mM Tris, 100 mM sodium acetate and 0.02% (w/v) sodium azide) (pH 7.6) at 23°C. Substrates were dissolved in MATS buffer and quantified by spectrophotometry ($\varepsilon_{340\ nm} = 6200\ M^{-1}cm^{-1}$ for NADPH and $\varepsilon_{282\ nm} = 28{,}400\ M^{-1}cm^{-1}$ for DHF). MTX was dissolved in 0.05M KOH and quantified by spectrophotometry in 0.1M NaOH using $\varepsilon_{258\ nm} = 22\ 100\ M^{-1}cm^{-1}$ and $\varepsilon_{302\ nm} = 23\ 300\ M^{-1}cm^{-1}$. Kinetic parameters for the hDHFR mutants were determined with a Cary 100 Bio UV/Vis spectrophotometer

(Varian Canada Inc., Montréal, QC) by monitoring the NADPH and DHF depletion ($\Delta\varepsilon_{340\ nm}$ = 12 800 $M^{-1}cm^{-1}$)[58] in 1-cm cells with 10 nM enzyme, unless otherwise stated. All assays were performed in at least 4 independent experiments and the average values are reported. The initial rates during the first 15% of substrate conversion were recorded for all assays. Kinetic and inhibition parameters were obtained from a non-linear regression fit to the Michaelis-Menten equation using Graphpad Prism (Graphpad Software, San Diego, CA). The k_{cat} values were determined in presence of saturating substrate concentrations (100 μM each of DHF and NADPH) in 1-cm cells according to $k_{cat} = V_{max}/[E]$. K_M values for DHF (K_M^{DHF}) for the MTX-resistant mutants were determined in presence of 20 μM NADPH by varying the concentration of DHF (0.5 μM to 20 μM). For WT His_6-hDHFR, K_M^{DHF} was obtained by spectrophotometric determination in 10-cm cells containing 1 nM enzyme, 10 μM NADPH and a range of DHF concentrations (0.05 μM to 10 μM). The kinetic parameters of two mutants determined in 1-cm cells were also confirmed in 10-cm cells. IC_{50}^{MTX} for WT His_6-hDHFR and mutants were determined in presence of saturating concentrations of substrates (100 μM each of DHF and NADPH) and increasing concentrations of MTX (0.025 μM to 100 μM). Inhibition constants for MTX (K_i^{MTX}) were calculated from the determined IC_{50}^{MTX} according to the equation for competitive inhibitor binding.[59]

Determination of equilibrium dissociation constants

Ternary equilibrium dissociation constants for MTX (K_D^{MTX}) were determined in a 1-cm path-lenght quartz cell using a Cary Eclipse Bio fluorometer (Varian Canada Inc., Montréal, QC), by titrating the fluorescence quenching resulting from formation of the enzyme-ligand complex with increasing concentrations of MTX. For each variant tested, enzyme and NADPH were mixed at final concentrations of 200 nM and 5 μM (saturating concentration), respectively, and serial additions of MTX were added (0 to 1600 nM) in a final volume of 3 mL. The total volume of added MTX represented approximately 10% of the entire sample volume. After each addition of MTX, the solution was mixed with a magnetic stirrer for 2 minutes. Fluorescence quenching was monitored at λ_{ex} = 280 nm and λ_{em} = 435 nm. All assays were performed in at least 3 independent experiments, and

the average values are reported. The K_D^{MTX} values for each variant were obtained by fitting relative fluorescence (ΔF) to the following equation:[60]

$$\Delta F = \frac{\Delta F_{\max}\left([hDHFR]_0 + [MTX] + K_D - \sqrt{([hDHFR]_0 + [MTX] + K_D)^2 - (4[hDHFR]_0[MTX])}\right)}{2[hDHFR]_0}$$

Molecular modelling

Molecular modelling was performed using the InsightII package (version 2000, Accelerys), with 1U72.pdb (WT hDHFR with bound MTX and NADPH)[7] as starting coordinates. Following removal of the crystallographic water molecules, the BIOPOLYMER module was used to mutate residues 31, 34 and 35 and to add hydrogen atoms at the normal ionization state of amino acids at pH 7. Energy minimization of the enzyme-ligand complex was performed using 1000 steps of steepest descents minimization, followed by a conjugate gradient minimization until convergence of 0.001 kcal/mol/Å. Minimizations were performed with no constraints, using a dielectric constant of 80 and a cut-off value of 100 Å.

Protection of eukaryotic cells with MTX-resistant hDHFRs

Genes encoding the MTX-resistant mutants with the highest K_i^{MTX} values were amplified by PCR with primer 5A: *fwd* $^{5'}$ ACACAC*GAATTC*ATCCACCATGGTTGGTTCGCTAAACTGCAT and primer 5B: *rev* $^{5'}$ ACACAC*CTCGAG*AGCTTAATCATTCTTCTC and sub-cloned into pcDNA3.1 (+)-Zeo (Invitrogen) using the *Eco*RI and *Xho*I restriction sites (in italics). The WT and L22Y hDHFR genes were also amplified and cloned as described above, to serve as negative and positive controls for MTX resistance, respectively. The resulting constructs do not encode a His_6 tag. A mock transfection with pcDNA3.1 (+)-Zeo also served as a negative control. Cells were stained using trypan blue and counted using a Bright-Line hemacytometer (American Optical Corporation, Buffalo, NY). CHO DUKX B11 cells were propagated at 37°C, 5% CO_2 (v/v) in 10-cm plates and passaged every 48 h at 1.5 × 10^6 cells per plate in α-MEM containing 10% (v/v) dialyzed FBS, 4 mM glutamine, 10 μg/mL each of adenine, deoxyadenosine and thymidine, 100 units/mL penicillin and 100 μg/mL streptomycin (complete α-MEM medium). For passages, cells were washed twice

with 1 × PBS and trypsinized for 5 min at 37 °C. Before transfection, 5×10^5 cells at passage 10 or less were propagated for 18 h on 10-cm plates (70% confluence). A 3µg sample of plasmid DNA was mixed with 20 µL of Lipofectamine 2000 (Invitrogen) and incubated at room temperature for 45 min in 800 µL Opti-MEM. The mixture was added to the cells, which were further incubated at 37 °C with 5% CO_2 for 4 h. The transfection media was replaced by α-MEM media for 36 h. The transfected cells were split into 6 cm plates containing approximately 1×10^5 cells. The cells were exposed to different concentrations of MTX (0 - 200 µM) in α-MEM media in the absence of adenine, deoxyadenine and thymidine. As a reference, the same number of cells was plated in complete α-MEM medium. The stock solution (2 mM MTX) was prepared in 0.05M KOH to ensure dissolution; MTX could not be added at a higher concentration than 200 µM as this marked the limit of the buffering capacity of the medium. The cells were counted after 48 h. Transfection efficiency was evaluated first by transfecting the *lacZ* reporter gene (pBabe-LacZ)[61] and by counting the number of blue cells in the presence of X-Gal; and secondly by comparing the number of cells in absence and in presence of nucleotides in the media. The percentage of cell survival is given as the ratio of cells counted in the presence or in the absence of MTX (in absence of nucleotides). EC_{50}^{MTX} were generated with a non-linear sigmoidal fit using Graphpad Prism software. All MTX-resistance studies were performed in at least 3 independent experiments and the average EC_{50}^{MTX} values are reported. Expression of hDHFR variants was verified by Western blotting, following resolution of supernatant from transfected CHO DUKX B11 cells by SDS-PAGE (15% (w/v) polyacrylamide gel) and semi-dry transfer on PVDC membrane. The membranes were blocked with 5% (w/v) powdered milk before overnight incubation at 4 ºC with primary polyclonal anti-mDHFR antibody from rabbit. Membranes were washed twice with PBS, 0.5% (v/v) Tween before incubation for 1 h at 4 °C with the secondary monoclonal anti-rabbit-alkaline phosphatase coupled antibody (Sigma-Aldrich). Protein bands were revealed with BCIP/NBT (Sigma-Aldrich) for 10 min at room temperature.

Table 2.1. Amino acids encoded at residues 31, 34 and 35 of the hDHFR mutant library

Native residue	Encoded amino acids	Justification
F31	**F**, **A**, **G**, **R**,**S**, C, L, P, V	Reducing contact surface with inhibitor
F34	**F**, **A**, **I**, **S**, **T**, **Q** L	Reducing contact surface with inhibitor
Q35	**Q**, **D**, **G**, **N**, **R**, **S**, E, H, K,	Changing helical propensity

Wild-type residues at positions 31, 34 and 35 are underlined. Intended substitutions are in bold. The remaining amino acids were encoded as a result of the degeneracy of the genetic code.

Table 2.2. Kinetic and inhibition constants for the selected MTX-resistant hDHFR mutants

Enzyme[a]	k_{cat} (s^{-1})	K_M^{DHF} (μM)	k_{cat}/K_M^{DHF} (s^{-1} μM^{-1})	IC_{50}^{MTX} (nM)	K_i^{MTX} (nM)	K_D^{MTX} [b] (nM)
WT (FFQ)	10±2	≤0.075	≥140	41±14	≤0.031	<2
Point mutant						
F31P (PFQ)	6.4±1.0	1.5±0.30	4.3	110±40	1.7±0.6	<2
Double mutants						
GFN	4.3±1.0	1.7±0.39	2.6	570±180	9±3	16±5
PFH	1.7±0.12	2.1±0.51	0.80	470±70	10±1	6.9±1.4
PFE	1.7±0.05	2.7±0.63	0.60	470±170	12±4	4.1±1.6
RFE	1.3±0.17	0.69±0.13	1.9	3100±1600	21±11	21±0.2
SFE	9.4±0.31	3.3±0.70	2.8	930±340	30±11	25±4
Triple mutants						
RAN	0.50±0.06	2.2±0.62	0.20	550±80	12±2	<2
RTS	1.0±0.09	1.7±0.27	0.60	4500±2500	59±26	110±12
RTR	1.0±0.10	2.0±0.25	0.50	3500±1600	86±49	11±0.9
AVH	1.1±0.39	4.3±1.3	0.30	4400±1700	180±69	150±44

[a] hDHFR variants are designated by the one-letter code of the amino acids occurring at positions 31, 34 and 35.
[b] K_D^{MTX} for the ternary complex.

Table 2.3. *EC_{50}* MTX for CHO DUKX B11 cells transfected with MTX-resistant hDHFR mutants

Transfected variant	EC_{50}^{MTX} (μM)
Null	0
WT	0.054
L22Y	12
RFE	31
SFE	32
RTS	56
AVH	>200

Combinatorial mutants are designated by the one-letter code of the amino acids occurring at positions 31, 34 and 35.

Table 2.4. Comparison of MTX-resistant hDHFR mutated at positions F31 and F34

hDHFR variant	K_i^{MTX} (nM)	k_{cat}/K_M^{DHF} ($\mu M^{-1} s^{-1}$)	Reference
WT (FFQ)	≤0.031	≥140	This work
L22Y[a]	11	10	29
F31X			
F31S	0.24	16	14
F31A	0.27	30	14
F31G	0.35	26	14
F31P (PFQ)	1.7	4.3	This work
F31R	7.2	1.5	41
F34X			
F34T	9.6[b]	0.11	10
F34V	10[b]	0.49	10
F34A	34[b]	0.24	10
Combinatorial mutants[c]			
GFN	9	2.6	This work
RAN	12	0.2	″
RFE	21	1.9	″
SFE	30	2.8	″
RTS	59	0.6	″
RTR	86	0.5	″
AVH	180	0.3	″

[a] Variant L22Y was used as a positive control for MTX resistance.
[b] Values of ternary K_D^{MTX}.
[c] Combinatorial mutants are designated by the one-letter code of the amino acids occurring at positions 31, 34 and 35.

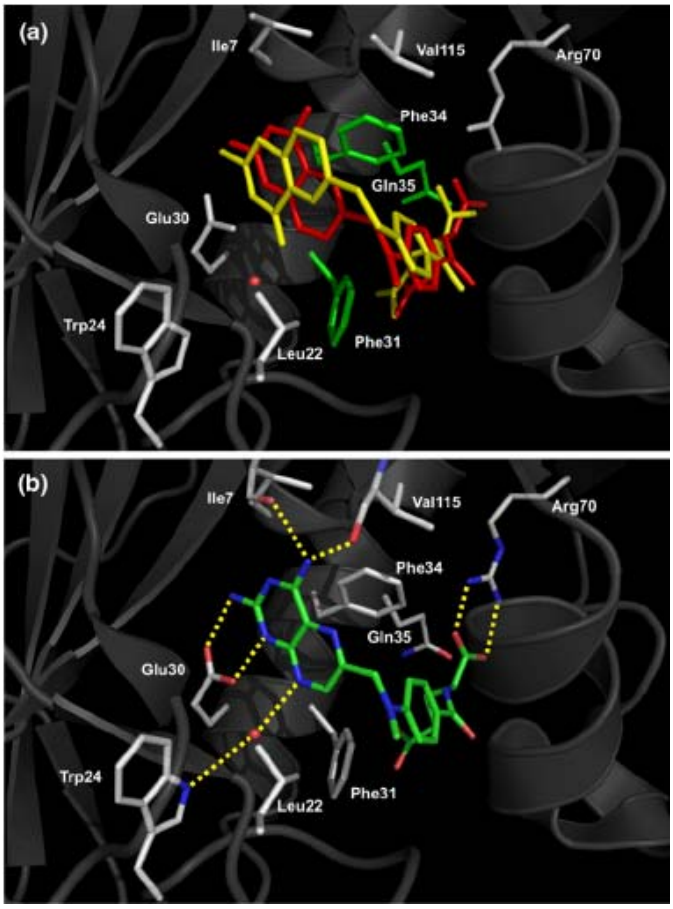

Figure 2.1. Ligand binding at the active-site of WT hDHFR. A: Superimposition of hDHFR with bound folate (yellow; 1DRF.pdb[62]) and its competitive inhibitor methotrexate (red; 1U72.pdb[7]). The active site is shown, highlighting the flip of the bicyclic pteroyl ring. Stick representations of side-chains from Ile7, Leu22, Trp24, Glu30, Arg70 and Val115 are shown in white. The residues targeted for mutation, Phe31, Phe34 and Gln35, are in green. A conserved active-site water molecule is depicted as a red sphere. **B:** Hydrogen bonding network of bound MTX at the active site of hDHFR. Side-chains and MTX are in sticks representation, coloured by atom (nitrogen (blue), oxygen (red) and carbon (white for side chains and green for MTX)). A conserved active-site water molecule is depicted as a red sphere. For clarity, only the coordinates of 1U72.pdb are represented.

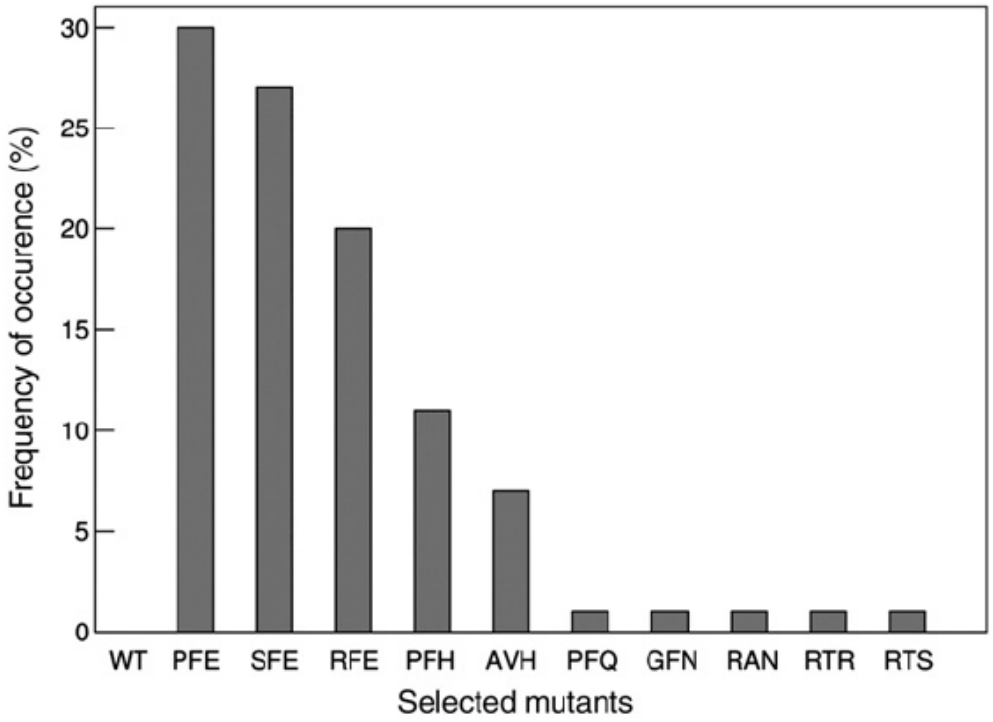

Figure 2.2. Frequency of occurrence of the novel MTX-resistant mutants. Seventy mutants were isolated following selection of the hDHFR mutant library on ATM-1000 medium. Mutants are designated by the one-letter code of the amino acid occurring at positions 31, 34 and 35, respectively. Mutant PFQ corresponds to point mutant F31P.

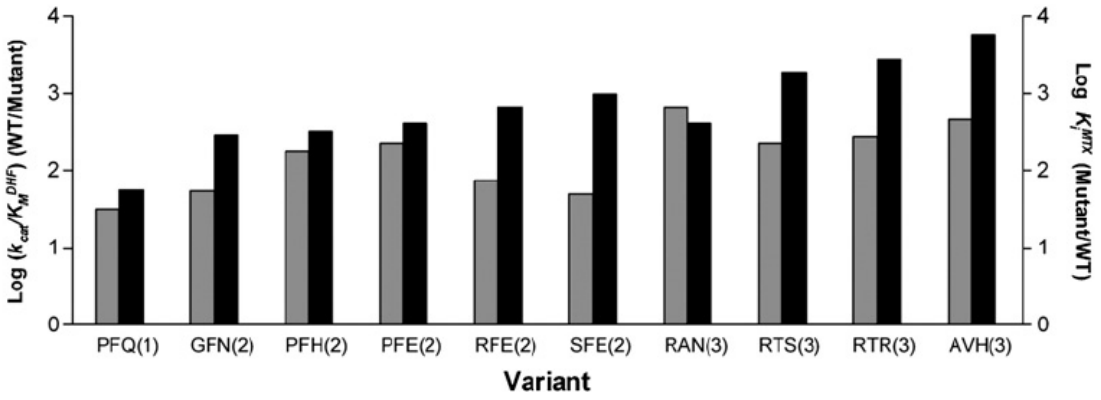

Figure 2.3. Relation between the number of hDHFR mutations and k_{cat}/K_M^{DHF} or K_i^{MTX} relative to WT His_6-hDHFR. Mutants are designated by the one-letter code of the amino acid occurring at positions 31, 34 and 35, respectively. Numbers in parentheses correspond to the number of mutations in the variant. Log k_{cat}/K_M^{DHF} relative to WT is shown in grey while log K_i^{MTX} relative to WT is in black.

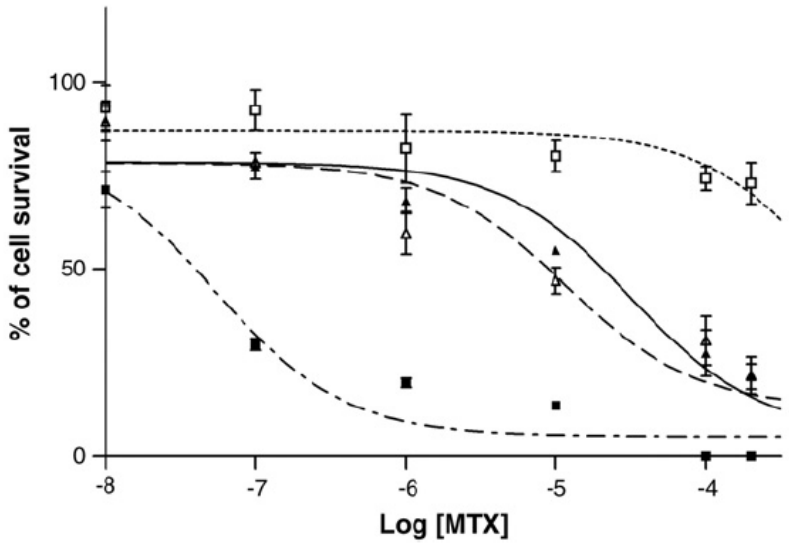

Figure 2.4. Survival of CHO DUKX B11 cells transfected with selected mutants in presence of MTX. Data is presented for two representative mutants: double mutant SFE (—▲—) and triple mutant AVH (····□····). The positive control L22Y (- -△- -) and the negative control WT hDHFR (.-.■.-.) are given as references. SFE and AVH are designated by the one-letter code of the amino acid occurring at positions 31, 34 and 35, respectively. Percentage of cell survival represents the ratio of cells counted in presence and absence of MTX after 48hrs at 37ºC, 5% CO_2.

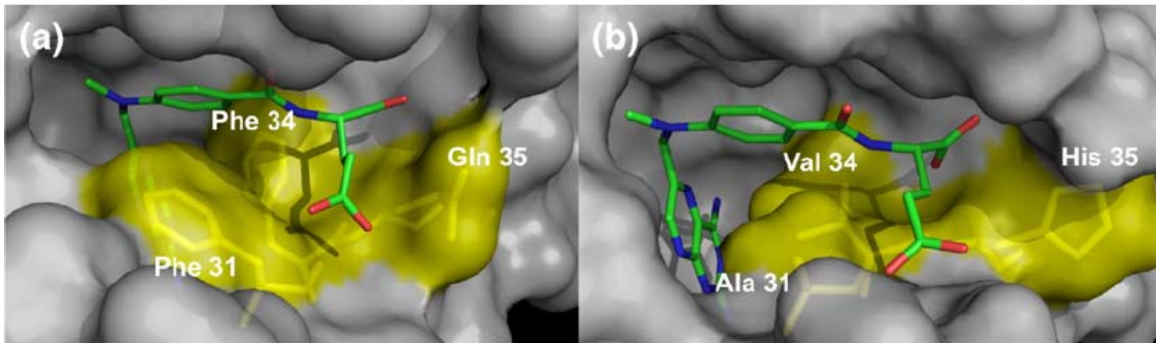

Figure 2.5. *In silico* comparison of MTX binding between (A) WT hDHFR (1U72) and (B) mutant AVH. Protein structures are shown in surface representation with residues 31, 34 and 35 coloured yellow, and MTX coloured by atom (nitrogen, blue; oxygen, red; and carbon, green), in sticks representation. AVH coordinates were obtained by mutating residues 31, 34, 35 using PDB file 1U72 as starting coordinates, followed by minimization in presence of bound MTX and NADPH. NADPH is not shown.

REFERENCES

1. Chu, E. & Allegra, C. J. (1996). Antifolates. *In Cancer Chemotherapy and Biotherapy* (Chabner, B. A. & Longo, D. L., eds.), 2nd edit., pp. 149-212. Lippincott-Raven, Philadelphia, PA.
2. Mennes, M., Stiers, P., Vandenbussche, E., Vercruysse, G., Uyttebroeck, A., De Meyer, G. & Van Cool, S. W. (2005). Attention and information processing in survivors of childhood acute lymphoblastic leukemia treated with chemotherapy only. *Pediatr. Blood Cancer* **44**, 478-486.
3. Daw, N. C., Billups, C. A., Rodriguez-Galindo, C., McCarville, M. B., Rao, B. N., Cain, A. M., Jenkins, J. J., Neel, M. D. & Meyer, W. H. (2006). Metastatic osteosarcoma. *Cancer* **106**, 403-412.
4. Slamon, D. J., Romond, E. H. & Perez, E. A. (2006). Advances in adjuvant therapy for breast cancer. *Clin. Adv. Hematol. Oncol.* **4**(Suppl. 7), 4-9.
5. Strojan, P., Soba, E., Budihna, M. & Auersperg, M. (2005). Radiochemotherapy with Vinblastine, Methotrexate, and Bleomycin in the treatment of verrucous carcinoma of the head and neck. *J. Surg. Oncol.* **92**, 278-283.
6. Appleman, J. R., Prendergast, N., Delcamp, T. J., Freisheim, J. H. & Blakley, R. L. (1988). Kinetics of the formation and isomerization of methotrexate complexes of recombinant human dihydrofolate reductase. *J. Biol. Chem.* **263**, 10304-10313.
7. Cody, V., Luft, J. R. & Pangborn, W. (2005). Understanding the role of Leu22 variants in methotrexate resistance: comparison of wild-type and Leu22Arg variant mouse and human dihydrofolate reductase ternary crystal complexes with methotrexate and NADPH. *Acta Crystallogr. Sect. D.* **61**, 147-155.
8. Meiering, E. M., Li, H., Delcamp, T. J., Freisheim, J. H. & Wagner, G. (1995). Contributions of tryptophan 24 and glutamate 30 to binding long-lived water molecules in the ternary complex of human dihydrofolate reductase with methotrexate and NADPH studied by site-directed mutagenesis and nuclear magnetic resonance spectroscopy. *J. Mol. Biol.* **247**, 309-325.

9. Ercikan, E., Waltham, M., Dicker, A., Schweitzer, B. & Bertino, J. R. (1993). Effect of codon 22 mutations on substrate and inhibitor binding for human dihydrofolate reductase. *Advan. Expt. Med. Biol.* **338**, 515-519.

10. Nakano, T., Spencer, H. T., Appleman, J. R. & Blakley, R. L. (1994). Critical role of phenylalanine 34 of human dihydrofolate reductase in substrate and inhibitor binding and in catalysis. *Biochemistry* **33**, 9945-9952.

11. Schweitzer, B. I., Srimatkandada, S., Gritsman, H., Sheridan, R., Venkataraghavan, R. & Bertino, J. R. (1989). Probing the role of two hydrophobic active site residues in the human dihydrofolate reductase by site-directed mutagenesis. *J. Biol. Chem.* **264**, 20786-20795.

12. Thompson, P. D. & Freisheim, J. H. (1991). Conversion of arginine to lysine at position 70 of human dihydrofolate reductase: generation of a methotrexate-insensitive mutant enzyme. *Biochemistry* **30**, 8124-8130.

13. Blakley, R. L., Appleman, J. R., Chunduru, S. K., Nakano, T., Lewis, W. S. & Harris, S. E. (1993). Mutations of human dihydrofolate reductase causing decreased inhibition by methotrexate. *Advan. Expt. Med. Biol.* **338**, 473-479.

14. Chunduru, S. K., Cody, V., Luft, J. R., Pangborn, W., Appleman, J. R. & Blakley, R. L. (1994). Methotrexate-resistant variants of human dihydrofolate reductase. Effects of Phe31 substitutions. *J. Biol. Chem.* **269**, 9547-9555.

15. Lewis, W. S., Cody, V., Galitsky, N., Luft, J. R., Pangborn, W., Chunduru, S. K., Spencer, H. T., Appleman, J. R. & Blakley, R. L. (1995). Methotrexate-resistant variants of human dihydrofolate reductase with substitutions of leucine 22. Kinetics, crystallography, and potential as selectable markers. *J. Biol. Chem.* **270**, 5057-5064.

16. Ercikan-Abali, E. A., Waltham, M. C., Dicker, A. P., Schweitzer, B. I., Gritsman, H., Banerjee, D. & Bertino, J. R. (1996). Variants of human dihydrofolate reductase with substitutions at leucine-22: effect on catalytic and inhibitor binding properties. *Mol. Pharmacol.* **49**, 430-437.

17. Thillet, J., Absil, J., Stone, S. R. & Pictet, R. (1988). Site-directed mutagenesis of mouse dihydrofolate reductase. Mutants with increased resistance to methotrexate and trimethoprim. *J. Biol. Chem.* **263**, 12500-12508.

18. Melera, P. W., Davide, J. P. & Oen, H. (1988). Antifolate-resistant Chinese hamster cells. Molecular basis for the biochemical and structural heterogeneity among dihydrofolate reductases produced by drug-sensitive and drug-resistant cell lines. *J. Biol. Chem.* **263**, 1978-1990.

19. Srimatkandada, S., Schweitzer, B. I., Moroson, B. A., Dube, S. & Bertino, J. R. (1989). Amplification of a polymorphic dihydrofolate reductase gene expressing an enzyme with decreased binding to methotrexate in a human colon carcinoma cell line, HCT-8R4, resistant to this drug. *J. Biol. Chem.* **264**, 3524-3528.

20. Dicker, A. P., Waltham, M. C., Volkenandt, M., Schweitzer, B. I., Otter, G. M., Schmid, F. A., Sirotnak, F. M. & Bertino, J. R. (1993). Methotrexate resistance in an in vivo mouse tumor due to a non-active-site dihydrofolate reductase mutation. *Proc. Natl. Acad. Sci. USA* **90**, 11797-11801.

21. Chunduru, S. K., Appleman, J. R. & Blakley, R. L. (1993). Kinetic investigation of methotrexate resistant human dihydrofolate reductase (hDHFR) mutants at Phe31. *Advan. Expt. Med. Biol.* **338**, 507-510.

22. Wyss, P. C., Gerber, P., Hartman, P. G., Hubschwerlen, C., Locher, H., Marty, H. P. & Stahl, M. (2003). Novel dihydrofolate reductase inhibitors. Structure-based versus diversity-based library design and high-throughput synthesis and screening. *J. Med. Chem.* **46**, 2304-2312.

23. Spencer, H. T., Sorrentino, B. P., Pui, C. H., Chunduru, S. K., Sleep, S. E. & Blakley, R. L. (1996). Mutations in the gene for human dihydrofolate reductase: an unlikely cause of clinical relapse in pediatric leukemia after therapy with methotrexate. *Leukemia* **10**, 439-446.

24. Lynch, G., Magill, G. B., Sordillo, P. & Golbey, R. B. (1982). Combination chemotherapy of advanced sarcomas in adults with "CYOMAD" (S7). *Cancer* **50**, 1724-1727.

25. Sauerbrey, A., McPherson, J. P., Zhao, S. C., Banerjee, D. & Bertino, J. R. (1999). Expression of a novel double-mutant dihydrofolate reductase-cytidine deaminase fusion gene confers resistance to both methotrexate and cytosine arabinoside. *Hum. Gene Ther.* **10**, 2495-2504.

26. Capiaux, G. M., Budak-Alpdogan, T., Alpdogan, O., Bornmann, W., Takebe, N., Banerjee, D., Maley, F. & Bertino, J. R. (2004). Protection of hematopoietic stem cells from pemetrexed toxicity by retroviral gene transfer with a mutant dihydrofolate reductase-mutant thymidylate synthase fusion gene. *Cancer Gene Ther.* **11**, 767-773.

27. Zhao, S. C., Banerjee, D., Mineishi, S. & Bertino, J. R. (1997). Post-transplant methotrexate administration leads to improved curability of mice bearing a mammary tumor transplanted with marrow transduced with a mutant human dihydrofolate reductase cDNA. *Hum. Gene Ther.* **8**, 903-909.

28. May, C., Gunther, R. & McIvor, R. S. (1995). Protection of mice from lethal doses of methotrexate by transplantation with transgenic marrow expressing drug-resistant dihydrofolate reductase activity. *Blood* **86**, 2439-2448.

29. Ercikan-Abali, E. A., Mineishi, S., Tong, Y., Nakahara, S., Waltham, M. C., Banerjee, D., Chen, W., Sadelain, M. & Bertino, J. R. (1996). Active site-directed double mutants of dihydrofolate reductase. *Cancer Res.* **56**, 4142-4145.

30. Rui, L., Cao, L., Chen, W., Reardon, K. F. & Wood, T. K. (2005). Protein engineering of epoxide hydrolase from Agrobacterium radiobacter AD1 for enhanced activity and enantioselective production of (R)-1-phenylethane-1,2-diol. *Appl. Environ. Microbiol.* **71**, 3995-4003.

31. Schmitzer, A. R., Lepine, F. & Pelletier, J. N. (2004). Combinatorial exploration of the catalytic site of a drug-resistant dihydrofolate reductase: creating alternative functional configurations. *Protein Eng. Des. Sel.* **17**, 809-819.

32. Santoro, S. W. & Schultz, P. G. (2002). Directed evolution of the site specificity of Cre recombinase. *Proc. Natl. Acad. Sci. USA* **99**, 4185-4190.

33. Tsutsui, H., Karasawa, S., Shimizu, H., Nukina, N. & Miyawaki, A. (2005). Semi-rational engineering of a coral fluorescent protein into an efficient highlighter. *EMBO Rep.* **6**, 233-238.

34. Shaner, N. C., Campbell, R. E., Steinbach, P. A., Giepmans, B. N., Palmer, A. E. & Tsien, R. Y. (2004). Improved monomeric red, orange and yellow fluorescent proteins derived from Discosoma sp. red fluorescent protein. *Nature Biotechnol.* **22**, 1567-1572.

35. Davies, J. F., 2nd, Delcamp, T. J., Prendergast, N. J., Ashford, V. A., Freisheim, J. H. & Kraut, J. (1990). Crystal structures of recombinant human dihydrofolate reductase complexed with folate and 5-deazafolate. *Biochemistry* **29**, 9467-9479.

36. Williams, E. A. & Morrison, J. F. (1992). Human dihydrofolate reductase: reduction of alternative substrates, pH effects, and inhibition by deazafolates. *Biochemistry* **31**, 6801-6811.

37. Klon, A. E., Heroux, A., Ross, L. J., Pathak, V., Johnson, C. A., Piper, J. R. & Borhani, D. W. (2002). Atomic structures of human dihydrofolate reductase complexed with NADPH and two lipophilic antifolates at 1.09 Å and 1.05 Å resolution. *J. Mol. Biol.* **320**, 677-693.

38. Chou, P. Y. & Fasman, G. D. (1974). Prediction of protein conformation. *Biochemistry* **13**, 222-245.

39. Kopytek, S. J., Dyer, J. C., Knapp, G. S. & Hu, J. C. (2000). Resistance to methotrexate due to AcrAB-dependent export from *Escherichia coli*. *Antimicrob. Agents Chemother.* **44**, 3210-3212.

40. Prendergast, N. J., Delcamp, T. J., Smith, P. L. & Freisheim, J. H. (1988). Expression and site-directed mutagenesis of human dihydrofolate reductase. *Biochemistry* **27**, 3664-3671.

41. Patel, M., Sleep, S. E., Lewis, W. S., Spencer, H. T., Mareya, S. M., Sorrentino, B. P. & Blakley, R. L. (1997). Comparison of the protection of cells from antifolates by transduced human dihydrofolate reductase mutants. *Hum. Gene Ther.* **8**, 2069-2077.

42. Thillet, J. & Pictet, R. (1990). Transfection of DHFR- and DHFR+ mammalian cells using methotrexate-resistant mutants of mouse dihydrofolate reductase. *FEBS Letters* **269**, 450-453.

43. Banerjee, D., Schweitzer, B. I., Volkenandt, M., Li, M. X., Waltham, M., Mineishi, S., Zhao, S. C. & Bertino, J. R. (1994). Transfection with a cDNA encoding a Ser31 or Ser34 mutant human dihydrofolate reductase into Chinese hamster ovary and mouse marrow progenitor cells confers methotrexate resistance. *Gene* **139**, 269-274.

44. Banerjee, D., Zhao, S. C., Tong, Y., Steinherz, J., Gritsman, K. & Bertino, J. R. (1994). Transfection of a nonactive site mutant murine DHFR cDNA (the tryptophan 15 mutant) into Chinese hamster ovary and mouse marrow progenitor cells imparts MTX resistance *in vitro*. *Cancer Gene Ther.* **1**, 181-184.

45. Aharoni, A., Gaidukov, L., Khersonsky, O., Mc, Q. G. S., Roodveldt, C. & Tawfik, D. S. (2005). The 'evolvability' of promiscuous protein functions. *Nature Genet.* **37**, 73-76.

46. Cody, V., Luft, J. R., Pangborn, W. & Gangjee, A. (2003). Analysis of three crystal structure determinations of a 5-methyl-6-N-methylanilino pyridopyrimidine antifolate complex with human dihydrofolate reductase. *Acta Crystallogr. sect. D.* **59**, 1603-1609.

47. Cody, V., Galitsky, N., Luft, J. R., Pangborn, W. & Gangjee, A. (2003). Analysis of two polymorphic forms of a pyrido[2,3-d]pyrimidine N9-C10 reversed-bridge antifolate binary complex with human dihydrofolate reductase. *Acta Crystallogr. Sect. D.* **59**, 654-661.

48. Mildvan, A. S. (2004). Inverse thinking about double mutants of enzymes. *Biochemistry* **43**, 14517-14520.

49. Baccanari, D. P., Stone, D. & Kuyper, L. (1981). Effect of a single amino acid substitution on *Escherichia coli* dihydrofolate reductase catalysis and ligand binding. *J. Biol. Chem.* **256**, 1738-1747.

50. Chothia, C. (1976). The nature of the accessible and buried surfaces in proteins. *J. Mol. Biol.* **105**, 1-12.

51. Blakley, R. L. & Sorrentino, B. P. (1998). In vitro mutations in dihydrofolate reductase that confer resistance to methotrexate: potential for clinical application. *Hum. Mutat.* **11**, 259-263.

52. Flasshove, M., Banerjee, D., Bertino, J. R. & Moore, M. A. (1995). Increased resistance to methotrexate in human hematopoietic cells after gene transfer of the Ser31 DHFR mutant. *Leukemia,* **9(**Suppl. 1), S34-S37.

53. Blakley, R. L. (1960). Crystalline dihydropteroylglutamic acid. *Nature*, 231.

54. Sidhu, S. S., Lowman, H. B., Cunningham, B. C. & Wells, J. A. (2000). Phage display for selection of novel binding peptides. *Methods Enzymol.* **328**, 333-363.

55. Fidock, D. A. & Wellems, T. E. (1997). Transformation with human dihydrofolate reductase renders malaria parasites insensitive to WR99210 but does not affect the intrinsic activity of proguanil. *Proc. Natl. Acad. Sci. USA* **94**, 10931-10936.

56. Sarkar, G. & Sommer, S. S. (1990). The "megaprimer" method of site-directed mutagenesis. *Biotechniques* **8**, 404-407.

57. Fernandez-Patron, C., Castellanos-Serra, L. & Rodriguez, P. (1992). Reverse staining of sodium dodecyl sulfate polyacrylamide gels by imidazole-zinc salts: sensitive detection of unmodified proteins. *Biotechniques* **12**, 564-573.

58. Hillcoat, B. L., Nixon, P. F. & Blakley, R. L. (1967). Effect of substrate decomposition on the spectrophotometric assay of dihydrofolate reductase. *Anal. Biochem.* **21**, 178-189.

59. Segel, I. H. (1993). Simple inhibition systems. In *Enzyme Kinetics: Behavior and Analysis of Rapid Equilibrium and Steady-State Enzyme Systems*, pp. 100-160, John Wiley and Sons, New York.

60. Kawaura, T., Inagaki, M., Tanaka, A., Kato, M., Nishikawa, S. & Kashimura, N. (2003). Contributions of polysaccharide and lipid regions of lipopolysaccharide to the recognition by spike G protein of bacteriophage phi X174. *Biosci. Biotechnol. Biochem.* **67**, 869-876.

61. Mallette, F. A., Goumard, S., Gaumont-Leclerc, M. F., Moiseeva, O. & Ferbeyre, G. (2004). Human fibroblasts require the Rb family of tumor suppressors, but not p53, for PML-induced senescence. *Oncogene,* **23**, 91-99.

62. Oefner, C., D'Arcy, A. & Winkler, F. K. (1988). Crystal structure of human dihydrofolate reductase complexed with folate. *Eur. J. Biochem.* **174**, 377-385.

ACKNOWLEDGEMENTS

The authors thank Frédérick-Antoine Mallette and Gerardo Ferbeyre for discussions and suggestions concerning cell culture, Stéphane Roy for the use of cell culture facilities, Huy Ong for the use of a Cary 100 spectrophotometer, as well as Krista Morley, Lucie Poulin, Roberto A. Chica and Nicolas Doucet for critical reading of the

manuscript. This work was supported by Canadian Institutes of Health Research (CIHR) grant 68851.

Chapter 3 (Article 2) – Two-tier bacterial and *in vitro* selection of active and methotrexate-resistant variants of human dihydrofolate reductase

Section 3.0 – Preface

Article 2 describes the development of an efficient and rapid screening strategy to identify active and antifolate resistant mutants of hDHFR. Moreover, the article provides new information regarding the specific role of key active-site residues in binding.

Five little characterized active-site positions (Ile7, Gly15, Trp24, Arg70 and Val115) were individually mutated by saturation mutagenesis, creating small libraries (20 mutants/library) suitable for further methodological development.

The selection strategy described in chapter 2 (article 1) was sufficiently efficient to identify highly MTX-resistant mutants. However, bacterial survival under selective conditions (high concentration of MTX in this specific case) is not a direct read-out of catalytic activity *in vitro*. In fact, factors like expression level, solubility and stability can be compatible with minimal activity in an *in vivo* context (and therefore with bacterial propagation), but inadeguate for *in vitro* characterization. As a result, it may not be possible to discriminate among the variety of good and mediocre positive hits from the selection. In order to optimize the screening process for larger-scale application (analysis of large-size libraries of mutants) a lower throughput but more informative second-tier *in vitro* assay was added to screen all positive hits from bacterial selection. The assay consisted in measuring residual enzymatic activity in the presence of a concentration of inhibitor which is user-defined, where a higher concentration provides more stringent screening. The *in vitro* assay was performed directly from cell lysates (with no need for purification) using a plate reader, and also allowed determination of a quantitative descriptor for MTX-resistance (IC_{50}^{MTX}).

Moreover, we extended the flexibility of our directed evolution approach by developing a two-tier selection strategy for detection of activity (which requires DHF binding) and resistance to the antifolate pemetrexed (which requires reduced binding of the inhibitor), demonstrating the broad applicability of the strategy for studying binding of different compounds at the active-site of hDHFR.

I was responsible of the majority of the experimental work. Joelle Pelletier and I were responsible of the design of the experimental approach and the edition of the paper. Jordan Volpato was responsible of the choice of the active-site residues to be mutated, the creation of 2 of the 5 libraries of mutants created, the creation of figure 1 and of critical discussion both related to the experimental work and to the edition of the paper. Lucie Poulin performed half of DNA sequencing. David-Antoine Dugas created library 115 under my supervision. Vanessa Guerrero performed part of the screening (screening for activity and MTX-resistance of libraries 15 and 24 and part of the screening for pemetrexed resistance) under my supervision.

An *erratum corrigendum* about the kinetic and inhibition parameters of one of the hDHFR mutants characterized was added to the chapter, right after the references section.

2-TIER BACTERIAL AND *IN VITRO* SELECTION OF ACTIVE AND METHOTREXATE-RESISTANT VARIANTS OF HUMAN DIHYDROFOLATE REDUCTASE

Elena Fossati, Jordan P. Volpato,[1] Lucie Poulin,[2] Vanessa Guerrero,[1] David-Antoine Dugas[1] and Joelle N. Pelletier[1,2]

[1]Département de biochimie and [2]Département de chimie
Université de Montréal
C.P. 6128, Succursale Centre-ville
Montréal (Québec)
H3C 3J7, CANADA

J. Biomol. Screen., 2008, **13** (6), 504-514

ABSTRACT

We report a rapid and reliable 2-tier selection and screen for detection of activity as well as drug-resistance in mutated variants of a clinically-relevant drug-target enzyme. Human dihydrofolate reductase point-mutant libraries were subjected to a 1st-tier bacterial complementation assay, such that bacterial propagation served as an indicator of enzyme activity. Alternatively, when selection was performed in the presence of the inhibitor methotrexate (MTX), propagation indicated MTX resistance. The selected variants were then subjected to a 2nd-tier *in vitro* screen in 96-well plate format using crude bacterial lysate. Conditions were defined to establish a threshold for activity or for MTX resistance. The 2nd-tier assay allowed rapid detection of the best variants among the leads and provided reliable estimates of relative reactivity, (k_{cat}) and IC_{50}^{MTX}. Screening saturation libraries of active-site positions 7, 15, 24, 70 and 115 revealed a variety of novel mutations compatible with reactivity as well as 2 novel MTX-resistant variants: V115A and V115C. Both variants displayed K_i^{MTX} = 20 nM, a 600-fold increase relative to the wild-type. We also present preliminary results from screening against further antifolates following simple modifications of the protocol. The flexibility and robustness of this method will provide new insights into interactions between ligands and active-site residues of this clinically relevant human enzyme.

Key words: Human dihydrofolate reductase, methotrexate, drug resistance, saturation mutagenesis, high-throughput screening

INTRODUCTION

Dihydrofolate reductase (DHFR, EC 1.5.1.3) catalyzes the NADPH-dependent reduction of 7,8-dihydrofolate (DHF) to 5,6,7,8-tetrahydrofolate (THF), an essential metabolite involved in the biosynthesis of purines and thymidylate.[1] Due to its crucial role in cell proliferation, human DHFR (hDHFR) has long been a target in the treatment of psoriasis,[2] rheumatoid arthritis[2,3] and neoplastic diseases.[4] A specific competitive inhibitor of hDHFR, the antifolate methotrexate (MTX), has been extensively used to

treat various cancers.[4] Limitations to cancer treatment with MTX include lack of specificity for cancerous cells[1] and development of drug resistance.[5]

Among the recognized MTX-resistance mechanisms,[5] we are specifically interested in mutations that weaken MTX binding. Despite their structural similarity, the substrate DHF and the inhibitor MTX bind to the active site in different orientations, making different contacts with the enzyme.[6,7] Active-site mutations may thus reduce MTX binding while maintaining sufficient DHF affinity for catalysis.[8-10] Gaining a better understanding of substrate and inhibitor binding at the hDHFR active site by characterizing ligand binding in active-site variants will offer insight toward the synthesis of alternative antifolates.[4,10] In a clinical context, MTX-resistant hDHFR variants can offer protection of haematopoietic stem cells from the cytotoxicity of MTX *via* gene therapy.[11] Furthermore, MTX-resistant hDHFR variants show excellent potential as selectable markers for gene transfer in stem cells, improving the outcome of gene therapy.[11] For these applications, ideal hDHFR variants should possess a high K_i for MTX (weak binding) and efficient catalytic properties (low K_M^{DHF} and high k_{cat}) in addition to good stability, solubility and high expression levels.

We previously performed directed evolution to identify highly MTX-resistant variants of hDHFR from a combinatorial library of mutants using a rapid bacterial selection strategy.[8] The strategy relies on the capacity for variants of human DHFR to allow bacterial propagation in the presence of high MTX concentrations. While characterization of the selected variants confirmed successful identification of active and highly MTX-resistant hDHFR variants with no significant background from false-positive hits, there remain issues to be addressed to allow its broader application. First, we need to assess if the bacterial-based selection strategy is robust; that is, what is the incidence of false-negatives? While bacterial selection offers the undeniable advantage of speed, it is challenging to tune the sensitivity to specific enzyme properties. Differences in mutant enzyme stability, expression levels and limitations set by bacterial metabolic requirements (upper or lower threshold for requirement of a specific metabolite) contribute to phenotypic responses that do not reflect kinetic properties of the enzyme variants. Second, classic methods for characterizing the kinetic parameters defining activity and MTX-resistance of the selected variants were lengthy and labour-intensive,

precluding application at a larger scale. Finally, the selection assay had been designed exclusively for the purpose of identifying the phenotype of MTX-resistance. However, a further phenotype of interest is that of conservation of native-like activity upon mutation.

Herein, we present a streamlined, 2-tier selection and screening protocol to rapidly identify hDHFR variants that are active and/or MTX-resistant and that possess properties justifying further, more detailed kinetic characterization. As a 1st step, the bacterial selection strategy was expanded to select either for native-like activity or for a combination of activity and MTX-resistance. Then, an *in vitro* activity assay was conveniently performed directly on cell lysates in 96-well plate format to rapidly provide a reliable estimate of catalytic activity and/or MTX-resistance. Toward this goal, active-site residues 7, 15, 24, 70 and 115 of hDHFR, each known or suspected to affect ligand binding, were subjected to saturation mutagenesis. The 5 libraries were selected for conservation of native-like activity and for MTX resistance. A variety of mutations compatible with activity were identified and 2 novel MTX-resistant variants were identified and characterized. Preliminary results from screening against further antifolates are also reported, demonstrating the adaptability of the approach.

MATERIALS AND METHODS

Reagents

Restriction and DNA modifying enzymes and dNTPs were purchased from MBI Fermentas (Burlington, ON). Folic acid, methotrexate (MTX), β-NADPH, trimethoprim (TMP), buffers and CelLytic™ B Cell Lysis Reagent were from Sigma-Aldrich (Oakville, ON). Pemetrexed (ALIMTA) was from Eli Lilly (Toronto, ON). Alimta was supplied as 1:1 mixture of pemetrexed and D-mannitol. Dihydrofolate (DHF) was synthesized from folic acid.[12] Standard mutagenic oligonucleotide primers were from Alpha DNA (Montréal, QC), while primers containing degenerate codons were from Integrated DNA Technologies (Coralville, IA). The QIAquick® Gel extraction kit, QIAprep® Spin plasmid purification kits, and Ni-NTA agarose were from Qiagen

(Mississauga, ON). Isopropyl 1-thio-β-D-galactopyranoside (IPTG) was from BioShop Canada (Burlington, ON). DNA sequencing was performed by dideoxy-chain termination using a Thermo Sequenase Cycle Sequencing Kit (GE healthcare) and dye-labelled primers (*fwd* $^{5'}$CGGATAACAATTTCACACAG$^{3'}$ or *rev* $^{5'}$GTTCTGAGGTCATTACTGG$^{3'}$) (Li-Cor Biotechnology, Lincoln, NB) with a Li-Cor 4200 automated sequencer. *Escherichia coli* strain SK037[13] was a generous gift from Gwen Snapp and James Hu (Texas A&M).

Creation of the hDHFR saturation mutant libraries

The construct WT hDHFR-pQE32 encoding WT human DHFR cloned into pQE32 (Qiagen) between the BamHI and HindIII sites was previously described.[8] It expresses WT His_6-hDHFR (*N*-terminally 6-histidine tagged) and was the template in creation of the mutated libraries. The external primer set 1 (primer 1A: *fwd* $^{5'}$ ACACACGGATCCAAATGGTTGGTTCGCTAAACTGCATC$^{3'}$ [BamHI restriction site underlined]; primer 1B: *rev* $^{5'}$GTTCTGAGGTCATTACTGG$^{3'}$) allowed for PCR amplification of the entire coding region. Libraries 7 and 15, named according to the numbering of the mutated residue, were constructed in a single-step PCR using primers *fwd*7
($^{5'}$ACCATGGGATCCAAATGGTTGGTTCGCT**T**AACTGCNNSGTCGCTGTGTC CCAGA$^{3'}$; a silent mutation [bold] was introduced as a tracer) or *fwd*15 ($^{5'}$ACCATGGGATCCAAATGGTTGGTTCGCTAAACTGCATCGTCGCTGTGTCCC AGAACATGNNSATCGGCAAGAACGG$^{3'}$), respectively, with primer 1B. Library 24 was constructed by 2-step megaprimer PCR[14] using primer 24 (*rev* $^{5'}$TCCTTAAGGGTGGSNNCGGCAGGTCCCCGT$^{3'}$) and external primer set 1. Libraries 70 and 115 were created by 3-step overlap extension PCR[15] using primers 70A (*fwd* $^{5'}$CGACCTTTAAAGGGTNNSATTAATTTAGTTAG$^{3'}$) and 70B (*rev* $^{5'}$CTGAGAACTAAATTAATSNNACCCTTTAAAGGTCG$^{3'}$) or primers 115A (*fwd* $^{5'}$GACATGGTCTGGATANNSGGTGGCAGTTCTGTTTATAAGG$^{3'}$) and 115B (*rev* $^{5'}$CCTTATAAACAGAACTGCCACCSNNTATCCAGACCATGTC$^{3'}$), and the external primer set 1. Degenerate codons are underlined. The resulting libraries were cloned into pQE32 between BamHI and HindIII and transformed into electrocompetent *E. coli*

SK037, yielding approximately 1×10^4 colonies per library. The quality of each library was verified by sequencing DNA from clones propagated on LB agar containing 100 μg/ml ampicillin.

Selection for activity and MTX resistance

Library-transformed *E. coli* SK037 was selected first for hDHFR activity, then for MTX resistance. *E. coli* SK037 transformed with pQE2 (Qiagen) was the negative control. Cells were plated in equal dilutions on M9 minimal agar containing 0.08% w/v casamino acids and 100 μg/ml ampicillin (MM_A; non-selective conditions), on MM_A containing 0.1 μg/ml trimethoprim (TMP) (MM_AT; selective conditions for hDHFR activity) and MM_AT containing 1 mM MTX (ATM_1000;[8] selective conditions for MTX resistance). Colony formation took place at 37 °C over 18 h on both MM_A and MM_AT and over 22 h on ATM_1000. The survival rate for each library was the ratio of colonies observed on selective MM_AT or ATM_1000 relative to non-selective MM_A medium. Following selection, plasmid DNA was sequenced to identify the mutations at the targeted positions. In all cases, the entire coding sequence was verified, and in certain cases, both strands were verified.

Protein expression and cell lysis

For expression, transformed *E. coli* SK037 were propagated in LB (100 μg/ml ampicillin) at 37 °C, 225 rpm in 96-well assay blocks with 2 ml wells (Costar, Cambridge, MA). Fresh LB medium (1 ml) was inoculated with overnight cultures (25 μl) and propagated until $OD_{600} \approx 0.6$. Protein expression was induced by addition of IPTG to a final concentration of 1 mM and further propagation for 3 hrs. The assay blocks were centrifuged (30 min, 2700 × *g,* 4 °C), the supernatant was removed and the pellets were resuspended in 150 μl of lysis reagent (15 min, 225 rpm, room temperature). The lysates were clarified by centrifuging as above and were preserved on ice until required.

Determination of activity and antifolate resistance from crude cell lysates in 96-well plates

All rate measurements were in MATS buffer (25 mM MES, 25 mM acetic acid, 50 mM Tris, 100 mM sodium acetate and 0.02% w/v sodium azide) pH 7.6, 23 °C. Substrates were dissolved in buffer and quantified by spectrophotometry ($\varepsilon_{340\ nm}$ = 6 200 $M^{-1}cm^{-1}$ for NADPH; $\varepsilon_{282\ nm}$ = 28 400 $M^{-1}cm^{-1}$ for DHF). MTX was dissolved in 0.05 M KOH and quantified in 0.1 M NaOH ($\varepsilon_{258\ nm}$ = 22 100 $M^{-1}cm^{-1}$ and $\varepsilon_{302\ nm}$ = 23 300 $M^{-1}cm^{-1}$). Pemetrexed (ALIMTA) was dissolved and quantified in 0.9 % w/v NaCl ($\varepsilon_{226\ nm}$ = 31200 $M^{-1}cm^{-1}$). Catalytic activity of mutants was determined in 96-well flat-bottom plates (Costar #3595, Cambridge, MA) with a FLUOstar OPTIMA UV-Vis plate reader (BMG Laboratories, Offenburg) by monitoring concurrent NADPH and DHF depletion ($\Delta\varepsilon_{340\ nm}$ = 12 800 M^{-1} cm^{-1}).[16] Reaction rates were determined in a final volume of 300 µl using crude cell lysate and 100 µM each DHF and NADPH. To evaluate the background due to bacterial DHFR, reactions were conducted in presence or absence of 1 µg/ml TMP.

To ensure high signal to background while keeping the reaction sufficiently slow to allow measurement of initial rates, an initial estimate of reaction rate was obtained using various dilutions of the lysates. The dilutions were then adjusted for rate measurement of each variant. These dilutions were also used for determination of k_{cat} according to $k_{cat} = V_{max}$ / [hDHFR], where the concentration of soluble hDHFR variant in each lysate was estimated following migration on 15 % SDS-PAGE and Coomassie blue staining. Protein quantification was performed using the image analysis software Scion Image (NIH, rsb.info.nih.gov/nih-image) from digitalized images of the stained gels.

For assessment of MTX resistance, residual activities were determined as the ratio of activity in presence of 200 or 1000 nM MTX *versus* activity in absence of MTX. The concentration of hDHFR variant in each lysate was verified to ensure that saturating concentrations of MTX were used. For library 115, the approximate IC_{50}^{MTX} values of active mutants were determined from cell lysates by monitoring initial reaction rates in presence of 100 µM each DHF and NADPH and increasing concentrations of MTX: 0, 50, 500, 1000, 5000 and 10000 nM. IC_{50}^{MTX} values were obtained from a non-linear

regression fit to the hyperbolic model for one-site binding using Graphpad Prism (Graphpad Software, San Diego, CA) and the data from three independent experiments.

For assessment of PMTX resistance, residual activities were determined as the ratio of activity in presence of 5 μM or 20 μM PMTX *versus* activity in absence of PMTX. For assessment of TMP sensitivity, reactions were conducted in presence or absence of 0.1 μg/ml (0.34 μM) and 1 μg/ml (3.4 μM) TMP.

Purification and characterization of individual selected variants

The MTX-resistant and the PMTX-resistant mutants identified by screening as well as mutant I7F were expressed and purified by Ni-NTA affinity chromatography as previously described[8] from 50 ml of culture medium. Solubility and relative expression level were verified by loading volume-equivalent amounts of total cell extracts, cell pellet and lysis supernatant for resolution by 15 % SDS-PAGE. Purity was evaluated using the Scion Image software following separation by 15 % SDS-PAGE and Coomassie blue staining. Protein concentration was determined using the Bradford assay (Bio-Rad, Hercules, CA). Kinetic and inhibition constants were determined in presence DHF and NADPH (100 μM each) in 1-cm cells with a Cary 100 Bio UV/Vis spectrophotometer (Varian Canada, Montréal, QC).[8] For determination of K_M^{DHF}, the concentration of DHF was varied (0.5 μM to 20 μM). For determination of IC_{50}^{MTX}, the following MTX concentrations were used: 0, 0.025, 0.050, 0.1, 0.5, 1, 10 μM. For determination of IC_{50}^{PMTX}, the following PMTX concentrations were used: 0, 0.1, 0.5, 1, 5, 10, 100 μM. K_i^{MTX} and K_i^{PMTX} were calculated from IC_{50}^{MTX} and IC_{50}^{PMTX}, respectively, according to the equation for competitive inhibitor binding.[17] DHF was held constant at 100 μM for all IC_{50} determinations. The mock-purified *E. coli* SK037 expressing no hDHFR served as a negative control.

RESULTS AND DISCUSSION

Selection of target residues for mutagenesis

In silico visualization of active-site hDHFR residues known to interact with DHF and/or MTX was performed to identify residues for mutation. The crystal structure coordinates of the ternary complex of hDHFR with MTX and NADPH (1U72.pdb)[7] and the binary complex of hDHFR with folic acid (1DHF.pdb)[6] were visualized. Folate and MTX are constituted of a pteridine ring moiety, a *p*-aminobenzoyl group (*p*-ABA) and a L-glutamyl γ-carboxylate tail. The molecules are chemically and sterically similar. However, because of their differences, MTX binds to DHFR with its pteroyl moiety flipped 180° about the C_6-C_9 bond relative to folate (**figure 3.1A and 3.1B**). As a result, active-site residues form different contacts with the two molecules and binding of the inhibitor MTX is 2000-fold stronger than binding of the substrate DHF.

MTX-resistant point mutants of DHFR from human or other mammalian sources have been identified either *in vitro*, *in vivo* or *ex-vivo*. Point mutations at residues Ile7,[18,19] Gly15,[20] Leu22,[21,22] Trp24,[19] Phe31,[8,23] Phe34,[24] Gln35,[19] Arg70[25] and Val115[19] have yielded DHFR variants with decreased MTX-affinity. In particular, saturation mutagenesis[26] and *in vitro* characterization of mutants at residues 22[21,22] and 31[8,23] have identified the specific mutations at these positions that confer MTX-resistance *in vitro*.

Herein, we investigated five non-contiguous positions where no saturation mutagenesis had been performed previously: Ile7, Gly15, Trp24, Arg70 and Val115 (**figure 3.1C**). The backbone carbonyl groups of Ile7 and Val115 form hydrogen bonds with the 4-amino pteroyl group of bound MTX; these bonds are not formed with folate.[7] Trp24 and Arg70 are strictly invariant residues in all vertebrate and bacterial DHFRs. The indole nitrogen of Trp24 is hydrogen-bonded to the C_4-oxygen of folate (N_8 of MTX) *via* a conserved water molecule. Arg70 makes ionic interactions with the α-carboxylate of the L-glutamate moiety of both folate and MTX. The mutation R70K weakens binding to both ligands.[25] Gly15, also selected for mutagenesis, is a highly conserved residue located on a loop outside the active site (**figure 3.1C**). It has no known interaction, direct or indirect, with NADPH, DHF or MTX. Nonetheless, mutant G15W

was isolated *in vivo* from a MTX-resistant subline of murine leukemic cells implanted in mice,[27] justifying further investigation.

Mutagenesis and expression

Saturation mutagenesis was performed to obtain individual libraries encoding the 20 amino acids at positions 7, 15, 24, 70 and 115 of hDHFR (libraries 7, 15, 24, 70 and 115, respectively). The libraries were subcloned into pQE32 to provide His_6-tagged variants for ease of purification. The His_6-tag causes no detectable variation in WT hDHFR kinetic parameters.[8] The libraries were transformed into *E. coli* SK037, a MTX-sensitive strain that is a knock-out of the *tolC* component of a multi-drug-resistance (MDR) efflux pump.[13] Approximately 1×10^4 colonies were obtained per library. DNA sequencing of randomly chosen clones propagated on non-selective medium revealed little or no sequence biases and no non-specific mutations. For library 115, DNA sequencing of 42 clones selected for activity and 46 nonselected clones allowed identification of 18 out of the 20 possible variants (mutants V115D and V115E were not identified).

Selection and screening for catalytically active mutants

The 2-tier selection strategy to identify catalytically active mutants is depicted in **figure 3.2A**. To verify whether the 2-tier strategy could reliably select active variants, we validated it against library 115. This library had shown a range of activity levels upon preliminary screening and was judged a good candidate to assess sensitivity and prevalence of false positives or false negatives. The 1st-tier assay is a bacterial complementation assay allowing high-throughput selection of active variants. For this assay, the library was plated on selective MM_AT medium containing trimethoprim (TMP). TMP inhibits the endogenous bacterial DHFR, making bacterial propagation on minimal medium obligatorily dependent on the activity of the expressed variant of hDHFR. *E. coli* SK037 transformed with pQE2 or with WT hDHFR-pQE32 was used as negative and positive controls, respectively. No bacterial growth was observed for the negative control whereas a survival rate varying between 88% and 100% was observed for the positive control. DNA sequencing of 42 selected colonies yielded 8 unique

hDHFR variants (7 mutants and the WT) (**figure 3.3A**). The WT (Val115) was the most frequently selected variant (48%), followed by V115I (32%), V115M (10%) and V115C, V115L, V115F, V115Y and V115A (2% each) (**figure 3.4A).** We observed no bias resulting from the distribution of the 32 codons of the 'NNS' approach to saturation mutagenesis. Thus, the NNS codon encodes the WT Val at a frequency of 2/32, the V115I, M, C, F and Y at a frequency of 1/32 and the V115L at a frequency of 3/32; nonselected mutations are also encoded at frequencies varying between 1/32 and 3/32.

Not all variants identified as active by bacterial complementation were necessarily suitable for *in vitro* characterization. If the threshold for significant activity is higher *in vitro* than *in vivo*, some variants that allow cellular propagation may appear to be inactive *in vitro* and would thus constitute false positive hits from bacterial selection. Factors such as expression level, solubility and stability may have differing effects *in vivo* and *in vitro*. Moreover, if a greater number of selected colonies had been sequenced, further active variants at position 115 may have been identified. Failure to identify these would result in false negatives from bacterial selection.

To evaluate prevalence of false negatives, both the active, selected variants as well as the active but non-selected variants (14 variants in total, see **figure 3.4**) were individually plated under the bacterial selective conditions. All variants identified in the 1st-tier selection step conferred high survival rates while all others resulted in negligible or no survival **(figure 3.4A)**. Thus, bacterial selection of library 115 gave no false negatives.

To evaluate prevalence of false-positive hits in the 1st-tier selection, the 2nd-tier 96-well plate-based screening assay was applied to library 115 variants. Despite having lower throughput than the selection step, it has the advantage of rapidly providing an estimate of the kinetic constant k_{cat}. To assess activity independently of bacterial selection, the selected variants as well as the nonselected variants were subjected to the *in vitro* activity assay (18 variants). DHFR activity was assayed directly from cell lysates in 96-well plate-based assays. When available, at least 2 clones were assayed per mutant. No significant differences in reaction rates were observed in absence or presence of TMP. This indicates that there is no significant background due to endogenous bacterial DHFR.

E. coli SK037 transformed with pQE2 also served as a negative control. Again, the bacterial DHFR gave a negligible signal relative to the overexpressed hDHFR variants. The WT was always identified as being active both in bacterial selection and *in vitro*, which was an essential validation of the reliability of the method.

Clones with > 2-fold the *in vitro* activity of the negative control pQE2/SK037 were considered active. This threshold was established on the basis of the reproducibly weak signal obtained for the negative controls (at least 2 negative controls were included on each 96-well plate) as well as the sensitivity of plate-reader. Because the assay was performed with crude lysate rather than purified enzyme, any active but poorly expressed, poorly soluble or unstable mutant would be classified as inactive if the overall activity were < 2-fold pQE2/SK037. All library 115 variants that were identified in the first-tier bacterial selection were also active *in vitro*, confirming that the selection yielded no false positive hits (**figure 3.3A and 3.4B**). The k_{cat} for all active variants from library 115 roughly correlated with the frequency of occurrence of the mutants during bacterial selection (**figure 3.4B** and **table 3.1**). When more than 1 clone was assayed for a given mutation, the data were generally in agreement. However, mutants V115T, V115Q, V115N, V115S, V115K and V115G, which had not been selected *in vivo* and which yielded no significant cellular propagation when individually plated (**figure 3.4A**), were also identified as active *in vitro*. The most active mutant, V115T, exhibited a native-like k_{cat}. While these mutants possessed readily assayed activity, their overall properties (potentially including K_M changes) did not provide sufficient turnover to support bacterial growth. These variants were not false negatives according to the criteria required for bacterial propagation, which is the ultimate goal of our work. Nonetheless, they illustrate that there can be a loss of underlying structure-activity information if only the bacterial-selected variants are subjected to the 2nd-tier assay for *in vitro* activity, as this assay can reveal individual properties of specific interest.

Having validated the reliability of the 2-tier selection procedure, it was applied to the remaining libraries. Following 1st-tier selection for activity, 16 selected clones per library were subjected to DNA sequencing analysis, allowing identification of mutations compatible with cell survival (**figure 3.3A**). Survival rates for the different libraries varied between 3% and 7% and a variety of mutations were tolerated at each targeted

position. The mutants conferring survival were then tested *in vitro* in the 2nd-tier assay, allowing for identification of stable, soluble and active mutants (**figure 3.3A**). For libraries 7 and 24, most of the bacterial-selected mutants were active *in vitro*, with elimination of at most 1 false positive hit per library. Five false-positive mutants were eliminated from each of library 15 and 70. In library 70 only the native Arg showed detectable activity *in vitro*. Contrary to the results of library 115, where no false-positives were identified, not all mutants obtained in the 1st-tier selection showed significant *in vitro* activity. The correlation between *in vivo* and *in vitro* activity appears to depend on the particular library and on the threshold chosen to define activity, where mutations at the different positions have differing effects on the overall properties of the enzyme.

Mutations that support catalytic activity

Position 115 tolerated the greatest number of mutations. The active variant V115P was previously reported in the highly homologous mouse DHFR (mDHFR) but was unstable,[27] and its hDHFR counterpart was incompatible with bacterial propagation in this study. Positions 7 and 15 tolerated only a restricted subset of conservative mutations. Gly15, located farther from the active site than the other targeted residues, tolerated the conservative mutation G15A. The only reported mutation of hDHFR at position 15, G15W, was described as active but unstable.[20] This is consistent with it having been identified in the 1st-tier bacterial selection but eliminated in the 2nd-tier *in vitro* assay. Position 7 tolerated only the conservative mutations I7L and I7V. As in the case of Val115, the main-chain carbonyl of Ile7 is hydrogen-bonded to MTX but not to DHF.[7] The only active hDHFR mutation previously described at position 7 was I7F.[18] This mutant was identified in the 1st-tier bacterial selection but was rejected in the *in vitro* assay, its activity being slightly inferior to the chosen threshold. Considering that its expression level and solubility were comparable to the WT (data not shown), its low *in vitro* activity is likely a result of its reported instability and its high K_M^{DHF}.[18] Because its activity *in vitro* was not negligible, we determined its kinetic parameters using purified enzyme (k_{cat} = 2.1 ± 0.1 s^{-1}, K_M^{DHF} = 14.9 ± 3.6 μM; k_{cat}/K_M^{DHF} = 0.16 $\mu M^{-1}s^{-1}$), confirming the reported data (k_{cat} = 5.0 ± 0.2 s^{-1}, K_M^{DHF} = 20 ± 2.1 μM; k_{cat}/K_M^{DHF} = 0.25 $\mu M^{-1}s^{-1}$).[18] The exclusion of this variant following the *in vitro* assay does not point to

disagreement with previous studies but highlights the advantage of comparing all variants on the basis of a user-defined threshold for a specific parameter, where only variants surpassing that value are considered to be sufficiently fit for a given application.

Residues Trp24 and Arg70 are highly conserved in various species and are known to be important for DHF binding.[25,28] Moreover, Arg70 appears to be involved in maintaining the structure of the binding site.[25] Position 70 tolerated no substitution that allowed significant *in vitro* catalytic activity. The conservative hDHFR mutation R70K has been previously described (k_{cat} = 1.75 s^{-1}, K_M^{DHF} = 0.47 μM; k_{cat}/K_M^{DHF} = 3.7 $\mu M^{-1}s^{-1}$ at pH 7.5).[25] Its stability was comparable to the WT.[25] The mutation R70K was identified in the 1st-tier bacterial selection, but was then eliminated in the following step (**figure 3.3A**; 2 independent clones tested). Factors such as lower expression level or solubility may have contributed to reduce its *in vitro* fitness below the established threshold. Position 24 tolerated the conservative substitutions W24F and W24Y (**figure 3.3A**). The hDHFR mutation W24F was previously described as being compatible with activity (K_M^{DHF} increased 25-fold and a 3-fold increase in k_{cat} relative to WT) but its stability was 3-fold lower than the WT. NADPH binding was also weakened and the rate of hydride transfer was markedly decreased, illustrating its importance for substrate binding and catalysis;[28] nonetheless, its resulting activity was above the threshold. Mutation W24R in mDHFR was reported to be very poorly active,[19] and was not tolerated by hDHFR in this study (**figure 3.3A**).

Overall, the parallel comparison of a large number of mutations of a human gene by the rapid means of bacterial propagation was shown to provide a reliable indicator of global activity. Further sorting by the 2nd-tier *in vitro* assay allowed efficient retention of the variants that best met the user-specified parameters. The selected variants were overwhelmingly in agreement with published data and readily allowed identification of novel, active point mutants of hDHFR.

Selection and screening for MTX resistance

In parallel with the activity assay, a 2-tier selection strategy was developed to identify MTX-resistant hDHFR mutants (**figure 3.2B**). In the 1st-tier bacterial selection step, the 5 libraries were selected on medium containing 1 mM MTX (ATM-1000). MTX

inhibits the hDHFR variants that are not resistant, making the survival of bacteria on minimal medium dependent on the activity of the hDHFR variants that are active as well as MTX-resistant. It should be noted that, despite the increased MTX sensitivity of *E. coli* SK037, it exhibited relatively high intrinsic MTX resistance such that > 200 μM MTX was required for efficient bacterial selection. No bacterial growth was observed for the negative control expressing only endogenous bacterial DHFR. When the WT hDHFR was expressed, very low survival was observed (0.002%), consistent with its sensitivity to MTX. Survival of all libraries was low (≤ 0.03%), suggesting that few MTX-resistant variants were present and highlighting the importance of verifying the occurrence of false-positives. DNA sequencing following selection allowed identification of 2 to 6 mutations at each targeted position (**figure 3.3B**).

The 2nd-tier screening step using the 96-well plate screening assay was used to eliminate false positives. The clones identified as being MTX-resistant by bacterial selection were assayed for residual activity in the presence of 200 nM MTX (**table 3.1**) or 1000 nM MTX (not shown), relative to activity in the absence of MTX. These 2 concentrations were selected based on IC_{50}^{MTX} (estimated at 100 μM DHF) for previously-characterized, MTX-resistant point mutants: L22Y ($IC_{50}^{MTX} \cong$ 2000 nM, where K_M^{DHF} = 0.53 μM and K_i^{MTX} = 10.9 nM);[22] L22W ($IC_{50}^{MTX} \cong$ 1000 nM, where K_M^{DHF} = 0.42 μM and K_i^{MTX} = 4.31 nM);[22] L22R ($IC_{50}^{MTX} \cong$ 290 nM, where K_M^{DHF} = 1.6 and K_i^{MTX} = 4.57)[22] as well as I7F ($IC_{50}^{MTX} \cong 272 \pm 72$ nM, this study). The assays were conducted using the same cell-lysate dilutions as for the activity test. Cell lysate from SK037 expressing no hDHFR or expressing WT hDHFR-pQE32 were used as negative controls for MTX-resistance. Previously characterized hDHFR mutants displaying a broad range of MTX-resistance levels were used as positive controls: mutant F31A/F34V/Q35H (AVH; K_i^{MTX}= 180 nM), mutant F31R/F34T/Q35R (RTR; K_i^{MTX}= 86 nM) and point-mutant F31P (K_i^{MTX}= 1.7 nM).[8] Mutants AVH and RTR showed residual activity higher than 40% at both concentrations of MTX tested, consistent with their high IC_{50}^{MTX} under these conditions (4400 nM and 3500 nM, respectively). F31P showed a residual activity > 40% at 200 nM MTX but not at 1000 nM, consistent with its IC_{50}^{MTX} under these conditions (110 nM). On the basis of these observations, a threshold of

residual activity > 40% at 200 nM MTX was established as being minimally required to consider a mutant as MTX-resistant.

Two mutants from library 115 (V115A and V115C) were effectively resistant to MTX on the basis of the threshold (**figure 3.3B** and **table 3.1**). These had never been previously reported. Other mutants had residual activities higher than WT hDHFR but were rejected because these values were below the established threshold. Previously reported MTX-resistant mutants of hDHFR I7F[18] and R70K[25] were identified at the 1st-tier level but rejected at the 2nd-tier screening as their overall activity *in vitro* did not meet the required criteria, as discussed above. Despite the fact that the purified I7F mutant was effectively MTX-resistant, with a K_i^{MTX} = 31.9 ± 8.5 nM (> 1000-fold increase relative to WT), the > 200-fold increase in K_M^{DHF} [18] and/or further modified properties contributed to decrease *in vitro* activity below the established threshold. G15W has also been reported as being MTX-resistant but unstable;[20] its fitness was too low even to allow 1st-tier selection for resistance.

As a further control for robustness of the strategy, the mutants encoded in library 115 (18 variants) were all individually tested for residual activity at 200 and 1000 nM MTX. The only mutants with a residual activity > 40% in presence of 200 nM MTX were V115A and V115C. Thus, the bacterial selection for MTX-resistance yielded no false negatives in library 115.

The IC_{50}^{MTX} values for all library 115 mutants that showed non-negligible *in vitro* activity were measured in 96-well plates directly from cell lysates (**table 3.1** and **figure 3.5A**). This assay was less rapid but more precise than the simple assay of residual activity. Only mutants V115A and V115C presented an IC_{50}^{MTX} higher than 200 nM. Other mutants (e.g V115L, V115K, V115T and V115G) had an IC_{50}^{MTX} higher than the WT hDHFR but lower than the established threshold of resistance (200 nM MTX). These results confirm the validity of relying on the simple indicator of residual activity to reliably identify MTX resistance. Thus, the rapid 2-step protocol consisting of bacterial selection followed by *in vitro* measurement of residual activity provided sufficient information to identify hDHFR variants satisfying our specific requirements for resistance.

Screening for modified binding to additional antifolate compounds

To verify the flexibility of the method, it was applied to testing against the antifolate TMP. Because human DHFR is intrinsically resistant to TMP (K_i^{TMP} WT hDHFR = 960 ± 30 nM relative to K_i^{TMP} WT *E. coli* DHFR = 0.08 nM)[29], we screened for increased sensitivity rather than resistance. The 1st-tier bacterial selection step cannot be applied to this compound because the endogenous bacterial DHFR will confer bacterial growth in absence of TMP. We performed the 2nd-tier *in vitro* reaction rate measurements for library 115 in absence or presence of 0.34 μM and 3.4 μM TMP. As mentioned previously, there was no significant background *in vitro* due to endogenous bacterial DHFR. In no case was a significant difference in reaction rates observed, indicating that no library 115 variants tested were rendered TMP-sensitive as a result of mutation. This confirmed that TMP sensitivity was not the cause of reduced cellular propagation in the bacterial selection presented above.

Preliminary tests were performed to assess resistance to the clinically relevant antifolate pemetrexed (PMTX). Pemetrexed inhibits multiple folate-utilizing enzymes, including thymidylate synthase and hDHFR[4]. Because bacterial selection using pemetrexed could not be interpreted solely on the basis of hDHFR resistance, only the 2nd-tier *in vitro* screen was performed. Active clones from the 5 libraries considered in this study were assayed in crude lysate for residual activity in the presence of 5 μM PMTX (**table 3.1**) or 20 μM (not shown) PMTX, relative to activity in the absence of PMTX. These concentrations were selected based on the value of $IC_{50}^{PMTX} \cong 0.75 \pm 0.3\mu M$ determined for the purified WT hDHFR. Using the same negative controls as for MTX-resistance, mutants with residual activity significantly greater than the WT residual activity at 5 μM PMTX were considered PMTX-resistant (**table 3.1**). Screening results suggest that, as for MTX, variants V115A and V115C may be PMTX-resistant. Variants V115L and V115I also showed potential PMTX resistance according to residual activity.

Kinetic and inhibition parameters of the novel antifolate-resistant mutants

The WT and the novel MTX and/or PMTX-resistant mutants (V115A and V115C, V115I, V115L) identified in the 2nd-tier screen were expressed, purified to 90-95% purity and characterized according to their kinetic and inhibition parameters (**table 3.2**).

Their expression levels were comparable, and as for WT hDHFR, mutants were approximately 50% soluble (data not shown). Catalytic efficiencies (k_{cat}/K_M^{DHF}) for variants V115A and V115C were reduced by approximately 700 and 1400-fold, respectively, relative to WT. K_M^{DHF} for V115A and V115C was increased at least 100-fold relative to WT while turnover (k_{cat}) was reduced only 4 and 15-fold, respectively, relative to WT. The inhibition constants confirmed that both variants were effectively MTX-resistant, having K_i^{MTX} = 20 nM, which is > 600-fold higher than the WT and compares favorably to the well-characterized resistant point mutant L22Y (K_i^{MTX} = 10.9 nM).[22] It should be noted that IC_{50}^{MTX} for V115A and V115C from crude lysate or in purified form were comparable (**table 3.1** and **table 3.2; figure 3.5**). This demonstrates the accuracy of the rapid determination of IC_{50}^{MTX} directly from cell lysate in the 96-well plate format. Variants V115A and V115C were also shown to be PMTX-resistant as their K_i^{PMTX} values were > 250-fold greater than the WT hDHFR.

Variant V115L showed ~ 5-fold increase in IC_{50}^{MTX} relative to WT (**table 3.1**; **table 3.2**), which was below our user-defined threshold for resistance. Nonetheless, determination of its K_i^{MTX} confirmed that it confers MTX-resistance, albeit at a lower level than variants V115A and V115C (**table 3.2**). This variant showed the greatest increase in K_i^{PMTX}, with a > 700-fold increase relative to WT. Taken with the results for variant V115A, which shows high MTX resistance and moderate PMTX resistance, our results suggest that variants at position 115 may confer a differential degree of resistance to the specific antifolates tested, despite the structural similarity of the compounds. We are pursuing more detailed studies relative to this question.

Variant V115I was not MTX resistant but was identified as being potentially PMTX resistant according to residual activity (**table 3.1**). However, further analysis demonstrated that it is not PMTX resistant and thus constitutes a false-positive hit from the second-tier residual activity screen.

CONCLUSIONS

An efficient 2-tier selection strategy was applied to the selection of active and MTX-resistant hDHFR variants from 5 hDHFR libraries created by saturation mutagenesis of active-site residues. This allowed, for the 1st time, exhaustive screening and identification of mutations compatible with hDHFR activity at these positions. The 2 tiers showed reliability and complementarity with respect to identification of active hDHFR variants. The 1st-tier bacterial selection results of library 115 confirmed that the most frequently selected variants conferred better survival rates. All selected mutants from library 115 were also active in the 2nd tier, *in vitro* assay. Because the 2nd-tier assay has user-defined parameters, varying the threshold for activity or the assay conditions (substrate and cofactor concentrations) will yield additional information relative to the effect of mutations on catalytic activity. In general, where active, stable and soluble variants have been reported, they were selected in the 2nd-tier activity assay, further validating the selection strategy. Thus, the bacterial selection for activity was shown to be robust and the *in vitro* screening allowed rapid preliminary kinetic characterization of novel active hDHFR variants.

The addition of MTX to the 2-tier procedure allowed identification of MTX-resistant point mutants at these positions, among which 2 are novel variants. There was no evidence of false-negatives upon bacterial selection. False-positives were readily eliminated upon *in vitro* screening, for which the IC_{50}^{MTX} values obtained from crude lysate were comparable to those obtained with purified enzyme. The concentrations of MTX for tests of residual growth were set by the operator and determined the extent of resistance that was sought. In this work, the concentrations of MTX were selected according to properties of previously-characterized point mutants, since our aim was to match or surpass that level of resistance. By increasing the threshold, only the most highly resistant mutants would be identified.

The method described is ideal for screening large libraries, the 1st-tier bacterial selection being high-throughput and the 2nd-tier assay allowing rapid detection of the best variants among the leads, according to user-defined parameters. The approach has proven efficient in rapidly assessing key kinetic parameters in enzyme variants. Simple

modification of the protocol readily allowed screening against further compounds; preliminary screening has allowed identification of three novel pemetrexed-resistant variants by this approach. The 2-tier strategy should also prove adaptable to screening other metabolically-essential enzymes that can complement a bacterial strain rendered metabolically deficient via chemical or genetic methods, and where a colorimetric or fluorogenic assay can reliably report activity in crude bacterial lysate.

Table 3.1. Reactivity (k_{cat}) and MTX or PMTX resistance determined in 96-well plates using crude lysates of active hDHFR variants from library 115.

Library 115 variants [a]	k_{cat} relative to WT	Residual activity (%) at 200 nM MTX [b]	IC_{50}^{MTX} (nM) [c]	Residual activity (%) at 5 μM PMTX [d]
V (WT)	1	11	20 ± 12	30
I	5.0	8	0.4 ± 0.3	**49**
M	0.68	12	19 ± 4	11
C	0.27	**67**	**400 ± 69**	**51**
L	0.45	30	130 ± 25	**80**
A	0.27	**49**	**220 ± 17**	**50**
F	0.23	– [e]	47 ± 41	–
Y	0.29	18	38 ± 8	16
T	0.94	35	76 ± 13	30
S	0.35	24	76 ± 7	22
K	0.33	34	96 ± 18	28
G	0.21	30	67 ± 5	30
Q	0.024	–	27 ± 7	–
N	0.020	–	51 ±18	–

Variants are grouped according to frequency of bacterial selection for activity (**figure 3.4**).
[a] IC_{50}^{MTX} could be calculated only where a non-negligible k_{cat} was recorded.
[b] Variants in bold-type were considered MTX-resistant according to the user-defined threshold of residual activity at 200 nM MTX being greater than 40%, as defined under Results.
[c] Mean ± SD; $n = 3$. Variants in bold-type were considered MTX-resistant according to the user-defined threshold of $IC_{50}^{MTX} \geq 200$ nM, as defined under Results.
[d] Variants in bold-type were considered PMTX-resistant according to the user-defined threshold of residual activity at 5 μM PMTX being significantly greater than the WT residual activity.
[e] '-' indicates that activity was not detectable.

Table 3.2. Kinetic and inhibition constants [a] of purified MTX or PMTX-resistant hDHFR mutants.

hDHFR variant	k_{cat} (s^{-1})	K_M^{DHF} (μM)	k_{cat}/K_M^{DHF} ($\mu M^{-1}\ s^{-1}$)	IC_{50}^{MTX} (nM)	K_i^{MTX} (nM)	IC_{50}^{PMTX} (μM)	K_i^{PMTX} (nM)
Wild-type	10 ± 2.0	< 0.075	> 138	41 ± 14	< 0.031	0.75 ± 0.3	< 0.5
V115C	0.65 ± 0.02	7 ± 1	0.1	330 ± 29	20 ± 4	4.3 ± 1.6	283 ± 44
V115A	2.8 ± 0.2	15 ± 2	0.2	150 ± 18	20 ± 5	1 ± 0.3	131 ± 87
V115L	ND [b]	4 ± 0.5	ND	190 ± 60	7.3 ± 2.7	9 ± 4	378 ± 118
V115I	1.3 ± 0.05	< 1	> 1.3	20 ± 8	< 0.2	0.2 ± 0.03	< 2

[a] Mean ± SD; $n = 3$ except for mutant V115L where $n = 2$.
[b] ND: not determined

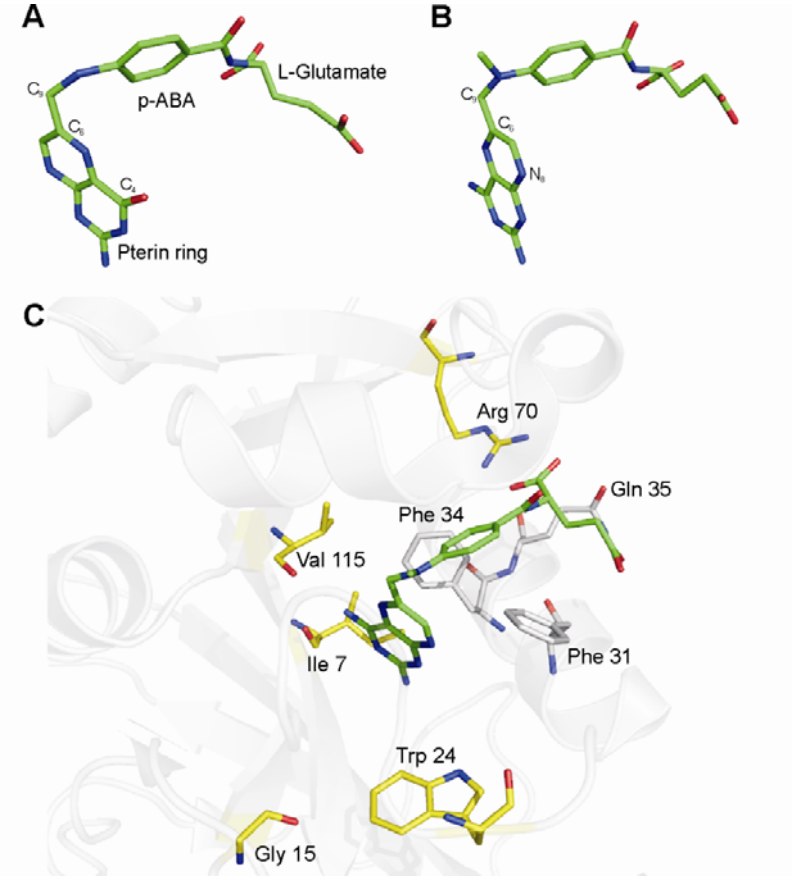

Figure 3.1. (A) Structures of folate (1DRF.pdb) and MTX (1U72.pdb) bound to hDHFR active site, with atom numbering. **(B)** The active-site area of hDHFR with bound MTX (1U72.pdb), illustrating the residues targeted for saturation mutagenesis (yellow sticks) as well as residues mutated in a previous study[8] (white sticks).

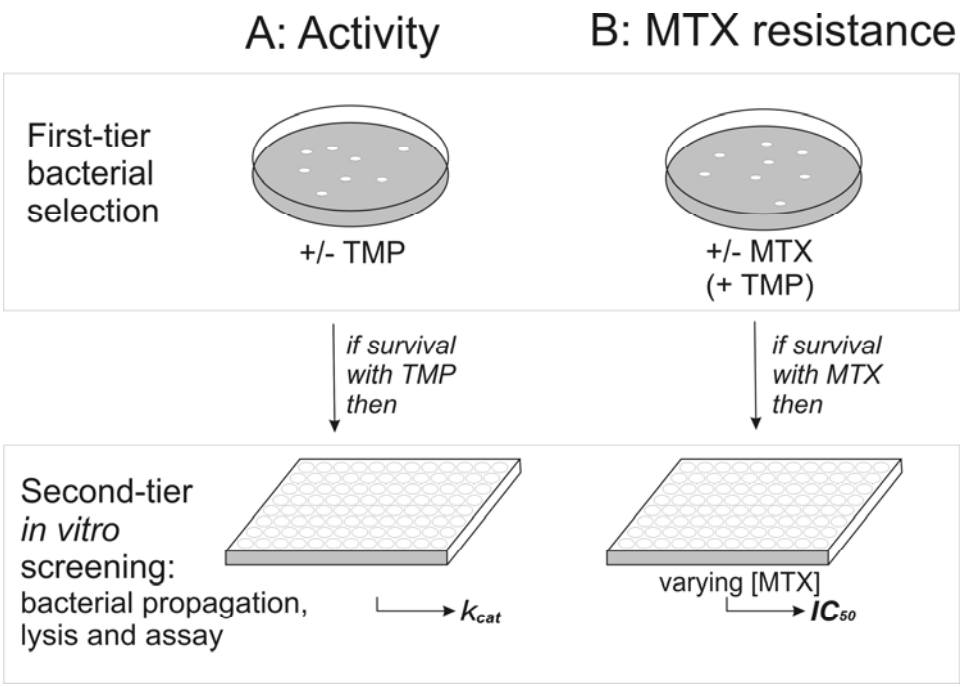

Figure 3.2. Flow-chart of the two-tier strategy to select mutated hDHFR library variants for A) catalytic activity or B) methotrexate (MTX) resistance. The first-tier selection relies on bacterial propagation in the presence of trimethoprim (TMP). Colonies are picked into 96-well plates for second-tier screening using crude bacterial lysate.

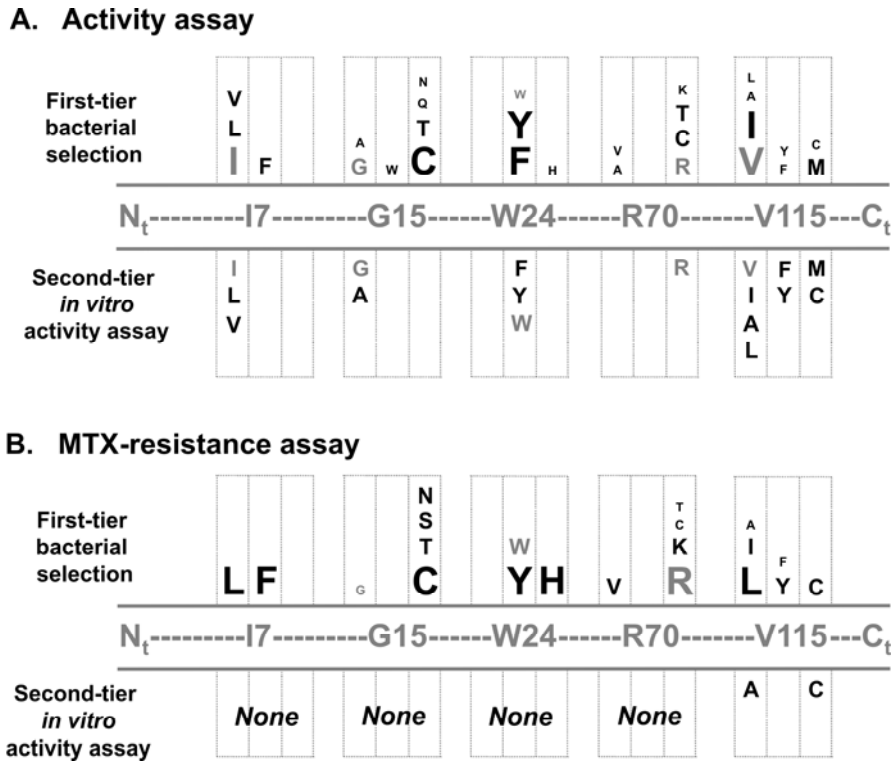

Figure 3.3. Comparison of hDHFR mutations that allow for conservation of activity (A) or MTX resistance (B) on the basis of the two-tier selection strategy. Residues subjected to mutagenesis are depicted relative to the WT hDHFR primary sequence. Above the sequence are the mutants identified in the first-tier bacterial selection. The size of the font is related to the frequency of occurrence in the selection: small (< 10 %), medium (10 to 30%), large (> 30%). Below the sequence are the mutations identified in the second-tier *in vitro* assay. Clones with (A) > 2-fold the *in vitro* activity of the negative control were considered active and clones with (B) residual activity > 40% at 200 nM MTX were considered MTX-resistant. Mutations at each targeted position are grouped as follows: small, hydrophobic (first column); aromatic (second column); polar and charged (third column). The WT residue at each targeted position is shown in grey.

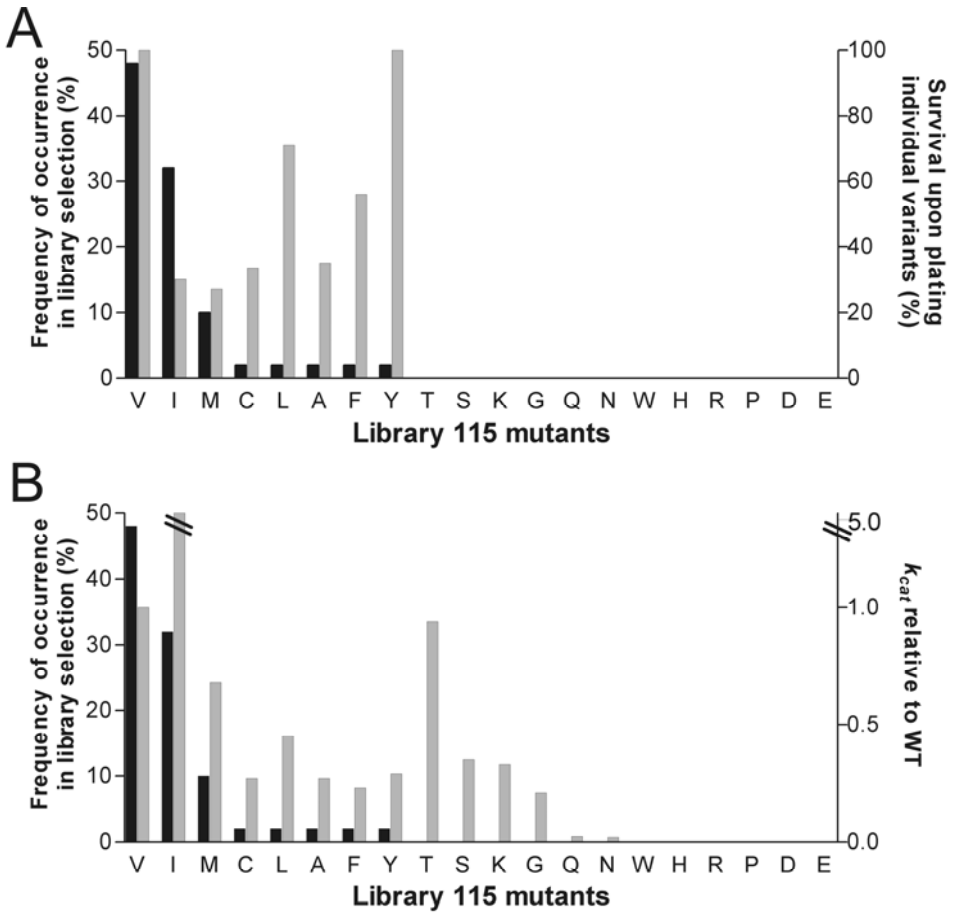

Figure 3.4. The two-tier selection results for library 115. (A) Comparison of the frequency of occurrence of mutations following bacterial library selection (black bars) and bacterial survival rates from plating individual variants (grey bars). Variants T, S, K, G, Q and N showed negligible selection rates (between 0.02 % and 0.002 %) while variants W, H, R and P were not selected (= 0). All variants showing *in vitro* activity (see Panel B) were individually plated. (B) Frequency of occurrence of mutations following bacterial library selection (black bars) and k_{cat} relative to WT (Val115) for individual variants (grey bars). Variants D and E were not individually tested.

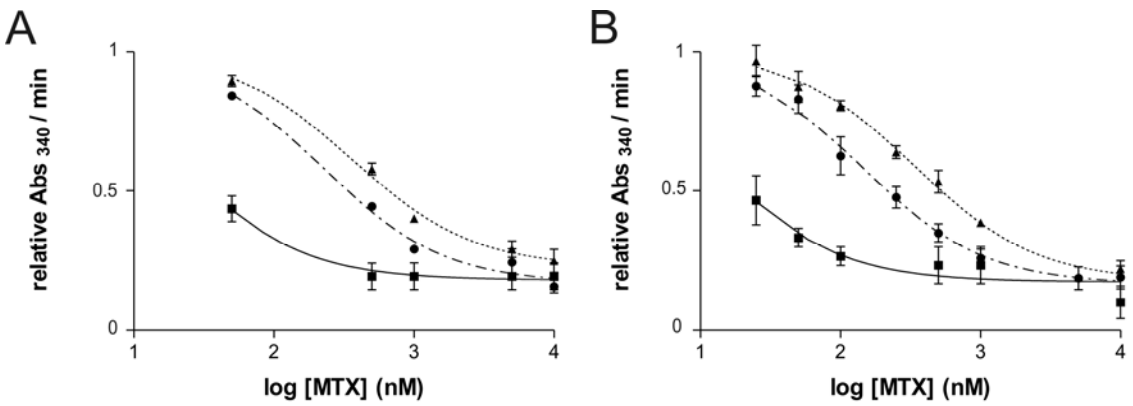

Figure 3.5. IC_{50}^{MTX} concentration-response curves (mean ± SD; n = 3) of WT hDHFR (■), V115A (●) and V115 C (▲) using (**A**) crude lysate or (**B**) purified enzyme.

REFERENCES

1 Schweitzer BI, Dicker AP, Bertino JR: Dihydrofolate reductase as a therapeutic target. *Faseb J* 1990; 4:2441-2452.

2 International Bone Marrow Transplant Registry: Effect of methotrexate on relapse after bone marrow transplantation for acute lymphoblastic leukemia. *Lancet* 1989; 1:535-537.

3 Kremer JM, Lee JK: A long-term prospective study of the use of methotrexate in rheumatoid arthritis: update after a mean of fifty-three months. *Arthritis Rheum* 1988; 31:577-584.

4 Walling J: From methotrexate to pemetrexed and beyond: a review of the pharmacodynamic and clinical properties of antifolates. *Invest New Drugs* 2006; 24:37-77.

5 Zhao R, Goldman ID: Resistance to antifolates. *Oncogene* 2003; 22:7431-7457.

6 Davies JF, 2nd, Delcamp TJ, Prendergast NJ, Ashford VA, Freisheim JH, Kraut J: Crystal structures of recombinant human dihydrofolate reductase complexed with folate and 5-deazafolate. *Biochemistry* 1990; 29:9467-9479.

7 Cody V, Luft JR, Pangborn W: Understanding the role of Leu22 variants in methotrexate resistance: comparison of wild-type and Leu22Arg variant mouse and human dihydrofolate reductase ternary crystal complexes with methotrexate and NADPH. *Acta Crystallogr D Biol Crystallogr* 2005; 61:147-155.

8 Volpato JP, Fossati E, Pelletier JN: Increasing methotrexate resistance by combination of active-site mutations in human dihydrofolate reductase. *J Mol Biol* 2007; 373:599-611.

9 Blakley RL, Sorrentino BP: In vitro mutations in dihydrofolate reductase that confer resistance to methotrexate: potential for clinical application. *Hum Mutat* 1998; 11:259-263.

10 Gangjee A, Jain HD, Phan J, Lin X, Song X, McGuire JJ, Kisliuk RL: Dual inhibitors of thymidylate synthase and dihydrofolate reductase as antitumor agents: design, synthesis, and biological evaluation of classical and nonclassical pyrrolo[2,3-d]pyrimidine antifolates(1). *J Med Chem* 2006; 49:1055-1065.

11 Budak-Alpdogan T, Banerjee D, Bertino JR: Hematopoietic stem cell gene therapy with drug resistance genes: an update. *Cancer Gene Ther* 2005; 12:849-863.

12 Blakley R: Crystalline dihydropteroylglutamic acid. *Nature* 1960; 188:231-232.

13 Kopytek SJ, Dyer JC, Knapp GS, Hu JC: Resistance to methotrexate due to AcrAB-dependent export from Escherichia coli. *Antimicrob Agents Chemother* 2000; 44:3210-3212.

14 Sarkar G, Sommer SS: The "megaprimer" method of site-directed mutagenesis. *Biotechniques* 1990; 8:404-407.

15 Ho SN, Hunt HD, Horton RM, Pullen JK, Pease LR: Site-directed mutagenesis by overlap extension using the polymerase chain reaction. *Gene* 1989; 77:51-59.

16 Hillcoat BL, Nixon PF, Blakley RL: Effect of substrate decomposition on the spectrophotometric assay of dihydrofolate reductase. *Anal Biochem* 1967; 21:178-189.

17 Segel IH: *Enzyme Kinetics: Behaviour and Analysis of Rapid Equilibrium and Steady-State Enzyme Systems*. New York: John Wiley and Sons, 1993.

18 Patel M, Sleep SE, Lewis WS, Spencer HT, Mareya SM, Sorrentino BP, Blakley RL: Comparison of the protection of cells from antifolates by transduced human dihydrofolate reductase mutants. *Hum Gene Ther* 1997; 8:2069-2077.

19 Thillet J, Absil J, Stone SR, Pictet R: Site-directed mutagenesis of mouse dihydrofolate reductase. Mutants with increased resistance to methotrexate and trimethoprim. *J Biol Chem 1988*; 263:12500-12508.

20 Spencer HT, Sorrentino BP, Pui CH, Chunduru SK, Sleep SE, Blakley RL: Mutations in the gene for human dihydrofolate reductase: an unlikely cause of clinical relapse in pediatric leukemia after therapy with methotrexate. *Leukemia* 1996; 10:439-446.

21 Ercikan-Abali EA, Waltham MC, Dicker AP, Schweitzer BI, Gritsman H, Banerjee D, Bertino JR: Variants of human dihydrofolate reductase with substitutions at leucine-22: effect on catalytic and inhibitor binding properties. *Mol Pharmacol* 1996; 49:430-437.

22 Lewis WS, Cody V, Galitsky N, Luft JR, Pangborn W, Chunduru SK, Spencer HT, Appleman JR, Blakley RL: Methotrexate-resistant variants of human dihydrofolate reductase with substitutions of leucine 22: kinetics, crystallography, and potential as selectable markers. *J Biol Chem* 1995; 270:5057-5064.

23 Chunduru SK, Cody V, Luft JR, Pangborn W, Appleman JR, Blakley RL: Methotrexate-resistant variants of human dihydrofolate reductase: effects of Phe31 substitutions. *J Biol Chem* 1994; 269:9547-9555.

24 Nakano T, Spencer HT, Appleman JR, Blakley RL: Critical role of phenylalanine 34 of human dihydrofolate reductase in substrate and inhibitor binding and in catalysis. *Biochemistry* 1994; 33:9945-9952.

25 Thompson PD, Freisheim JH: Conversion of arginine to lysine at position 70 of human dihydrofolate reductase: generation of a methotrexate-insensitive mutant enzyme. *Biochemistry* 1991; 30:8124-8130.

26 Morris JA, McIvor RS: Saturation mutagenesis at dihydrofolate reductase codons 22 and 31: a variety of amino acid substitutions conferring methotrexate resistance. *Biochem Pharmacol* 1994; 47:1207-1220.

27 Dicker AP, Waltham MC, Volkenandt M, Schweitzer BI, Otter GM, Schmid FA, Sirotnak FM, Bertino JR: Methotrexate resistance in an in vivo mouse tumor due to a non-active-site dihydrofolate reductase mutation. *Proc Natl Acad Sci U S A* 1993; 90:11797-11801.

28 Beard WA, Appleman JR, Huang SM, Delcamp TJ, Freisheim JH, Blakley RL: Role of the conserved active site residue tryptophan-24 of human dihydrofolate reductase as revealed by mutagenesis. *Biochemistry* 1991; 30:1432-1440.

29 Appleman JR, Prendergast N, Delcamp TJ, Freisheim JH, Blakley RL: Kinetics of the formation and isomerization of methotrexate complexes of recombinant human dihydrofolate reductase. *J Biol Chem* 1988; 263:10304-10313.

ACKNOWLEDGMENTS

The authors thank Christopher Clouthier for critical reading of the manuscript. This work was supported by Canadian Institutes of Health Research (CIHR) grant 68851.

Section 3.2 - Erratum corrigendum

Kinetic investigation with a new inhibitor allowed identification of a mistake occurred during previous characterization of mutant hDHFR V115L. Corrected values for V115L are

$K_M^{DHF} < 0.1$ μM,

$Ki^{MTX} < 0.048$ nM

$Ki^{PMTX} < 2.3$ nM

The mistake was due to erroneous interpretation of the kinetic data due to a very low signal. The mutant was repurified from two different clones and characterized in triplicate. For the characterization of K_M^{DHF} 10-cm quartz cells were used to amplify the signal.

As a consequence of the correction, V115L, like V115I, was found to be a false positive for MTX resistance. Substitution of Val115 with both the conservative residues Leu and Ile resulted in mutated variants with kinetic and inhibitory parameters comparable to those of the native enzyme. The kinetic and inhibition values for all the other mutants were confirmed.

A corrigendum note to JBS is being prepared.

Chapter 4 – Binding of fragments of MTX to hDHFR

4.0 - Preface

In order to better elucidate the determinants of ligand binding in the active site of hDHFR, we proposed to correlate the kinetic and inhibitory parameters of hDHFR mutants of interest to their structural properties. The kinetic and inhibitory characterization of the mutants indentified in this study was described in details in chapter 2 and 3. Here, a more detailed structure-function investigation of binding of MTX to hDHFR will be described. Productive binding (K_i) of MTX fragments to the native enzyme and to four highly MTX-resistant hDHFR mutants will be used as a parameter to evaluate how different parts of the inhibitor and different active-site residues contribute to the overall binding MTX to hDHFR.

4.1 - Introduction

Multiple interactions are generated within the enzyme around the ligand's functional groups. These interactions determine selectivity, strength of binding and ligand orientation. Do fragments of a ligand bind in the same orientation as the entire molecule? If this is the case, a quantification of the relative contributions of individual portions of the ligand in binding may offer considerable insight into the principles of drug recognition [103, 113, 114].

We investigated the relative importance of different parts of the inhibitor MTX in binding to the human DHFR by determining their inhibition constants (K_i) for the WT enzyme. Moreover, we have begun investigating the relative importance of residues located in different areas of the active-site by performing binding studies with these fragments towards mutant hDHFRs. The three different MTX fragments considered are illustrated in **figure 1.7.** DAP (2,4-diamino-6-(hydroxymethyl)pteridine) represents the pteridine moiety of MTX; DAMPA (4-[*N*-(2,4-diamino-6-pteridinylmethyl)-*N*-methylamino]

benzoic acid) the N10-methyl *p*-ABA pteroyl portion; *p*-ABA-Glu (N-(4-aminobenzoyl)-L-glutamic acid) the *p*-ABA-Glu portion**.**

Binding studies with MTX fragments DAP and *p*-ABA-Glu were previously reported for the DHFR from *Lactobacillus casei* [115-117]. On the basis of NMR evidence [115] supporting the hypothesis that both DAP and *p*-ABA-L-Glu bind to the enzyme similarly to MTX, Birdsall *et al.* determined the K_D for both DAP (1.28 mM) and *p*-ABA-L-Glu (0.83 mM) and for N-methyl-*p*-ABA-L-glutamate, which is a fragment more similar to MTX than *p*-ABA-L-Glu (1.05 mM) [117]. Thus, binding of all fragments was much weaker than binding of MTX (K_D^{MTX} = 2 pM) [117, 118].

Preliminary results with DAP and *p*-ABA-Glu were performed in our group by summer student Vanessa Guerrero and PhD student Mirja Krause, respectively (data not shown). Their results confirmed that DAP is a weak inhibitor also of hDHFR (IC_{50}^{DAMPA} for WT hDHFR was 16000-fold lower than IC_{50}^{MTX}, both measured using 100 μM DHF in the assay) while *p*-ABA-Glu does not inhibit hDHFR. Therefore, both DAP and *p*-ABA-Glu were not suitable for our purposes and were abandoned.

Preliminary results for binding of DAMPA to native hDHFR and mutants F31R/Q35E (RFE), F31R, Q35E and V115A will be presented and discussed in the following paragraphs.

4.2 - Materials and methods

4.2.1 Reagents and enzymes

DAMPA was purchased from Sigma. All other reagents were purchased or prepared as described in chapters 2 and 3. F31R/Q35E hDHFR and V115A were identified as highly MTX-resistant mutants and are described in chapters 2 and 3, respectively. Mutants F31R and Q35E were created by site-directed mutagenesis by PhD student Jordan Volpato.

4.2.2 Determination of binding parameters

Enzyme expression and purification, DHF and NADPH quantification and rate measurements were performed as previously described in both chapters 2 and 3. DAMPA was dissolved in 0.1 N NaOH and quantified by spectrophotometry (ε_{370nm} = 6568 $M^{-1}cm^{-1}$). IC_{50}^{DAMPA} were determined in 1-cm cells in the presence of 100 μM of both DHF and NADPH and different concentrations of DAMPA: 0, 0.1, 0.5, 1, 5, 10, 50, 200 μM for WT and Q35E; 0, 1, 5, 10, 50, 100, 200, 500, 1000 μM for RFE and F31R. K_i^{DAMPA} was calculated from IC_{50}^{DAMPA} assuming the mode of binding was competitive. IC_{50}^{MTX} for both F31R and Q35E was determined by summer student Vanessa Guerrero using 100, 350, 800, 1600, 3200, 6400 and 15000 μM and 0, 0.025, 0.05, 0.1,0.5, 1 and 10 μM of MTX, respectively. K_i^{MTX} for mutants F31R and Q35E were calculated according to the equation for competitive inhibitor binding. $\Delta\Delta G$ (kcal mol^{-1}) values were calculated from experimental K_i values using the following equation:

$$\Delta\Delta G = -RT \ln (K_i^{mut}/K_i^{WT})$$

R is the molar gas constant and T is the temperature in Kelvin.

4.3 Results and discussion

Mutants F31R/Q35E (RFE) and V115A were chosen as candidates for this preliminary study because they are located in different areas of the active site (therefore interact with different parts of the inhibitor) and they both confer high resistance to MTX. Mutants F31R and Q35E were created and characterized to evaluate the effect of the two individual mutations of RFE on binding of both MTX and DAMPA.

Results are presented in **table 4.1**. MTX and its fragment DAMPA differ in that DAMPA has no glutamate tail (**figure 1.7**). The ratio K_i^{DAMPA}/K_i^{MTX} was used to describe the effect on binding of the glutamate tail, assuming that DAMPA binds similarly to MTX. The thermodynamic contribution to inhibition ($\Delta\Delta G$) is used as quantitative parameter of binding. Kinetic characterization of K_M^{DHF} and V_{max} in presence of different concentrations of DAMPA remains to be performed to determine if this compound is

effectively a competitive inhibitor of hDHFR. However, only structural data will confirm the precise orientation of the inhibitor in the enzyme's binding site.

DAMPA binds very tightly to WT hDHFR (K_i < 2 nM). This result suggests that the binding is highly specific and likely to be structurally very similar to MTX binding. K_i^{DAMPA}/K_i^{MTX} for the native enzyme shows that the lack of the glutamate tail accounts for a 60-fold decrease in binding.

Mutation of residue 115 to Ala decreased binding of MTX and its fragments but, surprisingly, the effect on DAMPA was stronger than the effect on MTX. K_i^{DAMPA}/K_i^{MTX} V115A was 3-fold higher than for the WT. Since residue 115 is located far away from the glutamate portion of bound MTX (**figure 1.5B**), this suggests that distal effects are involved in binding the glutamate tail. Since distal effects cannot be detected from structural visualization, this result highlights the advantages of the presented approach to gain detailed information about binding.

To evaluate both the contribution of a given mutation taken alone and its contribution in a combinatorial context, we built a double mutant cycle for the F31R/Q35E hDHFR variant. **Table 4.1** and **figure 4.1A** illustrate that combination of point mutations F31R and Q35E in the double mutant F31R/Q35E enhances MTX- and DAMPA-resistance in a synergistic fashion, the major contribution resulting from point mutant F31R. Mutation Q35E slightly decreases the MTX binding and slightly increases the DAMPA binding. It is known that when the inhibitor does not occupy the active site, a sub-domain shift brings R70 into contact with Q35 [46]. When DAMPA is bound, it is possible that the insertion of a negative charge at position 35 (E35) favours its interaction with R70. In the case of MTX, putative repulsive forces between the glutamate tail of the inhibitor and E35 may be responsible for the slight increase in K_i^{MTX}.

The ratio K_i^{DAMPA}/K_i^{MTX} is similar for the WT and for mutant F31R/Q35E. However, K_i^{DAMPA}/K_i^{MTX} ratios are very different for the point mutants and reflect an unpredictable synergistic contribution to the binding in the double mutant (**table 4.1** and **figure 4.1B**).

In conclusion, these preliminary results represent a proof of principle for the validity of using the MTX fragment DAMPA to gain further insights on the MTX

binding. Kinetic characterization of further mutants of interest, determination of the mode of binding by a kinetic approach and structural characterization by X-ray crystallography with DAMPA will be performed.

Table 4.1. Inhibition constants[a] of MTX and DAMPA for WT and selected MTX-resistant hDHFR mutants.

hDHFR variant	MTX		DAMPA		
	K_i^{MTX} (nM)	$\Delta\Delta G$ *MTX* (kcal mol^{-1})	K_i^{DAMPA} (nM)	$\Delta\Delta G$ *DAMPA* (kcal mol^{-1})	K_i^{DAMPA}/K_i^{MTX}
WT	< 0.031	**-**	< 2	**-**	**> 65**
V115A	20 ± 5	**3.8**	3500 ± 1200	**4.38**	**175 (3×)**[b]
F31R	1.12 ± 0.6	**2.1**	241 ± 50	**2.81**	**215 (3×)**
Q35E	0.048	**0.26**	0.45± 0.26	**-0.87**	**10 (-6×)**
F31R/Q35E (RFE)	21 ± 11	**3.82**	921 ± 164	**3.59**	**45 (1×)**

[a] Mean ± SD; n=3

[b] Values in parenthesis indicate the fold of difference relative to the value for the WT enzyme. Thus, they represent the combined effect of mutation in the enzyme and lack of the glutamate tail portion in the ligand.

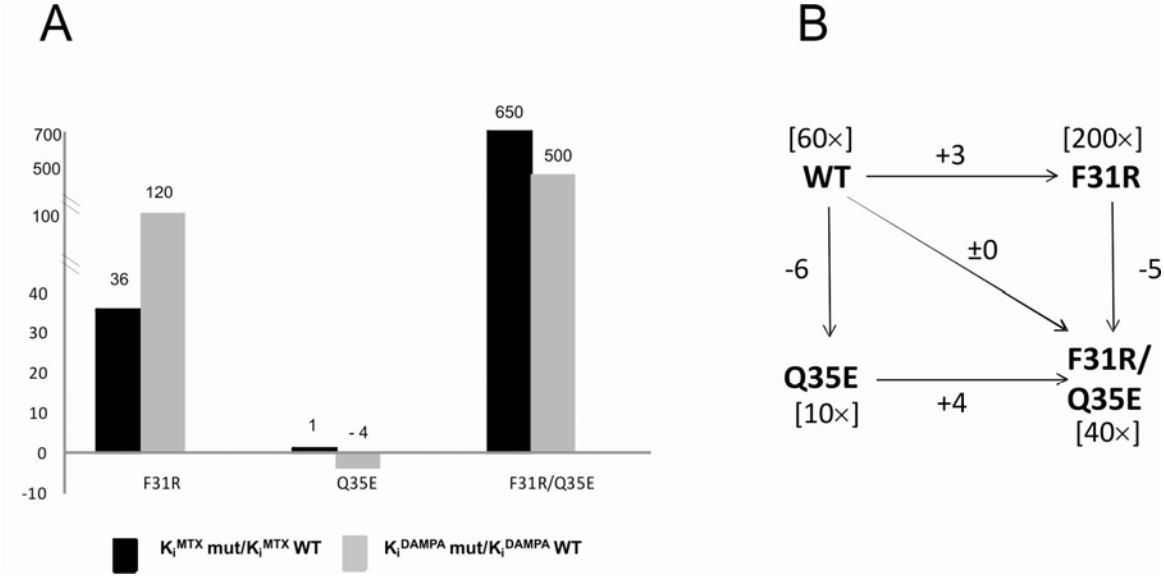

Figure 4.1. Comparison of binding of MTX and its fragment DAMPA in the double mutant F31R/Q35E (RFE) and the corresponding single mutants F31R and Q35E. A) Inhibition constants (K_i) for MTX and DAMPA of hDHFR mutants F31R, Q35E and F31R/Q35E hDHFRs relative to WT. **B**) SAR (structure-activity relationship) presented as a double mutant cycle for ligand binding to F31R/Q35E. Each enzyme variant is in bold. Values in square brackets indicate the ratio K_i^{DAMPA}/K_i^{MTX} for each variant. DAMPA and MTX differ by the lack of the glutamate tail in DAMPA (**figure 1.7**); thus the difference in binding of DAMPA and MTX reflects the contribution of the glutamate tail to binding. Values along the arrows represent the gain or loss in binding resulting both from mutation and from absence of the glutamate tail, determined from the ratio K_i^{DAMPA}/K_i^{MTX} for each mutant. Thus, the contribution of each mutation to the binding of each compound is revealed.

Chapter 5 – Docking for structure-function relationship analysis

5.0 Preface

Structural data are certainly a crucial element for structure-function relationship analysis, which is, ultimately, the main goal of this project. Our laboratory has an ongoing collaboration with the crystallography group of Prof. A. Berghuis at McGill University. The 1.7 Å-resolution structure of mutant F31R/Q35E complexed with MTX was recently obtained [119] and collaborative efforts to crystallize the variants presenting the greatest resistance in the presence of different relevant ligands are currently pursued. However, it is unrealistic to think of crystallizing and resolving the structure of many mutant-ligand complexes, because our experience has demonstrated that the mutated variants in the presence of various ligands do not readily yield high quality crystals. Therefore, it was necessary to identify an alternative, more efficient method to consider structural implication of mutations in ligand binding. Molecular modeling represents a solution to this problem. Among the modeling approaches available to us, we identified the method that best answered to our needs. While energy minimization (see chapter 2) is fast and can be informative when the orientation of the inhibitor in the binding site is known from structural data, it is not applicable to newer ligands for which this information is not available. In this section, the application of automated docking to predict ligand binding to the WT hDHFR will be described.

5.1 Introduction

Automated docking with Autodock 4 is a modeling approach to predict if and how small ligands bind to a target protein of known structure [120-122]. While simple energy minimization of mutant AVH complexed with MTX suggested reasonable insight into the structural causes of a reduced MTX binding (chapter 2) and proved to

be an informative approach for that study, we chose to test automated docking as a possible tool to predict binding of ligands for which no crystal structures in complex with hDHFR exists, such as DHF, PMTX and DAMPA. First, we validated the method by performing the docking with ligands for which DHFR-bound structure was available (FOL and MTX). Then, we used the same protocol to perform the docking of DHF and PMTX. The results of the PMTX binding were unexpected and highlighted the weak points of this methodology to perform structure-function analysis.

5.2 Materials and Methods

5.2.1 *In silico* automated docking of FOL, DHF, MTX and PMTX

The starting coordinates were taken from the PDB file 1U72 of WT hDHFR complexed with the cofactor NADPH and the inhibitor MTX [22]. The crystallographic water molecules and the MTX coordinates were removed directly from the PDB file text. All substrates (FOL, DHF, MTX and PMTX) were prepared as PDB files using ChemDraw 8.0 and Chem3D 8.0 (CambridgeSoft Corporation). Energy minimization of ligands conformations was performed using the integrated MM2 energy minimization script of Chem3D.

Automated docking runs were performed using the AutoDock 4 free software package (Scripps). Both the macromolecule (WT hDHFR complexed with NADPH) and the ligand were prepared as recommended by the Autodock protocol. AutoGrid was used to generate grid maps centered on the C_α of residue Phe34 and including the region that contained the entire folate-binding site and more than half of the NADPH-binding site (grid point spacing of 0.375 Å). For each ligand tested, 50 docking runs were performed using the Lamarckian genetic algorithm [123] and using a starting population of 150 random ligand conformations. All other parameters were kept as suggested in the Autodock docking protocol. Seven torsions were allowed for each ligand (C6-C9, C9-C10, and the five torsions in the glutamate tail assigned by AutoTors) in order to allow rotable bonds to rotate. Following docking, clusters were evaluated according to the total binding energies calculated by AutoDock 4, and the

minimal energy conformation coming from the cluster at the lowest energy was retained for analysis. Ligand conformations in each cluster were also analyzed.

5.3 Results and Discussion

Docking of MTX and FOL were used to validate the approach, expecting the ligand orientation and the critical contacts with the hDHFR active-site residues to be similar to existing structural information. MTX binds in the active site with its pteridine moiety flipped 180° relative to folate (**figure 1.6**). Main interactions between the ligands (FOL and MTX) and hDHFR were described in chapter 1 and they are listed in **table 1.1.** The crystal structures used as a reference for comparison were 1U72.PDB (ternary WT hDHFR·NADPH·MTX complex)[22] and 1DHF.PDB (binary WT hDHFR·FOL complex)[18].

Autodock analysis is based on positional root mean square deviation (rmsd) of the corresponding atoms. The docked conformations are ranked in clusters in order of increasing energy. The autoDock's analysis tool compares all docked conformations with one-another, and if two conformations have an rmsd between 0.5 Å and 2.0 Å (value set by the operator), they are both stored in the same cluster. Clusters are then ranked in order of increasing energy from the most negative to the most positive. The clustering results are indicated in **table 5.1.** In addition, conformations in **table 5.1** are classified on the basis of the orientation of their pteroyl moiety.

5.3.1 Docking of MTX

The docking result with MTX showed the correct orientation of the ligand in the folate binding site and a good prediction of the interactions of MTX with the macromolecule (**figure 5.1**). The docked MTX (conformation of lowest binding energy) superimposed well with MTX from 1U72.PDB, the main difference being a significant shift of the glutamate γ-COOH towards N64, possibly driven by H-bonding interaction with the N64 side chain (**figure 5.1**). Despite this difference, the docking result was considered consistent with the interactions observed in the crystal structure.

The cluster of lowest energy was constituted by 9 different conformations, 8 of which found the pterin 4-amino group oriented towards V115 (4-amino orientation), as

observed in the 1U72.PDB crystal structure, and 1 with its 4-amino group flipped (4-oxo orientation), such as the pterin 4-carbonyl of FOL (1DHF.PDB)(**table 5.1**). Thus, the pteroyl orientation of the majority of docked conformations in the cluster of lowest energy correlated well with the structural data.

5.3.2 Docking of FOL

The FOL ligand was docked into 1U72.PDB, and not into 1DHF.PDB, because we wanted to evaluate the effects of the docking of a ligand to a structure other than the one from which it had been stripped out.

Superimposition of the docked FOL (conformation of lowest binding energy), 1U72.PDB and 1DHF.PDB (**figure 5.2**) showed that the orientation of the molecule was, as expected, similar to the one observed in 1DHF.PDB, with the 4-oxo group pointing in the opposite direction compared to the 4-amino group of MTX. A rotation and an upwards shift of the FOL pteridine ring relative to both FOL from 1DHF.PDB and MTX from 1U72.PDB was observed. This was possibly due to ring stacking interactions with the nicotinamide ring of NADPH, which is missing in the 1DHF.PDB crystal structure. Following the docking, interactions with residues F31 (not shown in **figure 5.2**), N64 and R70 of the enzyme were all maintained. Again, the result of the modeling was consistent with the observed structural data.

Although the conformation of lowest energy was well oriented in the active site, the clustering results were poor. In fact, the cluster of the lowest energy was constituted by only 3 different conformations, 2 of which found the pterin 4-oxo group oriented towards W24 and E30 (4-oxo orientation), as observed in the crystal structure 1DHF.PDB, and 1 with its 4-oxo group oriented towards V115 (4-amino orientation), like the pterin 4-amino group of MTX (**table 5.1**).

5.3.3 Docking of DHF

The instability of this compound, which is readily oxidized to folate, makes impossible to crystallize it within the folate-binding site, making the docking an interesting alternative to better understand the DHF binding.

Following the docking, the orientation of the 4-carbonyl group of the conformation at lower energy was, as expected, the same as the FOL 4-oxo group. Most of the

docked conformations which entered the active site were in the expected 4-oxo orientation (**table 5.1**). However, the interactions with N64 and R70 were not preserved, due to a rotation of the *p*-ABA-Glu carbonyl and an inversion of α-COOH and γ-COOH of the glutamate tail (**figure 5.3**). The pteridine ring was positioned similarly to the pteridine ring of the docked FOL (result not shown in **figure 5.3**). Although it is likely that the *p*-ABA-Glu portion of bound FOL and DHF are oriented in the same way, important differences were observed following the docking, especially if we reason in the context of a SAR study.

5.3.4 Docking of PMTX

PMTX (**figure 1.7**) is a novel antifolate that inhibits the activity of human DHFR, as well as human thymidylate synthase (hTS) and to a lesser extent the purine biosynthesis enzymes GARFT and AICARFT [81]. PMTX contains a pyrrolo-pyrimidine ring instead of the classical pterin ring and N_{10} is replaced by a carbon covalently bound to a non-polar methyl group. Like FOL, the double-ring moiety of PMTX contains a 2-amino and a 4-oxo group, in contrast to MTX, which contains 2,4-diamino groups. Because of this difference, it has been suggested that PMTX binds the active site of hDHFR as FOL does, with the 4-oxo moiety pointing towards residues Glu30 and Trp24 [73]. This hypothesis is supported by the observation that 5-deazafolate (**figure 1.7**), which is also a 4-oxo pteridine system and is structurally similar to both FOL and PMTX, binds in the same orientation as FOL [18]. Moreover, using molecular modeling, Gangjee A. *et al*. [73] suggested that PMTX binds to DHFR in the same orientation as FOL.

Unexpectedly, the lowest energy conformation from the docking showed an orientation of the 6-5 ring-fused pyrrolo[2,3-*d*]pyrimidine moiety similar to that of MTX, with the PMTX 4-carbonyl group and the MTX 4 –amino group pointing in the same direction (**figure 5.4**). Out of the 11 docked conformations in the cluster at lowest energy, 7 were in the 4-amino orientation and 4 in the 4-oxo orientation. Of the other 11 conformations that docked into the FOL binding site, all bound in the 4-oxo mode (**table 5.1**). Unfortunately, due to the statistical representation of both orientations, it was impossible to make conlcusions on the binding mode of PMTX. The PMTX

modeling study from Gangjee A. *et al*.[73] was performed using Sybyl 6.3, but the modeling approach they used and the results were not described, so we could not compare our results with theirs.

5.4 Conclusion

All ligands tested efficiently entered the folate binding-site and overall results for MTX and FOL docking were relatively accurate. The results with PMTX were in disagreement with the previous modeling results from Gangjee A. *et al.*[73], the conformation at lowest energy being in the 4-amino orientation. In the absence of a strong modeling evidence, structural data will be required to elucidate the binding orientation of PMTX. Our lab is currently working to obtain this information in collaboration with the group of Prof. A. Berghuis (McGill University).

While automated docking is certainly a valuable tool to identify the inhibition potential of new molecules [124], it is also true that small differences can lead to erroneous interpretations when SAR (Structure-Activity Relationship) is the ultimate goal of the docking. AutoDock 4 ranks ligand conformations in clusters by calculating binding energies on the basis of its scoring function [123]. Depending on the size of the ligand and the number of torsion angles allowed, it is possible to obtain a high number of clusters containing a small number of significantly different conformations. Docking can certainly be a useful tool for SAR when little structural information is available, but a careful analysis of clustering number, energies, and ligand conformations should be taken into account. Although we do not exclude the possibility of using AutoDock in the future for similar SAR applications, in the case of PMTX we prefer obtaining structural evidence before speculating on PMTX binding properties and effects of hDHFR mutations on binding.

Table 5.1. Docking clustering: orientation of the pteroyl ring in the active site

Docked substrate	Known or expected orientation	Number of clusters[a]	Conformations in 4-oxo orientation	Conformations in 4-amino orientation	Conformations outside the active site[d]
MTX	4-amino orientation[22]	30	**1**_6[b]; **2**_1; **2**_2; **6**_1; **6**_2; **7**_1; **8**_1; **9**_1; **10**_1; **10**_2	**1**_1[c]-**1**_5; **1**_7-**1**_9; **24**_1	**3**_1; **4**_1-**4**_3; **5**_1; **11**_1; **12**_1; **13**_1; **14**_1; **14**_2; **15**_1; **15**_2; **16**_1; **17**_1-**17**_4; **18**_1; **19**_1; **20**_1; **21**_1; **21**_2; **22**_1; **23**_1; **25**_1; **26**_1; **26**_2; **27**_1; **28**_1; **29**_1; **30**_1
FOL	4-oxo orientation[18]	23	**1**_1; **1**_3; **4**_1; **12**_1; **14**_1	**1**_2; **2**_1; **2**_2	**3**_1-**3**_4; **5**_1-**5**_5; **6**_1; **6**_2; **7**_1; **8**_1-**8**_5; **9**_1; **9**_2; **10**_1; **11**_1-**11**_4; **13**_1; **13**_2; **14**_2; **15**_1; **16**_1; **16**_2; **17**_1; **18**_1-**18**_4; **19**_1; **19**_2; **20**_1; **20**_2; **21**_1; **22**_1; **23**_1
DHF	4-oxo orientation	25	**1**_1-**1**_7; **2**_1-**2**_4; **7**_1; **18**_1	**19**_1	**3**_1-**3**_4; **4**_1-**4**_6; **5**_1; **5**_2; **6**_1; **8**_1-**8**_3; **9**_1-**9**_3; **10**_1; **11**_1-**11**_4; **12**_1; **13**_1; **14**_1; **15**_1; **16**_1; **17**_1; **20**_1; **21**_1; **22**_1; **23**_1; **24**_1; **25**_1
PMTX	4-oxo orientation	12	**1**_5; **1**_8-**1**_10; **3**_1; **3**_2; **4**_1-**4**_6; **5**_1-**5**_3	**1**_1-**1**_7; **1**_11	**2**_1-**2**_6; **6**_1; **7**_1-**7**_7; **8**_1-**8**_6; **9**_1-**9**_4; **10**_1; **11**_1; **11**_2; **12**_1

[a] Cluster: group of docked conformations with rmsd between 0.5 Å and 2.0 Å.
[b] **1**_6: docked conformations are indicated on the base of the cluster they belong (number in bold) and their ranking energy within the cluster (number in normal style).
[c] docked conformation of lowest energy is underlined.
[d] docked conformations that docked outside the folate binding pocket.

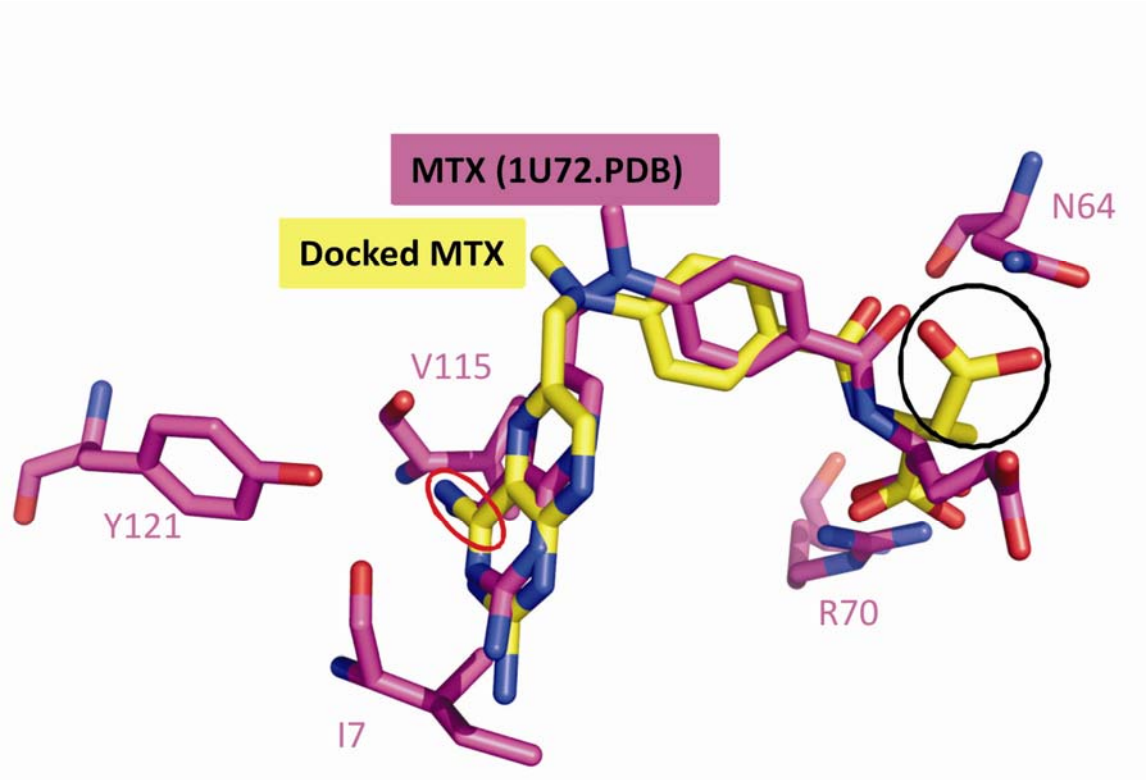

Figure 5.1. Docking of MTX into WT hDHFR·NADPH. Superimposition of docking result (MTX conformation of lowest binding energy) and 1U72.PDB (ternary complex WT hDHFR·NADPH·MTX). Docked MTX is in yellow. MTX from 1U72.PDB is in magenta. Active-site residues I7, V115, Y121, R70 and N64 from 1U72.PDB are highlighted as reference points. The 4-amino of docked MTX is circled in red. The γ-COOH of the glutamate tail of MTX is circled in black.

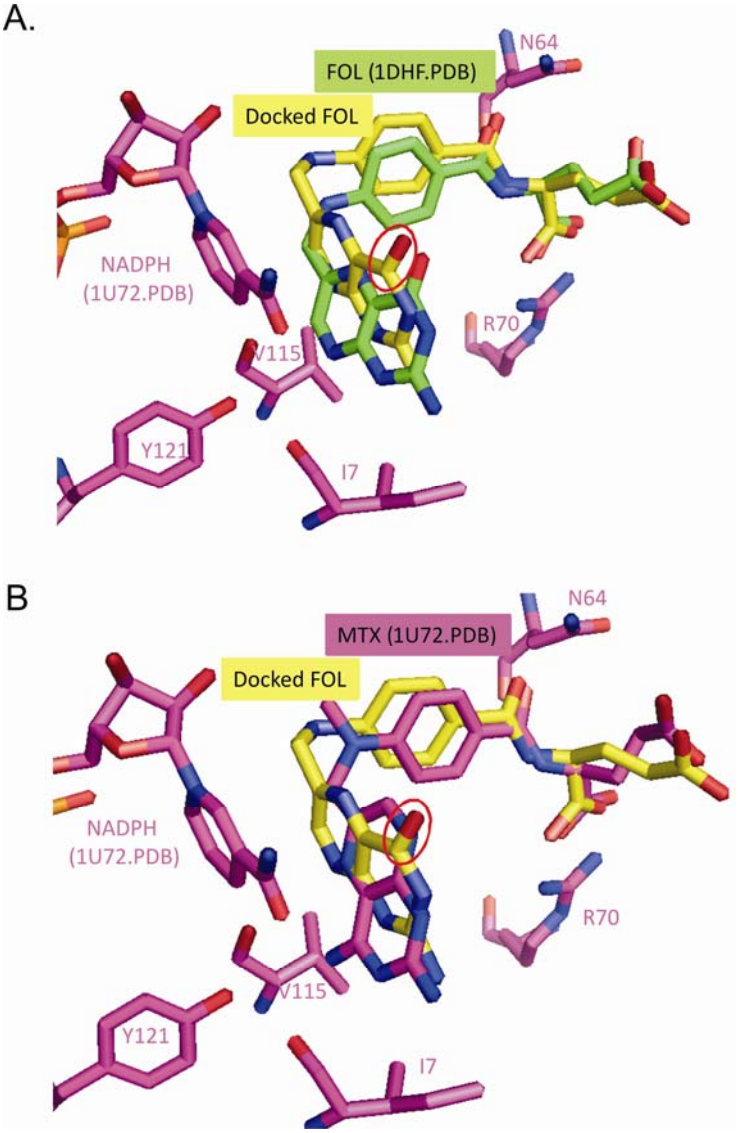

Figure 5.2. Docking of FOL into WT hDHFR·NADPH. Superimposition of docking result (FOL conformation of lowest binding energy), 1U72.PDB (ternary complex WT hDHFR·NADPH·MTX) and 1DHF.PDB (binary complex WT hDHFR·FOL). Active-site residues I7, V115, Y121, R70 and N64 and the NADPH nicotinamide ring from 1U72.PDB are highlighted. The 4-oxo group of docked FOL is circled in red. **A)** Docked FOL is in yellow and FOL from 1DHF.PDB is in green. **B)** Docked FOL is in yellow and MTX from 1U72.PDB in magenta.

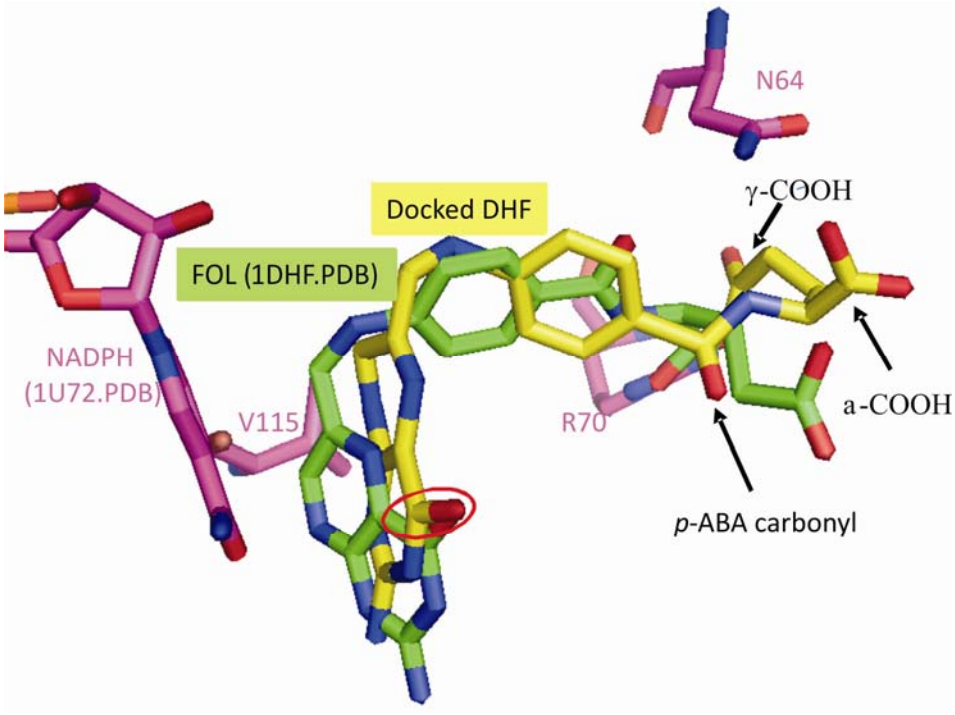

Figure 5.3. Docking of DHF into WT hDHFR·NADPH. Superimposition of docked DHF (conformation of lowest binding energy), 1U72.PDB (ternary complex WT hDHFR·NADPH·MTX) and 1DHF.PDB (binary complex WT hDHFR·FOL). Active-site residues V115, R70 and N64 and the NADPH nicotinamide ring from 1U72.PDB are shown as reference points. Docked DHF is in yellow. FOL from 1DHF.PDB is in green. The 4-oxo group of docked DHF is circled in red.

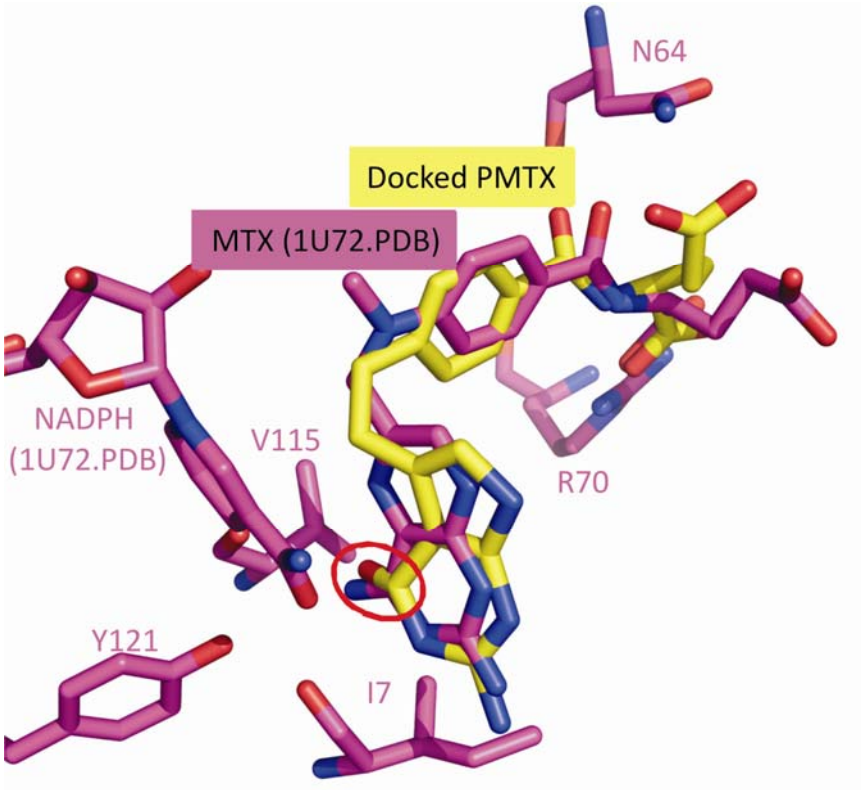

Figure 5.4. Docking of PMTX into WT hDHFR·NADPH. Superimposition of docked PMTX (conformation of lowest binding energy) and 1U72.PDB (ternary complex WT hDHFR·NADPH·MTX). Active-site residues I7, V115, Y121, R70 and N64 and the NADPH nicotinamide ring from 1U72.PDB are shown. Docked PMTX is in yellow. MTX from 1U72.PDB is in magenta. The 4-carbonyl group of docked PMTX is circled in red.

Chapter 6 – Conclusions and perspectives

In order to better understand the determinants of ligand binding, we applied directed evolution to the human DHFR, a well-characterized and clinically relevant enzyme which is an important target for the treatment of human proliferative diseases. A combined approach based on kinetic analysis, structural visualization and molecular modeling was used to begin a structure-activity relationship study.

First, we targeted different active-site residues (PhD student Jordan Volpato) and we mutated them, generally by saturation mutagenesis. Different combinatorial libraries (mutagenesis at multiple sites) were also created in the laboratory, of which only library 31/34/35 created by Jordan Volpato was described in chapter 2.

Then, we developed an efficient two-tier bacterial and *in vitro* selection strategy to identify mutants presenting the phenotypes of interest: activity (DHF binding) and antifolate resistance (reduced enzyme inhibition). Following the screening, we obtained new functional information regarding the targeted residues, which was the goal of the proposed work. **Position 115** is relatively permissive to mutations that conserve activity. All substitutions were hydrophobic (Ile, Leu, Ala, Tyr, Phe, Met) or had no H-bonding capacity (Cys). This feature appears to be required to preserve the activity. Novel MTX-resistant mutants V115A and V115C were identified. The reduced hydrophobic contact surface of Ala and Cys appears to a have a greater impact on the MTX binding (= resistance) than on the DHF binding (= maintenance of activity), and therefore confers ligand discrimination. Due to its permissivity (many mutations are accepted), residue 115 is surely an interesting candidate for further studies in a combinatorial context. In the case of **Ile7**, only highly conservative mutations I7L and I7V preserved activity, highlighting the importance of hydrophobicity at this position. No substitutions were compatible with activity at position 70. Mutants may have been inactive, poorly expressed or unstable. Arg70 is highly conserved across species and was not permissive

to mutations; thus, it is likely required for the substrate binding, the structure or both. For this reason, it will not be mutated in complex libraries.

We extended the utility of the screening method to identify further phenotypes of interest, like the resistance of mutant hDHFR to other antifolates. To be detected as inhibitor-resistant, a hDHFR mutant has to preserve a certain degree of catalytic activity. Therefore, in principle, every new antifolate can be tested *in vitro* towards any identified active mutant, as long as the molecule is soluble in the assay conditions. The results for PMTX resistance correlated with the ones for MTX-resistance, the only two PMTX-resistant mutants identified being V115A and V115C. However, while mutation V115A reduced K_i^{MTX} 600-fold and affected productive binding of both PMTX and DHF in a similar fashion (200-fold decrease effect on K_i^{PMTX} and K_M^{DHF}, respectively), mutation V115C reduced K_M^{DHF} only 100-fold but K_i^{MTX} and K_i^{PMTX} of about 600-fold. Therefore, independently of the orientation of the PMTX pterin ring, for which structural data is not available, it appears that residue 115 can effectively offer some degree of ligand discrimination. Variants that are mutated at other active site positions will be screened against PMTX to verify the occurrence of ligand discrimination at specific areas.

We have begun to build a SAR (Structure-Activity Relationship) with MTX, by investigating the binding of its constituent fragments DAP, *p*-ABA-Glu and DAMPA. Preliminary tests confirmed that, of the three tested fragments, only DAMPA efficiently inhibits WT hDHFR. The lack of the L-glutamate portion of MTX accounted for a 65-fold reduced inhibition (K_i^{DAMPA}/K_i^{MTX} for WT hDHFR). Mutation of residue 115 (V115A), which is located far from the glutamate tail of the bound MTX, unexpectedly affected the binding of DAMPA, showing the importance of distal effects that cannot be visualized from the structure. Characterization of the double mutant F31R/Q35E (RFE) and of its constituent point mutants showed unpredictable synergistic contribution to the binding in the double mutant

Finally, we performed *in silico* mutagenesis coupled with energy minimization to compare the predicted structure of the highly MTX-resistant triple mutant F31A/F34V/Q35H (AVH) to the native enzyme. Modeling suggested that an increased cavity volume lies at the root of the weakened ligand binding. The method is simple and allows postulating of reasonable structural hypothesis by correlating structural

visualization and kinetic/inhibitory parameters. We also used an automated docking approach to predict the binding of DHF and PMTX, for which structural data are not available. Although this remains a possible tool to test the inhibitory potential of a molecule, it is probably not precise enough for SAR studies.

Currently, we are attempting to obtain a crystal structure of WT hDHFR complexed with PMTX (Jordan Volpato and Mirja Krause) to observe the orientation of its pyrrolo-pyrimidine moiety in the active site, information for which the current modeling results are contradictory.

In conclusion, we developed an efficient approach to identify active and antifolate- resistant mutants of hDHFR and we have begun collecting structure-function information that will contribute to the development of highly specific drugs for this enzyme. Combinatorial libraries which target different areas of the active site and different antifolates will be screened and characterized in order to build a molecular map of the determinants of the ligand binding in the hDHFR active site. A BioMek bench-top robotic liquid-handler will be installed in the laboratory, allowing a larger number of variants to be characterized and a larger number of variables (substrate and inhibitor concentrations) to be examined. Kinetic characterization for inhibitor fragments and structural characterization both by X-ray crystallography and by modeling will be used as principal tools to reach the ultimate goal of a better understanding of the ligand binding. As complementary approach, STD-NMR (saturation transfer difference NMR)[125, 126], a NMR technique that allows the identification of the proximity of ligand atoms to the protein surface, should also be considered as a tool for SAR studies.

References

1. Blakley, R.L., *The biochemistry of folic acid and related pterines*. 1969: John Wiley & sons, New York.
2. Voet, D.V., J. G., *Biochemistry*. 1995, Toronto: John Wiley & Sons, Inc.
3. Matherly, L.H., *Molecular and cellular biology of the human reduced folate carrier.* Prog Nucleic Acid Res Mol Biol, 2001. **67**: p. 131-62.
4. Anderson, R.G., et al., *Potocytosis: sequestration and transport of small molecules by caveolae.* Science, 1992. **255**(5043): p. 410-1.
5. Walling, J., *From methotrexate to pemetrexed and beyond. A review of the pharmacodynamic and clinical properties of antifolates.* Invest New Drugs, 2006. **24**(1): p. 37-77.
6. Yao, R., et al., *Human gamma-glutamyl hydrolase: cloning and characterization of the enzyme expressed in vitro.* Proc Natl Acad Sci U S A, 1996. **93**(19): p. 10134-8.
7. Moran, R.G., W.C. Werkheiser, and S.F. Zakrzewski, *Folate metabolism in mammalian cells in culture. I Partial characterization of the folate derivatives present in L1210 mouse leukemia cells.* J Biol Chem, 1976. **251**(12): p. 3569-75.
8. Appleman, J.R., et al., *Unusual transient- and steady-state kinetic behavior is predicted by the kinetic scheme operational for recombinant human dihydrofolate reductase.* J Biol Chem, 1990. **265**(5): p. 2740-8.
9. Viudes, A., et al., *Candidemia at a tertiary-care hospital: epidemiology, treatment, clinical outcome and risk factors for death.* Eur J Clin Microbiol Infect Dis, 2002. **21**(11): p. 767-74.
10. Morris, A., et al., *Current epidemiology of Pneumocystis pneumonia.* Emerg Infect Dis, 2004. **10**(10): p. 1713-20.
11. Dhople, A.M., *Antimicrobial activities of dihydrofolate reductase inhibitors, used singly or in combination with dapsone, against Mycobacterium ulcerans.* J Antimicrob Chemother, 2001. **47**(1): p. 93-6.
12. Linares, G.E. and J.B. Rodriguez, *Current status and progresses made in malaria chemotherapy.* Curr Med Chem, 2007. **14**(3): p. 289-314.

13. Appleman, J.R., et al., *Kinetics of the formation and isomerization of methotrexate complexes of recombinant human dihydrofolate reductase.* J Biol Chem, 1988. **263**(21): p. 10304-13.
14. Prendergast, N.J., et al., *Expression and site-directed mutagenesis of human dihydrofolate reductase.* Biochemistry, 1988. **27**(10): p. 3664-71.
15. Benkovic, S.J., C.A. Fierke, and A.M. Naylor, *Insights into enzyme function from studies on mutants of dihydrofolate reductase.* Science, 1988. **239**(4844): p. 1105-10.
16. Beard, W.A., et al., *Hydride transfer by dihydrofolate reductase. Causes and consequences of the wide range of rates exhibited by bacterial and vertebrate enzymes.* J Biol Chem, 1989. **264**(16): p. 9391-9.
17. Stone, S.R. and J.F. Morrison, *Dihydrofolate reductase from Escherichia coli: the kinetic mechanism with NADPH and reduced acetylpyridine adenine dinucleotide phosphate as substrates.* Biochemistry, 1988. **27**(15): p. 5493-9.
18. Davies, J.F., 2nd, et al., *Crystal structures of recombinant human dihydrofolate reductase complexed with folate and 5-deazafolate.* Biochemistry, 1990. **29**(40): p. 9467-79.
19. Meiering, E.M., et al., *Contributions of tryptophan 24 and glutamate 30 to binding long-lived water molecules in the ternary complex of human dihydrofolate reductase with methotrexate and NADPH studied by site-directed mutagenesis and nuclear magnetic resonance spectroscopy.* J Mol Biol, 1995. **247**(2): p. 309-25.
20. Volz, K.W., et al., *Crystal structure of avian dihydrofolate reductase containing phenyltriazine and NADPH.* J Biol Chem, 1982. **257**(5): p. 2528-36.
21. Matthews, D.A., et al., *Dihydrofolate reductase. The stereochemistry of inhibitor selectivity.* J Biol Chem, 1985. **260**(1): p. 392-9.
22. Cody, V., J.R. Luft, and W. Pangborn, *Understanding the role of Leu22 variants in methotrexate resistance: comparison of wild-type and Leu22Arg variant mouse and human dihydrofolate reductase ternary crystal complexes with methotrexate and NADPH.* Acta Crystallogr D Biol Crystallogr, 2005. **61**(Pt 2): p. 147-55.

23. Baccanari, D.P., D. Stone, and L. Kuyper, *Effect of a single amino acid substitution on Escherichia coli dihydrofolate reductase catalysis and ligand binding.* J Biol Chem, 1981. **256**(4): p. 1738-47.
24. Prendergast, N.J., et al., *Effects of conversion of phenylalanine-31 to leucine on the function of human dihydrofolate reductase.* Biochemistry, 1989. **28**(11): p. 4645-50.
25. Bowman, A.L., M.G. Lerner, and H.A. Carlson, *Protein flexibility and species specificity in structure-based drug discovery: dihydrofolate reductase as a test system.* J Am Chem Soc, 2007. **129**(12): p. 3634-40.
26. Chan, D.C. and A.C. Anderson, *Towards species-specific antifolates.* Curr Med Chem, 2006. **13**(4): p. 377-98.
27. Volpato, J.P. and J.N. Pelletier, *Sequence and structural comparison of mammalian, bacterial and parasitic dihydrofolate reductases: cross-species 'hot-spots' provide antifolate resistance. Review.* . Submitted, August 2008. .
28. Oefner, C., A. D'Arcy, and F.K. Winkler, *Crystal structure of human dihydrofolate reductase complexed with folate.* Eur J Biochem, 1988. **174**(2): p. 377-85.
29. Cody, V., et al., *Analysis of three crystal structure determinations of a 5-methyl-6-N-methylanilino pyridopyrimidine antifolate complex with human dihydrofolate reductase.* Acta Crystallogr D Biol Crystallogr, 2003. **59**(Pt 9): p. 1603-9.
30. Johnson, J.M., et al., *NMR solution structure of the antitumor compound PT523 and NADPH in the ternary complex with human dihydrofolate reductase.* Biochemistry, 1997. **36**(15): p. 4399-411.
31. Kovalevskaya, N.V., et al., *Solution structure of human dihydrofolate reductase in its complex with trimethoprim and NADPH.* J Biomol NMR, 2005. **33**(1): p. 69-72.
32. Hutchings, B.L., J.H. Mowat, and et al., *Synthesis and some biological properties of 4-aminopteroylaspartic acid.* J Biol Chem, 1949. **180**(2): p. 857-63.
33. Farber, S., *Some observations on the effect of folic acid antagonists on acute leukemia and other forms of incurable cancer.* Blood, 1949. **4**(2): p. 160-7.
34. McGuire, J.J., *Anticancer antifolates: current status and future directions.* Curr Pharm Des, 2003. **9**(31): p. 2593-613.

35. Ercikan-Abali, E.A., et al., *Variants of human dihydrofolate reductase with substitutions at leucine-22: effect on catalytic and inhibitor binding properties.* Mol Pharmacol, 1996. **49**(3): p. 430-7.
36. Stone, S.R. and J.F. Morrison, *Mechanism of inhibition of dihydrofolate reductases from bacterial and vertebrate sources by various classes of folate analogues.* Biochim Biophys Acta, 1986. **869**(3): p. 275-85.
37. Volpato, J.P., E. Fossati, and J.N. Pelletier, *Increasing methotrexate resistance by combination of active-site mutations in human dihydrofolate reductase.* J Mol Biol, 2007. **373**(3): p. 599-611.
38. Emery, P., et al., *Comparison of methotrexate monotherapy with a combination of methotrexate and etanercept in active, early, moderate to severe rheumatoid arthritis (COMET): a randomised, double-blind, parallel treatment trial.* Lancet, 2008.
39. Taylor, W.J., et al., *Drug Use and Toxicity in Psoriatic Disease: Focus on Methotrexate.* J Rheumatol, 2008. **35**(7): p. 1454-1457.
40. Alyea, E.P., et al., *Sirolimus, tacrolimus, and low-dose methotrexate as graft-versus-host disease prophylaxis in related and unrelated donor reduced-intensity conditioning allogeneic peripheral blood stem cell transplantation.* Biol Blood Marrow Transplant, 2008. **14**(8): p. 920-6.
41. Zhao, R. and I.D. Goldman, *Resistance to antifolates.* Oncogene, 2003. **22**(47): p. 7431-57.
42. Melera, P.W., *Acquired versus intrinsic resistance to methotrexate: diversity of the drug-resistant phenotype in mammalian cells.* Semin Cancer Biol, 1991. **2**(4): p. 245-55.
43. Lewis, W.S., et al., *Methotrexate-resistant variants of human dihydrofolate reductase with substitutions of leucine 22. Kinetics, crystallography, and potential as selectable markers.* J Biol Chem, 1995. **270**(10): p. 5057-64.
44. Thillet, J., et al., *Site-directed mutagenesis of mouse dihydrofolate reductase. Mutants with increased resistance to methotrexate and trimethoprim.* J Biol Chem, 1988. **263**(25): p. 12500-8.

45. Nakano, T., et al., *Critical role of phenylalanine 34 of human dihydrofolate reductase in substrate and inhibitor binding and in catalysis.* Biochemistry, 1994. **33**(33): p. 9945-52.

46. Thompson, P.D. and J.H. Freisheim, *Conversion of arginine to lysine at position 70 of human dihydrofolate reductase: generation of a methotrexate-insensitive mutant enzyme.* Biochemistry, 1991. **30**(33): p. 8124-30.

47. Farber, S., *Chemotherapeutic studies of tumors, including leukemia, in children.* Am J Dis Child, 1950. **79**(5): p. 961-2.

48. Goker, E., et al., *Amplification of the dihydrofolate reductase gene is a mechanism of acquired resistance to methotrexate in patients with acute lymphoblastic leukemia and is correlated with p53 gene mutations.* Blood, 1995. **86**(2): p. 677-84.

49. Melera, P.W., et al., *Antifolate-resistant Chinese Hamster Cells. mRNA directed overproduction of multiple dihydrofolate reductases from a series of independently derived sublines containing amplified dihydrofolate reductase genes.* J Biol Chem, 1982. **257**(21): p. 12939-49.

50. Chu, E., et al., *Specific binding of human dihydrofolate reductase protein to dihydrofolate reductase messenger RNA in vitro.* Biochemistry, 1993. **32**(18): p. 4756-60.

51. Rothem, L., et al., *Reduced folate carrier gene silencing in multiple antifolate-resistant tumor cell lines is due to a simultaneous loss of function of multiple transcription factors but not promoter methylation.* J Biol Chem, 2004. **279**(1): p. 374-84.

52. Zhao, R., et al., *Molecular analysis of murine leukemia cell lines resistant to 5, 10-dideazatetrahydrofolate identifies several amino acids critical to the function of folylpolyglutamate synthetase.* J Biol Chem, 2000. **275**(34): p. 26599-606.

53. Lin, J.T., et al., *Basis for natural resistance to methotrexate in human acute non-lymphocytic leukemia.* Leuk Res, 1991. **15**(12): p. 1191-6.

54. Trippett, T., et al., *Defective transport as a mechanism of acquired resistance to methotrexate in patients with acute lymphocytic leukemia.* Blood, 1992. **80**(5): p. 1158-62.

55. Goker, E., et al., *Decreased polyglutamylation of methotrexate in acute lymphoblastic leukemia blasts in adults compared to children with this disease.* Leukemia, 1993. **7**(7): p. 1000-4.

56. Spencer, H.T., et al., *Mutations in the gene for human dihydrofolate reductase: an unlikely cause of clinical relapse in pediatric leukemia after therapy with methotrexate.* Leukemia, 1996. **10**(3): p. 439-46.

57. Patel, M., et al., *Comparison of the protection of cells from antifolates by transduced human dihydrofolate reductase mutants.* Hum Gene Ther, 1997. **8**(17): p. 2069-77.

58. Banerjee, D. and J.R. Bertino, *Myeloprotection with drug-resistance genes.* Lancet Oncol, 2002. **3**(3): p. 154-8.

59. Dicker, A.P., et al., *Methotrexate resistance in an in vivo mouse tumor due to a non-active-site dihydrofolate reductase mutation.* Proc Natl Acad Sci U S A, 1993. **90**(24): p. 11797-801.

60. Simonsen, C.C. and A.D. Levinson, *Isolation and expression of an altered mouse dihydrofolate reductase cDNA.* Proc Natl Acad Sci U S A, 1983. **80**(9): p. 2495-9.

61. McIvor, R.S. and C.C. Simonsen, *Isolation and characterization of a variant dihydrofolate reductase cDNA from methotrexate-resistant murine L5178Y cells.* Nucleic Acids Res, 1990. **18**(23): p. 7025-32.

62. Melera, P.W., et al., *Phenotypic expression in Escherichia coli and nucleotide sequence of two Chinese hamster lung cell cDNAs encoding different dihydrofolate reductases.* Mol Cell Biol, 1984. **4**(1): p. 38-48.

63. Srimatkandada, S., et al., *Amplification of a polymorphic dihydrofolate reductase gene expressing an enzyme with decreased binding to methotrexate in a human colon carcinoma cell line, HCT-8R4, resistant to this drug.* J Biol Chem, 1989. **264**(6): p. 3524-8.

64. Cody, V., et al., *Crystal structure determination at 2.3 A of recombinant human dihydrofolate reductase ternary complex with NADPH and methotrexate-gamma-tetrazole.* Anticancer Drug Des, 1992. **7**(6): p. 483-91.

65. Chunduru, S.K., et al., *Methotrexate-resistant variants of human dihydrofolate reductase. Effects of Phe31 substitutions.* J Biol Chem, 1994. **269**(13): p. 9547-55.

66. Ercikan-Abali, E.A., et al., *Active site-directed double mutants of dihydrofolate reductase.* Cancer Res, 1996. **56**(18): p. 4142-5.

67. Budak-Alpdogan, T., D. Banerjee, and J.R. Bertino, *Hematopoietic stem cell gene therapy with drug resistance genes: an update.* Cancer Gene Ther, 2005. **12**(11): p. 849-63.

68. Zhao, S.C., et al., *Post-transplant methotrexate administration leads to improved curability of mice bearing a mammary tumor transplanted with marrow transduced with a mutant human dihydrofolate reductase cDNA.* Hum Gene Ther, 1997. **8**(8): p. 903-9.

69. Allay, J.A., et al., *In vivo selection of retrovirally transduced hematopoietic stem cells.* Nat Med, 1998. **4**(10): p. 1136-43.

70. Meisel, R., et al., *Efficient protection from methotrexate toxicity and selection of transduced human hematopoietic cells following gene transfer of dihydrofolate reductase mutants.* Exp Hematol, 2003. **31**(12): p. 1215-22.

71. Capiaux, G.M., et al., *Retroviral transduction of a mutant dihydrofolate reductase-thymidylate synthase fusion gene into murine marrow cells confers resistance to both methotrexate and 5-fluorouracil.* Hum Gene Ther, 2003. **14**(5): p. 435-46.

72. Volpato, J.P., et al., *Ex vivo selection of hematopoietic cells using highly MTX-resistant human dihydrofolate reductase double and triple mutants.* . Submitted, September 2008.

73. Gangjee, A., et al., *Design, synthesis, and X-ray crystal structure of a potent dual inhibitor of thymidylate synthase and dihydrofolate reductase as an antitumor agent.* J Med Chem, 2000. **43**(21): p. 3837-51.

74. Gangjee, A., et al., *Dual inhibitors of thymidylate synthase and dihydrofolate reductase as antitumor agents: design, synthesis, and biological evaluation of classical and nonclassical pyrrolo[2,3-d]pyrimidine antifolates(1).* J Med Chem, 2006. **49**(3): p. 1055-65.

75. Navarro-Peran, E., et al., *Effects of folate cycle disruption by the green tea polyphenol epigallocatechin-3-gallate.* Int J Biochem Cell Biol, 2007. **39**(12): p. 2215-25.

76. Wyss, P.C., et al., *Novel dihydrofolate reductase inhibitors. Structure-based versus diversity-based library design and high-throughput synthesis and screening.* J Med Chem, 2003. **46**(12): p. 2304-12.

77. Shih, C., et al., *Multiple folate enzyme inhibition: mechanism of a novel pyrrolopyrimidine-based antifolate LY231514 (MTA).* Adv Enzyme Regul, 1998. **38**: p. 135-52.

78. Adjei, A.A., *Pemetrexed (ALIMTA), a novel multitargeted antineoplastic agent.* Clin Cancer Res, 2004. **10**(12 Pt 2): p. 4276s-4280s.

79. Blanke, C.D., et al., *Phase II study of trimetrexate, fluorouracil, and leucovorin for advanced colorectal cancer.* J Clin Oncol, 1997. **15**(3): p. 915-20.

80. Punt, C.J., et al., *Trimetrexate as biochemical modulator of 5-fluorouracil/leucovorin in advanced colorectal cancer: final results of a randomised European study.* Ann Oncol, 2002. **13**(1): p. 81-6.

81. Shih, C., et al., *LY231514, a pyrrolo[2,3-d]pyrimidine-based antifolate that inhibits multiple folate-requiring enzymes.* Cancer Res, 1997. **57**(6): p. 1116-23.

82. Greer, J., et al., *Application of the three-dimensional structures of protein target molecules in structure-based drug design.* J Med Chem, 1994. **37**(8): p. 1035-54.

83. Ansede, J.H. and D.R. Thakker, *High-throughput screening for stability and inhibitory activity of compounds toward cytochrome P450-mediated metabolism.* J Pharm Sci, 2004. **93**(2): p. 239-55.

84. Ross, D.A., et al., *Multiplexed assays by high-content imaging for assessment of GPCR activity.* J Biomol Screen, 2008. **13**(6): p. 449-55.

85. Park, H., et al., *Discovery of Novel Cdc25 Phosphatase Inhibitors with Micromolar Activity Based on the Structure-Based Virtual Screening.* J Med Chem, 2008.

86. Kirchmair, J., et al., *Evaluation of the performance of 3D virtual screening protocols: RMSD comparisons, enrichment assessments, and decoy selection--what can we learn from earlier mistakes?* J Comput Aided Mol Des, 2008. **22**(3-4): p. 213-28.

87. Ding, F., M. Layten, and C. Simmerling, *Solution structure of HIV-1 protease flaps probed by comparison of molecular dynamics simulation ensembles and EPR experiments.* J Am Chem Soc, 2008. **130**(23): p. 7184-5.

88. Gastreich, M., et al., *Ultrafast de novo docking combining pharmacophores and combinatorics.* J Comput Aided Mol Des, 2006. **20**(12): p. 717-34.

89. Mattioni, B.E. and P.C. Jurs, *Prediction of dihydrofolate reductase inhibition and selectivity using computational neural networks and linear discriminant analysis.* J Mol Graph Model, 2003. **21**(5): p. 391-419.

90. Joseph-McCarthy, D., et al., *Lead optimization via high-throughput molecular docking.* Curr Opin Drug Discov Devel, 2007. **10**(3): p. 264-74.

91. Verkhivker, G.M., et al., *Towards understanding the mechanisms of molecular recognition by computer simulations of ligand-protein interactions.* J Mol Recognit, 1999. **12**(6): p. 371-89.

92. Morris, J.A. and R.S. McIvor, *Saturation mutagenesis at dihydrofolate reductase codons 22 and 31. A variety of amino acid substitutions conferring methotrexate resistance.* Biochem Pharmacol, 1994. **47**(7): p. 1207-20.

93. Mildvan, A.S., *Inverse thinking about double mutants of enzymes.* Biochemistry, 2004. **43**(46): p. 14517-20.

94. Reetz, M.T. and J. Sanchis, *Constructing and Analyzing the Fitness Landscape of an Experimental Evolutionary Process.* Chembiochem, 2008.

95. Venkatachalam, K.V., et al., *Characterization of TEM-1 beta-lactamase mutants from positions 238 to 241 with increased catalytic efficiency for ceftazidime.* J Biol Chem, 1994. **269**(38): p. 23444-50.

96. Arnold, F.H. and A.A. Volkov, *Directed evolution of biocatalysts.* Curr Opin Chem Biol, 1999. **3**(1): p. 54-9.

97. You, L. and F.H. Arnold, *Directed evolution of subtilisin E in Bacillus subtilis to enhance total activity in aqueous dimethylformamide.* Protein Eng, 1996. **9**(1): p. 77-83.

98. Stemmer, W.P., *Rapid evolution of a protein in vitro by DNA shuffling.* Nature, 1994. **370**(6488): p. 389-91.

99. Reetz, M.T., et al., *Expanding the substrate scope of enzymes: combining mutations obtained by CASTing.* Chemistry, 2006. **12**(23): p. 6031-8.

100. Chica, R.A., N. Doucet, and J.N. Pelletier, *Semi-rational approaches to engineering enzyme activity: combining the benefits of directed evolution and rational design.* Curr Opin Biotechnol, 2005. **16**(4): p. 378-84.

101. Reetz, M.T., *Controlling the enantioselectivity of enzymes by directed evolution: practical and theoretical ramifications.* Proc Natl Acad Sci U S A, 2004. **101**(16): p. 5716-22.

102. Turner, N.J., *Directed evolution of enzymes for applied biocatalysis.* Trends Biotechnol, 2003. **21**(11): p. 474-8.

103. Bershtein, S. and D.S. Tawfik, *Advances in laboratory evolution of enzymes.* Curr Opin Chem Biol, 2008. **12**(2): p. 151-8.

104. Taylor, S.V., P. Kast, and D. Hilvert, *Investigating and Engineering Enzymes by Genetic Selection.* Angew Chem Int Ed Engl, 2001. **40**(18): p. 3310-3335.

105. Fields, S. and O. Song, *A novel genetic system to detect protein-protein interactions.* Nature, 1989. **340**(6230): p. 245-6.

106. Droge, M.J., et al., *Directed evolution of Bacillus subtilis lipase A by use of enantiomeric phosphonate inhibitors: crystal structures and phage display selection.* Chembiochem, 2006. **7**(1): p. 149-57.

107. Lipovsek, D. and A. Pluckthun, *In-vitro protein evolution by ribosome display and mRNA display.* J Immunol Methods, 2004. **290**(1-2): p. 51-67.

108. Seelig, B. and J.W. Szostak, *Selection and evolution of enzymes from a partially randomized non-catalytic scaffold.* Nature, 2007. **448**(7155): p. 828-31.

109. Chen, G., et al., *Isolation of high-affinity ligand-binding proteins by periplasmic expression with cytometric screening (PECS).* Nat Biotechnol, 2001. **19**(6): p. 537-42.

110. Morley, K.L. and R.J. Kazlauskas, *Improving enzyme properties: when are closer mutations better?* Trends Biotechnol, 2005. **23**(5): p. 231-7.

111. Neuenschwander, M., et al., *A simple selection strategy for evolving highly efficient enzymes.* Nat Biotechnol, 2007. **25**(10): p. 1145-7.

112. Blakley, R.L. and B.P. Sorrentino, *In vitro mutations in dihydrofolate reductase that confer resistance to methotrexate: potential for clinical application.* Hum Mutat, 1998. **11**(4): p. 259-63.

113. Jackson, M., et al., *Calorimetric studies of ligand binding in R67 dihydrofolate reductase.* Biochemistry, 2005. **44**(37): p. 12420-33.

114. Stout, T.J., C.R. Sage, and R.M. Stroud, *The additivity of substrate fragments in enzyme-ligand binding.* Structure, 1998. **6**(7): p. 839-48.

115. Kimber, B.J., et al., *19 Fnuclear magnetic resonance studies of ligand binding to 3-fluorotyrosine-and 6-fluorotryptophan-containing dihydrofolate reductase from Lactobacillus casei.* Biochemistry, 1977. **16**(15): p. 3492-500.

116. Birdsall, B., A.S. Burgen, and G.C. Roberts, *Effects of coenzyme analogues on the binding of p-aminobenzoyl-L-glutamate and 2,4-diaminopyrimidine to Lactobacillus casei dihydrofolate reductase.* Biochemistry, 1980. **19**(16): p. 3732-7.

117. Birdsall, B., et al., *Cooperativity in ligand binding to dihydrofolate reductase.* Biochemistry, 1978. **17**(11): p. 2102-10.

118. Hood, K. and G.C. Roberts, *Ultraviolet difference-spectroscopic studies of substrate and inhibitor binding to Lactobacillus casei dihydrofolate reductase.* Biochem J, 1978. **171**(2): p. 357-66.

119. Volpato JP, Y.B., Blanchet J, guerrero V, Poulin L, Fossati E, Berghuis AM, Pelletier JN, *Multiple conformers in the active site of human dihydrofolate reductase F31R/Q35E double mutant suggest structural basis for methotrexate resistance.* Submitted, November 2008.

120. Huey, R., et al., *A semiempirical free energy force field with charge-based desolvation.* J Comput Chem, 2007. **28**(6): p. 1145-52.

121. Morris, G.M., et al., *Distributed automated docking of flexible ligands to proteins: parallel applications of AutoDock 2.4.* J Comput Aided Mol Des, 1996. **10**(4): p. 293-304.

122. Goodsell, D.S., G.M. Morris, and A.J. Olson, *Automated docking of flexible ligands: applications of AutoDock.* J Mol Recognit, 1996. **9**(1): p. 1-5.

123. Morris GM, G.D., Halliday RS, Huey R, Hart WE, Belew RK, Olson AJ, *Automated docking using a Lamarckian genetic algorithm and an empirical binding free energy function.* Journal of Computational Chemistry, 1998. **19**(14): p. 1639-1662.

124. Kim, R. and J. Skolnick, *Assessment of programs for ligand binding affinity prediction.* J Comput Chem, 2008. **29**(8): p. 1316-31.

125. Mayer, M. and B. Meyer, *Group epitope mapping by saturation transfer difference NMR to identify segments of a ligand in direct contact with a protein receptor.* J Am Chem Soc, 2001. **123**(25): p. 6108-17.

126. Meyer, B. and T. Peters, *NMR spectroscopy techniques for screening and identifying ligand binding to protein receptors.* Angew Chem Int Ed Engl, 2003. **42**(8): p. 864-90.